A Novel Variable Stiffness Gripper using a Bistable Metamaterial

Master Thesis Report

Martijn Oetelmans

TU Delft

A Novel Variable Stiffness Gripper using a Bistable Metamaterial

Master Thesis Report

by

Martijn Oetelmans

to obtain the degree of Master of Science
at the Delft University of Technology
to be defended publicly on July 3, 2024 at 13:45

Supervisors:	Prof. Cosimo Della Santina	*TU Delft*
	Prof. Edoardo Milana	*University of Freiburg*
Daily Supervisor:	Dr. Hugo Oliveira	*University of Freiburg*
Faculty:	Faculty of Mechanical Engineering	
Department:	Department of Biomechanical Engineering	
Project Duration:	January, 2024 - July, 2024	
Student number:	4677196	

Acknowledgements

This thesis report marks the end of my Master's in Mechanical Engineering, a journey that has been both challenging and immensely rewarding. Working on this thesis project has been a memorable experience, one that I enjoyed thoroughly from start to finish. This project has allowed me to apply knowledge from many different aspects of my studies and has sparked my interest in research. The opportunity to visit Freiburg for two months was particularly enriching, as it allowed me to conduct experiments and gain firsthand experience of working in academia.

I owe a great deal of gratitude to my daily supervisor, Dr. Hugo Oliveira, and my supervisor, Dr. Edoardo Milana. Their patient guidance and support were invaluable, not only in teaching me how to conduct proper research but also in making me feel welcome in Freiburg and including me in their academic community. Thank you both for the countless hours of help and the enjoyable moments we shared.

I am also deeply grateful to my supervisor, Dr. Cosimo Della Santina, whose assistance with the project's administrative aspects and insightful feedback on my findings and report were crucial to the completion of this work.

A special thanks to my housemates, whose mental support and timely dinners were a great comfort during stressful times. Your support made a significant difference in managing the pressures of this project. Additionally, I would like to thank my studymates who made the project so much more enjoyable, and in particular, Steven Tan, who generously allowed me unlimited access to his 3D printer.

Lastly, I want to extend my heartfelt gratitude to my girlfriend and my parents. Their unwavering support and willingness to listen throughout this project and my entire education has been invaluable. I could not have achieved this milestone without their constant encouragement and belief in me.

Thank you all for your contributions to this journey,

Martijn Oetelmans
Rotterdam, June 2024

Executive Summary

This thesis introduces the development of a novel Variable Stiffness Gripper (VSG) that leverages bistable metamaterials to shift between various stiffness states, addressing the limitations of current actuator technologies and enhancing the versatility and efficiency of robotic hands. The primary research objectives focus on analyzing the mechanical properties and behavior of bistable metamaterials and designing a lightweight VSG that incorporates these materials to achieve variable stiffness without requiring energy to maintain it.

The actuator design phase included the creation of a metamaterial optimized for torsional stiffness and bistability, along with the development of two designs for the Bistable Variable Stiffness Gripper (B-VSG), one actuated and one unactuated. These designs share some features but differ in their actuation mechanisms.

Experimental validation involved Finite Element Analysis (FEA) to simulate geometric ratios and material properties to predict torsional stiffness, and physical testing to confirm the FEA results and assess the dynamic behavior and stability of the bistable structure. The performance of the B-VSG was quantified by grip force and stiffness variation between states.

The findings highlighted the potential of bistable metamaterials in achieving variable stiffness, with significant differences in torsional stiffness observed between the bistable states. The design proved superior in efficiency and lightweight compared to existing technologies, although further optimization is necessary, particularly in improving the actuation unit and refining the unit cell designs.

In conclusion, the research successfully developed a novel, lightweight VSG using bistable metamaterials (B-VSG), proving the concept for integrating these materials into robotic actuators. Future research should look into more advanced manufacturing methods for size reduction and customization, integrate control systems for better stiffness adjustment, and perform long-term tests to see how the gripper performs in real-world conditions.

This study opens up new possibilities for using bistable metamaterials in robotics, suggesting a promising direction for creating more adaptable, efficient, and versatile actuators.

Contents

Nomenclature

List of Abbreviations

AM	Additive Manufacturing
B-VSG	Bistable Variable Stiffness Gripper
CAD	Computer-Aided Design
F-VSA	Flexure Variable Stiffness Actuator
FDM	Fused Deposition Modeling
FMM	Flexible Mechanical Metamaterial
SEA	Series Elastic Actuator
TPE	Thermoplastic Elastomer
VIA	Variable Impendance Actuator
VSA	Variable Stiffness Actuator
VSA	Variable Stiffness Gripper
VSM	Variable Stifness Machine

List of Symbols

$\Delta\%k$	Percentage Stiffness Difference
Δk	Stiffness Difference
δ	Gap between Supporting Segments
ϵ	Strain
ϕ	Angular Deformation
σ	Axial Stress
τ	Torsional Load
A	Cross-Sectional Area
b	Amplitude of Cosine-Shaped Section
b_l	Amplitude of Cosine-Shaped Section in the Larger Bistable Cell in the Three-celled Metamaterial
b_s	Amplitude of Cosine-Shaped Section in the Smaller Bistable Cells in the Three-celled Metamaterial
c	Damping Coefficient
D	Diameter of the Cylindrical Unit Cell
d	Wall Thickness of Cylindrical Unit Cell
E	Young's Modulus
E_{flex}	Flexural Modulus
F	Axial Load
F_c	Critical Force
G	Shear Modulus
h_1	Total Height of the Bistable Cell in Open State
h_2	Total Height of the Bistable Cell in closed state
I	Moment of Inertia
J	Polar Moment of Inertia
k	Stiffness
k_l	Stiffness in Linear Elastic Material
l	Width of Bistable Cell
M	Mass
R	Radius
t_1	Thickness of the Cosine-Shaped Section
t_2	Thickness of the Vertical Support Beam
U	Elastic Energy
x	Axial Deformation

List of Figures

List of Tables

1 Introduction

The lack of suitable actuators has slowed the development of high-performance machines that can match human capabilities, primarily due to the adaptable compliance, or variable stiffness, found in biological systems [1]. It has been shown that the passive nonlinear dynamics of human hand joints play a crucial role in achieving a stable grasp. Adding a passive component to a robotic system can enhance grasp stability in uncertain conditions [2]. Compliant robotic grippers can adapt to their environment to spread contact forces, facilitating compliant grasping without the need for complex sensors or actuators [3].

A compliant robotic hand is a good choice for mimicking the flexibility of the human hand, but it has drawbacks such as low fingertip force, low positioning accuracy, complex motion modeling, and challenging control [4]. Conversely, rigid manipulators can damage objects or cause undesired trajectories during grasp attempts. Using soft materials in grippers reduces design complexity, weight, and cost, as these materials can conform passively to an object's shape [5]. Soft robotic grippers offer a promising path for adaptive grasping, mimicking the dexterity and versatility of biological hands [3].

Tendons' natural spring-like behavior contrasts with traditional stiff actuators in industrial robotics, which require precise reference-trajectory tracking [6]. Over the past few decades, variable stiffness actuators (VSAs) have been developed to combine compliant elements, similar to muscles, with the precise tracking abilities of traditional rigid actuators. A robotic hand with variable stiffness benefits from the strengths of both soft and rigid hands [4].

VSAs are essential for advanced robotic systems, allowing robots to adjust stiffness based on task requirements, mimicking the compliant behavior of biological muscles and providing safety and performance benefits in dynamic environments [7]. These actuators enable robots to safely interact with humans and handle delicate objects by adjusting stiffness, enhancing precision and versatility in applications like prosthetics, rehabilitation, and industrial automation [6]. Research shows that hand prostheses with stiffness modulation can improve amputee performance when the prosthesis's impedance matches the task requirements [8].

VSAs were created to address the limitations of traditional actuators with fixed stiffness. While traditional actuators are effective for precise control in rigid environments, they struggle in uncertain or dynamic conditions [9]. Fixed stiffness actuators can be unsafe in human-robot interactions, as they do not absorb impact forces well, potentially causing injury or damage. They also lack the adaptability needed for tasks requiring variable compliance, such as handling fragile objects or navigating uneven terrain. Incorporating variable stiffness enhances safety by allowing compliance during unexpected impacts, reducing injury risk. It also improves robotic performance by adapting stiffness in real-time to suit specific tasks, leading to more efficient and versatile operation [10]. Despite the development of many novel variable stiffness joints, most have not been successfully applied to robotic arms due to complex tuning mechanisms, large sizes, and slow response times [11]. In robotic hands with variable stiffness specifically, size constraints, which require simplified variable stiffness structures, and achieving easy and active variable stiffness control are primary limitations [4]. Most research on variable stiffness in robotic systems is inspired by the human body, particularly for developing artificial limbs [2].

Flexible mechanical metamaterials (FMMs) present a groundbreaking approach that goes beyond mimicking human capabilities. FMMs offer a promising solution to enhance VSAs and open up new

possibilities in the field of robotics design and innovation. These materials have unique properties derived from their geometric structure rather than their material composition [12]. They can exhibit nonlinear elastic properties and multi-stability, which are potentially useful for actuators. Bistable metamaterials, a type of FMM, can switch between two stable states, enabling variable stiffness in monolithic structures [13]. Advances in additive manufacturing have enabled the creation of novel FMM structures with complex energy landscapes, showing great promise for VSAs [14, 15]. Recent research has led to the development of flexure variable stiffness actuators (F-VSAs) using FMM [15].

Despite the potential of FMMs, their use in VSAs remains underexplored, especially actuators that utilize FMM with buckling instabilities to switch between stiffness states. Most research on FMMs focuses on their fundamental properties rather than their integration into functional actuators. Comprehensive studies are needed to assess the feasibility and benefits of incorporating FMMs into VSAs, particularly regarding performance enhancement and mechanical simplicity.

This research aims to design a novel variable stiffness gripper (VSG), a VSA aimed for gripping, that uses bistability to switch between stiffness settings, making robotic actuators more versatile. Specific objectives include:

1. Analyzing the mechanical properties and behavior of bistable metamaterials.
2. Design of a variable stiffness gripper that integrates these metamaterials to achieve variable stiffness.
3. Validating the performance of the proposed actuator against the existing state of the art through computational modeling and experimental testing.

Integrating bistable metamaterials into VSAs has the potential to revolutionize the design and functionality of robotic actuators. This approach can lead to more efficient and versatile robotic systems by reducing size, mechanical complexity and energy consumption. In addition, bistable FMM can be used to design VSAs with a quick response time, a current limitation in the state of the art. Fabricating intricate FMM structures using additive manufacturing techniques can significantly enhance the functionality and customization of actuators [16]. This research aims to improve VSA performance and pave the way for improved robotic hand design in field such as prosthetics, where lightweight and efficient actuators are crucial for user comfort and functionality [17].

The novelty of the research lies in the use of bistable metamaterials as a compliant element and stiffness switching mechanism in a VSG. The proposed design allows for rapid, discreet inherent stiffness switches and reduces actuator size, weight and inertia. Not only is there very limited research on the use of metamaterials in VSAs, but this is also the first time bistable metamaterials are being used in such applications. When reviewing the state of the art of VSAs, a VSA that changes its stiffness due to geometric reorganization of a metamaterial would pioneer a new class of actuators.

This study employs a multi-faceted approach to develop and validate a novel VSG using bistable metamaterials (B-VSG). Initially, a comprehensive literature review is conducted to examine existing research on VSAs and (bistable) metamaterials, identifying knowledge gaps and state of the art technologies. Following this, the mechanical properties of bistable metamaterials are analyzed through computational modeling to understand their behavior under different loading conditions. After this, the research will dive into designing a VSG that integrates these bistable metamaterials, with a focus on optimizing the actuator's performance while minimizing mechanical complexity. Additive manufacturing techniques are then utilized to fabricate the actuator components with high precision and customization. Experimental validation is conducted to test the performance of the novel variable stiffness mechanism (VSM), including its stiffness modulation capabilities and overall mechanical behavior. Finally, the study combines these findings into the B-VSG design. This demonstrator serves as a proof-of-concept, highlighting the actuator's potential for real-world applications.

Part I

Preliminary Research

2

Literature Review

2.1. Variable Stiffness Actuators

In an effort to add spring-like behaviour to stiff actuators, *compliant actuators* were developed. Although less suitable for reference-trajectory tracking tasks than traditional stiff actuators, compliant actuators enhance user safety and enables motion that is more natural. However, compliant actuators, or soft actuators, face challenges such as complex modeling, difficult control, slow response in stiffness tuning, and bulkiness [18, 19, 11]. Soft actuators have been developed on the basis of a wide range of principles. These actuators have been designed to be specific to the application, facing the mentioned challenges in the context of their application.

While these compliant actuators may be less appropriate for conventional position controlled applications, they provide significant benefits in specific emerging applications, such as promoting a safe human–robot interaction, developing comfortable robotic prostheses and orthoses, and contributing to the design of legged robots [20]. Compliant actuators are divided into active and passive compliant actuators [21]. Active compliant actuators are systems consisting of an actuator, a sensor and a controller. Using feedback information, the actuator can emulate compliant performance. In contrast to passive compliant actuator that use an intrinsic compliant element to create passive compliance. Active compliant actuators are less energy efficient than their passive counterpart, are not able to store energy and have a limited bandwidth [22].

Being able to modulate the stiffness of a compliant actuator would solve the trade-off between position-controlled functionalities of traditional, stiff actuators and the motion, safety and energy advantages of a compliant actuator. In recent years, there has much development into variable impedance actuators (VIAs), which allow for stiffness modulation via active or passive adaptable compliance. In particular, a focus has been on a subgroup of VIAs, VSA, which does not include a damping unit [23].

Adaptable compliance enhances the safety and naturalness of interactions between robots and humans, a crucial aspect in many fields. There is a rising focus on the development and integration of VSAs or adaptable compliant actuators in, for example, wearable robotics, rehabilitation robotics, prosthetics, and walking robots [15]. This is driven by VSAs capacity to mimic biological muscle in shock absorption, ensuring safe interaction with users, and the ability to adjust the natural dynamics of a mechanical system, which leads to a motion closer to the desired motion, reducing energy consumption. In addition to biomimicking capabilities, VSAs are also capable of efficiently storing and releasing energy within passive elastic elements. Additionally, being able to tweak the stiffness improves the robot's ability to withstand unexpected disturbances and model errors. These uncertainties might come from changes in the environment, the robot's movements, or how a human interacts with it [17].

This section will focus on actuators with adaptable compliance, the VSA, comprehensively defining the actuator and discussing the current state of the art. It will delve into the existing actuators, the classifications, possible applications and define a background for further research into this topic. However, before diving into the existing state of the art, important background theory will be covered.

2.1.1. Stiffness: A Structural Property

It is important to note that whenever *stiffness*, or *compliance*, is mentioned in this review, the intended definition is that of a structural property. Compliance is defined as the inverse of stiffness. Stiffness is the

resistance to deformation of an elastic body, while compliance is the extent to which the material deforms under load. Both stiffness and compliance are related to elastic energy. Four primary types of stiffness exist, each relevant for a different type of deformation: *axial stiffness* (N/m) describes the resistance to tension or compression along the axis of deformation, *torsional stiffness* (Nm/rad), which indicates the resistance to rotational deformation, *flexural stiffness* (Nm^2/rad), that describes the resistance of a structure to bending, and *shear stiffness* (N/m), which measures the resistance to deformation by shear stress.

Depending on the structure that is under investigation, the formulation of stiffness can differ. When the structure maintains its original geometry under load or if it has no initial stress, the stiffness of the structure is equal to the *material stiffness*. However, when stressed members change orientation under load, *geometric stiffness* needs to be considered also. The *tangent stiffness* is the sum of the material stiffness and geometric stiffness in materials that change geometry under load [24].

The *tangent stiffness* represents the derivative of the applied load with respect to deformation at a specific point on the force-displacement curve, which shows the relation between the applied load and the deformation. When the relation between load and deformation is linear, the tangent stiffness is constant. The force-displacement curve depends on the structure of the material.

In linear elastic material, stress and strain in different directions are related by elastic moduli, such as the Young's modulus (E), shear modulus (G) and flexural modulus (E_{flex}). For instance, axial stress and strain are related by the Young's modulus, see Equation A.1. The Young's modulus is a material property, unlike stiffness which is a structural property and dependent on geometry as well as material properties such as the Young's modulus. Different material stiffnesses are related by different material moduli and the inertial properties of the material, such as moment of inertia (I), polar moment of inertia (J) and cross-sectional area (A).

Irrespective of the order of force-displacement relation, the tangent stiffness is equal to the gradient of the force-displacement curve. For linear springs, this implies a constant stiffness value, whereas for nonlinear springs, it implies a variable value. Because of this, the generalized equation between stiffness, axial load and variation of the length of the spring can be written as:

$$k(x) = \frac{\delta F(x)}{\delta x}, \tag{2.1}$$

where $k(x)$ denotes the tangent axial stiffness, $F(x)$ the load that is inflicted to the material and x is the difference in length of the spring from its nominal length. Note that the stiffness is no longer always constant, but could a function of the displacement x, depending on the order of the relation. This implies that the spring stiffness of nonlinear springs can be changed by increasing or decreasing the displacement of the spring.

2.1.2. Adaptable compliance actuators

Adaptable compliance actuators, also referred to as VSAs, are advanced mechatronic devices developed to create robotic devices that are inherently compliant, robust, and versatile [23]. The terminology used to characterize these actuators also includes adjustable compliance, variable compliance, adjustable stiffness, and controllable stiffness, highlighting the absence of standardized nomenclature for these devices [20]. For the purposes of this report, the terms *variable stiffness* or *adaptable compliance* will be used.

The idea of introducing variable stiffness came about primarily due to safety concerns [7]. VSAs have the potential to move loads more quickly and securely compared to solutions with rigid or flexible joints. Both robustness and performance considerations indicate that flexible robots may have superiority over traditional rigid ones. Because of the variable stiffness in VSA, these actuators are capable of both reference-trajectory tracking when in a high stiffness setting, and enhancing safer and more natural motion when in a low stiffness setting, effectively combining the advantages of both a rigid actuator and a compliant actuator.

As explained by Grioli et al. [7], there are two main advantages to VSAs in terms of system robustness and performance. First, incorporating compliant elements in a robot can prolong the lifespan of gearboxes by reducing stress peaks from sudden dynamic events (e.g. accidental contacts). Second, the inherent redundancy in the actuation of some VSAs (e.g. antagonist VSAs) enhances their reliability in case of

Table 2.1: Key attributes per use-case, as presented by [23]

Shock absorption	**Stiffness Variation at Constant Load**	**Stiffness Variation at Constant Position**	**Cyclic Movement**	**Explosive Movements**
Maximum elastic energy	Maximum stiffness	Stiffness versus torque diagram	Maximum deflection	Peak torque
Maximum deflection	Minimum stiffness	Maximum stiffness	Maximum stiffness	Maximum speed
	Stiffness variation time	Minimum stiffness	Minimum stiffness	Maximum elastic energy
			Maximum torque hysteresis	Stiffness variation time

mechanical failures. According to Grioli et al., VSAs perform up to 30% better compared to fixed mechanical compliance systems, such as series elastic actuators (SEAs).

Because of the widely recognized advantages of variable stiffness actuation across various applications, different VSAs have been developed to meet specific requirements. Stiffness regulation in these VSAs employs diverse mechanisms. However, the practical utilization of VSAs encounters limitations. Typically, a VSA occupies more space and has greater weight and inertia compared to traditional rigid or fixed compliant actuators [17]. Moreover, many VSAs consume a significant amount of energy for stiffness regulation and maintaining stiffness, restricting their use in various tasks [25]. Additionally, adjusting stiffness may impact the system's behavior, necessitating the adoption of sophisticated control approaches [26].

2.1.3. Design of a Variable Stiffness Actuator

Unfortunately, there is no one-size-fits-all design or solution for VSAs that works well across all applications [6]. However, when dealing with a specific task, it is possible to differentiate between more and less effective principles and implementations. This raises the question of how to choose the most suitable setup from various options. Depending on the use-case on the VSA, different attributes become more or less important [23].

Use-Cases of Variable Stiffness Actuators

As mentioned previously, VSAs are used in many applications and have therefore several different use-cases within these applications. These use-cases should be identified and prioritized to asses the requirements of the VSA design. According to Wolf et at. [23], the most common use-cases for VSAs are:

- Shock absorption
- Stiffness Variation at Constant Load
- Stiffness Variation at Constant Position
- Cyclic Movement
- Explosive Movements

The most important attributes to consider in the design process when working towards an application with intended use-cases, can be found in Table 2.1. Based on these attributes, the design requirements for new VSA designs can be constructed, or new use cases for existing design can be explored.

2.1.4. State of the art and Classifications of Variable Stiffness Actuators

Series Variable Stiffness Actuators

In this setup, one actuation unit with series springs is responsible for controlling the output link position, while another unit independently tweaks the stiffness. It is called the series approach because the first actuation unit is solely in charge of determining the desired position of the output link [17]. Typically, the second actuation unit doesn't focus on controlling the position but instead fine-tunes the stiffness of the output link.

The series configuration can be further divided into four classes [17], where VSAs are subdivided based on the principles they employ to change stiffness:

- Changing pretension of nonlinear spring
- Changing load-spring transmission ratio via lever arm ratio
- Changing load-spring transmission ratio via transmission angle
- Changing effective physical properties

In the class of changing pretension of a nonlinear spring, there are two types of actuators. The first type uses springs to control the position of the output link, while the second adjusts the pretension of these springs. The nonlinearity of the springs allows stiffness adjustment by altering the deflection. This method is simple but has the downside of not utilizing stored potential energy until the pretension is released, reducing energy capacity in stiff actuators [23]. Examples include: 1) *MACCEPA*, which uses a lever arm to pretension a single nonlinear spring [27]; 2) *MACCEPA 2.0*, which replaces the lever arm with a cam to adjust torque-angle and stiffness-angle relations [28]; 3) *Variable Stiffness Joint* (VS-joint), which uses a preload to push a roller to an equilibrium position [9]; 4) *Safe Joint Mechanism* (SJM-I), which uses a slider-crank mechanism and a linear spring [29]; and 5) *SJM-III*, which features an inclined link, a slider with rollers, and a linear spring [30]. Although the SJM-I and SJM-III use linear springs, they are considered as nonlinear spring mechanisms due to their nonlinear force-deflection profiles [17].

In stiffness regulation by changing the load-spring transmission ratio via lever arm ratio, VSAs adjust stiffness by changing the lever mechanism, which is effective since displacement is perpendicular to the applied force [6]. Examples include: 1) *Compact Variable Stiffness Actuator* (ComPact-VSA), which uses a cam-shaped lever arm [31]; 2) *Actuator with Adjustable Stiffness* (AwAS), which adjusts stiffness by altering the spring point position [32]; 3) *AwAS-II*, which adjusts stiffness by changing the pivot point position [33]; 4) *vsaUT-2*, which uses the concept of a changing pivot point [34]; 5) *mVSA-UT*, which is actuated by two differentially connected motors for adjusting output stiffness and position [35]; 6) *Hybrid Variable Stiffness Actuator* (HVSA) [36]; and 7) *Serial Variable Stiffness Actuator* (SVSA), which uses an Archimedean spiral relocation mechanism [37].

Another method involves changing the load-spring transmission ratio via transmission angle, adjusting the angle between the applied force and the spring's neutral axis. Examples include: 1) *Mechanism for Varying Stiffness via Changing Transmission Angle* (MESTRAN), which adjusts the angle between output force and deflection [38]; 2) *DLR FSJ*, which modifies stiffness by changing the pressure angle [39]; and 3) *VSA-HD*, which regulates the nonlinear relationship between input and output link angles using link length selection [40].

Lastly, VSAs can change the physical properties of the spring. This involves altering the effective properties (such as structure and stiffness) of the actuator's elements. For example, the *Mechanical Impedance Adjuster* changes the effective length of a leaf spring using a slider [41]. Another example that changes effective physical properties is the *Discrete Variable Stiffness Actuator* (DVSA) by Hussain et al.[11], which changes stiffness by varying the number of involved linear elastic elements. This design enables rapid stiffness switches using an energy-efficient, low-cost control mechanism [11]. New advancements in material science might pave the way for variation of the flexural modulus, which is a structural property, due to geometric reorganisation in elastic materials.

Antagonistic Variable Stiffness Actuators

The antagonistic approach mimics the antagonistic arrangement of muscles, such as the biceps and triceps in human arms. In the human body, contracting the biceps causes bending of the arm, while contracting the triceps causes extension. Contracting both muscles simultaneously causes high stiffness of the elbow and simultaneous relaxation results in a very compliant elbow. This mechanisms can be mechanically imitated to create a variable stiffness device. An advantage of the antagonistic approach, compared to the series approach, is that the stiffness curve can be designed [6]. In antagonistic VSAs this is realised by two actuators that actuate the output link using *nonlinear compliant elements*, with quadratic compliant elements being the most common because they provide a linear relationship between co-contraction and stiffness [42]. These elements need to be nonlinear in the antagonistic setup [20].

The antagonistic configuration can be further divided into three classes [17]: Unidirectional antagonistic, cross-coupled antagonistic and bidirectional antagonistic. In unidirectional antagonistic VSAs, each

actuation unit connects to the output link using a nonlinear unidirectional spring, which can only push or pull the output link in one direction. This means only one actuation unit can exert force to move the output link at any given moment. Consequently, the maximum joint torque is restricted to that of each individual motor, and there is no net torque available when the stiffness is at its maximum [6]. Some examples of unidirectional antagonistic VSAs are: 1) the *AMASC actuator*, where one motor controls the pretension of the opposing springs and the other motor controls the spring rest position [43]. 2) *Plated Pneumatic Artificial Muscles* (PPAM), that realises variable stiffness by inflating opposing artifical muscles[44]. 3) *Biologically inspired joint stiffness control*, that use rolamite springs as the complaint element [42].

Cross-coupled antagonistic VSAs are unidirectional antagonistic VSAs with an additional nonlinear spring connecting the two motors [17]. This extra springs allows for both motors to contribute to movement. An example of cross-coupled antagonistic VSAs is the *VSA-I* by Tonietti et al [45].

By adding a fourth nonlinear spring, connecting both motors to the output link with two springs, a bidirectional antagonistic VSA is created. Because of the extra spring, both motors are able to push and pull on the output link, allowing transmission of maximum generate force of each motor to the output link [17]. Some examples of bidirectional antagonistic VSAs are: 1) *VSA-II* [46], which is an improved to the VSA-I and uses a four-bar linkage system as transmission. 2) *VSA-CUBE* [47], which main focus was on cost reduction. 3) The *Bidirectional Antagonistic Joint* [48], which achieves bidirectional antagonism, by replacing the single string connecting a motor to the link with a loop that goes around both. 4) the *Flexure VSA* [49], where a compliant four-bar linkage mechanism utilizes elastic pivots to generate adaptable stiffness.s

Variable Stiffness Actuators based on Flexure Hinges

In recent year, efforts have been made to address the limitations of VSAs under the current classification. There is a clear trend in recent research of incorporating multiple, functionally different design component into a single integrated structure by using a novel material type named *flexible mechanical metamaterial* (FMM) [50]. Recent work has shown that FMMs can enhance the performance and simplify the design of engineered systems [51]. For example, recently researchers have designed an adaptable complaint actuator using FMM as transmission, joints and adaptable compliance elements [15].

Compliant joints, unlike traditional ones, do not have hinges and can be made as a monolithic structure. This reduces friction, wear, and backlash in the mechanism, making it easier to achieve a compact and lightweight design [52]. However, compliant mechanisms have a limited operational lifespan due to plastic deformation in hinges, eventually causing failure during cyclic loading [53]. Variable stiffness actuators based on flexure hinges, termed *F-VSAs* by Giraud et al. [15], stand out as an innovative solution because of its folding features, normally observed devices such as origami robots [54], offering improvements in both fabrication complexity and compactness compared to VSAs and SEAs [55].

To tackle the inherent mechanical intricacies of VSAs, researchers have delved into the use of flexure hinges and joints as compliant mechanisms. While existing VSA studies use flexure mechanisms as variable stiffness elements, they often function merely as compliant springs and attachments, connecting the motor to various components without fully addressing the complexity issues of VSAs [49, 56], for example in the *rotary flexure hinges based variable stiffness joint* [57], where four controlled rotary flexure hinges are utilized to control the stiffness via rotation of the flexure hinges. Additionally, determining the stiffness of flexure-based mechanisms proves challenging, especially in systems with complex folding patterns and closed kinematic chains [15].

The novel F-VSA proposed by Giraud et al. [15] incorporate flexure hinges and joints, serving not only as virtual springs but also adding elasticity to the system by acting as structural components of the actuator. Functioning as both links and joints, the flexure-based folds define the system's kinematics, eliminating the need for additional elastic elements to achieve variable stiffness. The inherent stiffness of the flexure joints in the transmission plays a crucial role in defining the overall stiffness of the F-VSA system. Altering the configuration allows for the variation of overall stiffness, providing control over force output and the position of the end-effector. Additionally, the flexure joint design minimizes the number of mechanical parts needed for achieving multi-Degrees of Freedom (DoF) structures, significantly reducing mechanical complexity and bulkiness while improving mechanical efficiency and assembly simplicity.

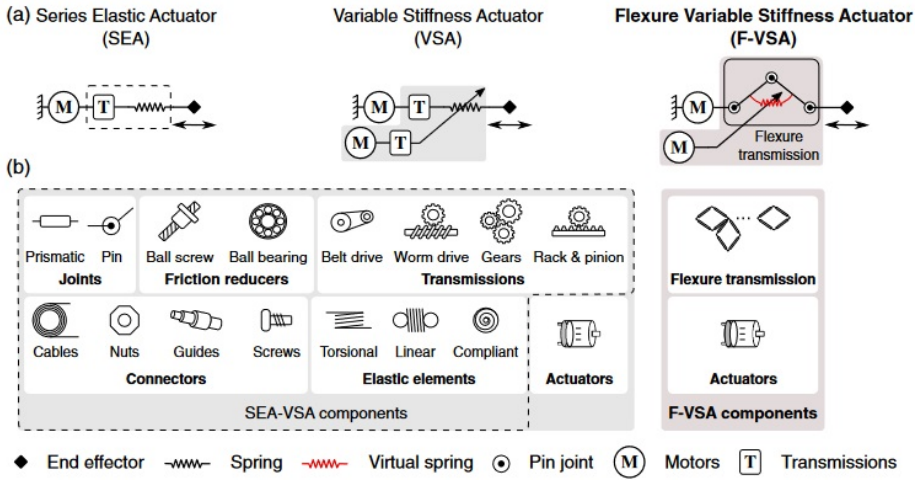

Figure 2.1: Comparison of components present in SEAs, VSAs, and F-VSAs, as presented by Giraud et al. [15]

2.2. Variable Stiffness in Flexible Mechanical Metamaterials

As explained in the previous section, FMMs shows enormous potential in the development of variable stiffness structures, which in turn can be utilized in innovative VSAs to achieve less complex, smaller, more durable actuators with a faster response time. At the time of writing this report, the implementation of FMM to tune stiffness of actuators is very limited. However, the developments into FMM and use of mechanical instabilities to adapt stiffness of these structures are currently under extensive investigation. In an effort to qualitatively compare FMMs against conventional compliant elements in VSAs, the recent developments into adaptable stiffness of FMMs will be reviewed, regardless of their intended application. The physical design of the FMM structures might be optimized for its intended use, but still show great promise for the application in VSAs. Before diving into the state of the art and potential of FMM, metamaterials in general will first be discussed.

Material derives its characteristics under external loads or stimuli from the constituents it is build from, which shows statistically relevant properties if further scaled [58]. *Metamaterial*, on the other hand, is material that is build up from the same matter but has inherently other characteristics under external loads or stimuli because of their geometrical structure. The word *metamaterial* is a conjunction of the Greek word ”meta” and the modern word ”material”, meaning *beyond material* [14]. Metamaterials are structured materials that consist of repeating building blocks or cells, often called *unit cells* [59]. Because these cells are carefully structured, it is possible to design a materials that exhibits properties and functionalities that are unseen in the conventional material that the unit cells are made off. Assembling these nonlinear or multistable building blocks to create mechanical metamaterials results in a variety of entirely novel functionalities. [12].

Originally used in optics and electromagnetism, the term ”metamaterial” was first associated with optical, acoustic and electromagnetic metamaterials [60, 61]. Lately, there is been increasing interest in *mechanical metamaterials*, even though this area has not been explored as much. These are a type of metamaterial that deals with motion, deformations, stresses, and mechanical energy [12]. Various types of mechanical metamaterials have been recognized for quite some time. For example, there is the idea of *auxetic materials*, which have a negative Poisson’s ratio [62].

2.2.1. State of the art of Stiffness Modulation in Flexible Mechanical Metamaterials

Mechanical metamaterials are key materials in today’s era, showing great potential for use in advanced engineering and physical systems [63]. Mechanical metamaterials have emerged in recent years and much research is currently being done to further develop this field. Although the interest for this thesis lies on stiffness adaptation, this is not the sole feature being developed in FMMs, of course. The field of FMMs encompasses motion, deformations, stresses and mechanical energy [12]. FMMs have gained interest because of the extraordinary manner they respond to external stimuli. Some of the recent research

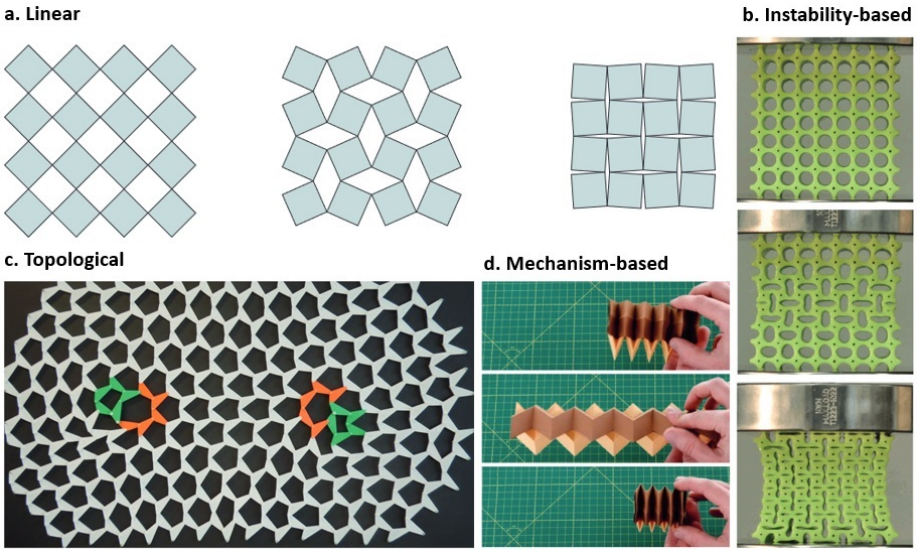

Figure 2.2: Categories of FMM as proposed by Bertoldi et al. [12]. a) Auxetic material, which followings the principle of linear mechanical metamaterials. b) Collective buckling instability in a rubber slab with circular holes, which follows the principle of instability-based mechanical metamaterials. c) Topology with dislocations which follows the principle of topological mechanical metamaterials. d) Deployment and retraction of a tube system, which follows the principle of mechanism-based mechanical metamaterials

focuses on multistablity, which enables a wide adaptability range, but is non-continuous and requires large deformation [64]. While other research focuses on the continuous (non)linear elastic responses, which is continuously adaptable, but does require constant energy to maintain the adaptation.

In the realm of FMMs, Bertoldi et al. [12] have identified four key design principles that contribute to the distinctive properties of metamaterials, see Figure 2.2. These principles are commonly incorporated in the development of advanced structures for FMMs. The first category, termed *linear mechanical metamaterials*, involves modulating the independent coefficients of the elasticity tensor of an anisotropic material through structural design choices. Examples of metamaterials aligned with this principle include auxetic materials and extremal materials, such as pentamode metamaterials. The second category is *mechanism-based metamaterials*, relying on the zero-energy, free motion of rigid elements connected by flexible hinges. Structures like origami and kirigami, known for their excellent 3D shaping ability and straightforward topology tailoring, illustrate this design principle [65].The third design principle is *topological metamaterial*, offering a pathway to robust functionalities as topologically protected properties remain unaffected by smooth deformations of the underlying geometry or the presence of disorder. The final design principle is *instability-based metamaterial*. By leveraging elastic instabilities and large deformations, strongly nonlinear relations between macroscopic stresses and strains can be established, even when the material stays in the near-linear regime.

Nonlinearities and instabilities underlie several advanced metamaterial functionalities, such as bistability and programmability [12]. The adaptability of stiffness in FMM is highly dependent of nonlinear elastic behaviour of the metamaterial structure under load. Within literature, two main methods to realise stiffness adaptation in FMMs are prevalent:

- Stiffness adaptation due to preloading all, or some, FMM unit cells in the structure.
- Utilization of different stiffness modes by exploiting multistability of flexible metamaterials structures.

Compliant mechanisms are often found in the state of the art of FMMs that are meant for stiffness modulation, for example the F-VSA by Giraud et al. [15], in the bio-inspired finger by Mohammadi et al. [52] and in the monolithic binary stiffness switches by Kuppens et al. [13]. Compliant mechanisms are structures consisting of rigid and flexible components that achieve motion through elastic deflection. Prevalent in the field of metamaterial are lattice structures, which are cellular materials that show a regular and repeating structure, such as the popular honeycomb structure [66]. Cellular solids are typically divided into structures

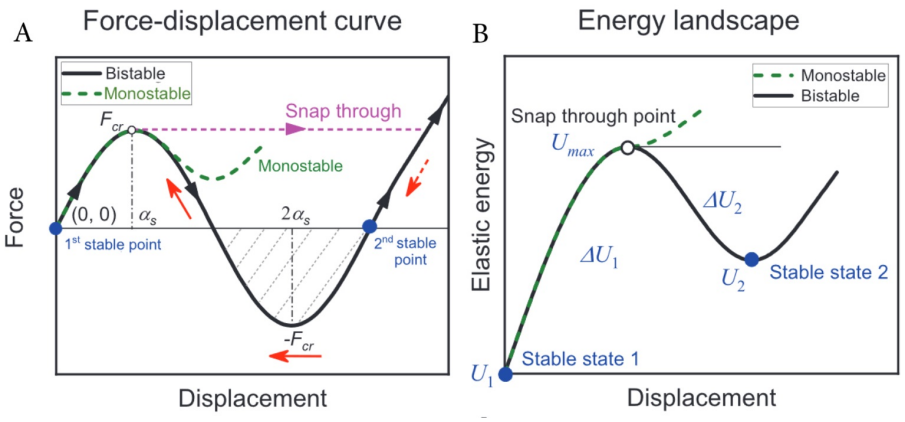

Figure 2.3: Snap-though behaviour and multistability [70]

dominated by stretching or bending. Bending is great for absorbing energy, while stretching is ideal for lightweight, load-bearing uses. Recent research has opted to combine these topologies, Wagner et al. [67] focused on creating programmable active lattice structures that can switch between stretch-dominated and bending-dominated topology when exposed to heat.

Compliant mechanisms are connected by compliant flexure joints or flexure hinges. These are mechanisms that transfer force, motion, or energy by using the elastic deformation of their flexure elements, causing relative motion between two links. Unlike traditional joints, compliant joints do not have hinges and can be fabricated as a single, integrated structure. A very important unit structure for compliant elements are slender elements [12]. The use of complaint hinges, instead of traditional joints, reduces friction, wear, and backlash in the mechanism, enabling a more compact and lightweight overall design [52].

Stiffness Adaptation due to Multiple Stiffness Modes in Multistable Systems

In general, effective multistable structures are build out of serially stacked bistable unit cells that exhibit local negative stiffness [68]. *Multistability* is accomplished by a morphological change of shape or topological transformation when loaded, causing structures with multiple stable states to shift from one equilibrium state to another [66, 67]. Multistable metamaterials and actuators can exist in various stable configurations and switch, with little change in size, between them when stimulated.

Depending on their geometry, metamaterials can exhibit three nonlinear elastic responses: *simple stability*, *monostability* and *bistability*. Both monostability and bistability show *snap-through* behaviour, see Figure 2.3. Snap-though behaviour occurs when the structures are deformed to a critical configuration. Because of this configuration an elastic instability occurs and the structure buckle towards a distant state [69]. All three nonlinear elastic responses are characterized by different force-displacement curves. The force-displacement curve of the metamaterial depends on the internal structure and arrangements of the unit cells. The force-displacement curve for a single unit cells can be derived by examining its structure.

In different modes, structural properties, like the flexural modulus of the metamaterial, can differ. Kaufmann et al. [71] developed a robotic arm using FMM configured in a Kresling origami structure that can modulate its stiffness by switching between stable states, see Figure 2.4. In the Kresling structure, the bending stiffness is directly related to the geometric design, and therefore easily controlled. Lele et al. [69] proposed a kirigami composite with a single slit and bistable patches, which experiences different stiffness depending on the state of the structure. In both the works of Kaufmann et al. and Lele et al. the stiffness adaptation is not explicitly applied on VSAs, but the proposed systems do show significant stiffness adaptations.

A FMM that exhibits local negative stiffness behavior, featuring bistability, has two unique capabilities. Firstly, it can **trap strain energy**, as shown in Figure B.1. This capability arises from the bistability that enables sequential snapping behaviors within the micro-structure [72, 73]. In contrast, a monostable system lacks the ability to trap energy. This energy trapping feature is particularly valuable in VSA applications involving explosive movements and shock absorption, where it can create rapid acceleration and enhance safety. Conversely, a monostable mechanical metamaterial shows promise in fields that demand repeated

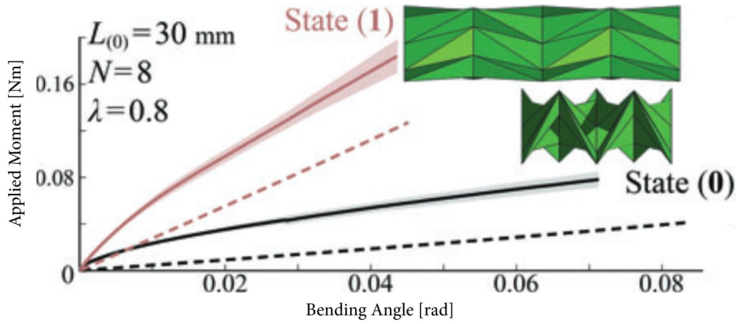

Figure 2.4: Stiffness modulation by mode switching of segments of the Kresling structure as designed by Kaufmann et al. [71].

energy dissipation and shock isolation, exhibiting potential in VSA applications involving cyclic movements and shock absorption. Utilizing a bistable system in cyclic movements would be impractical due to the additional force needed for recovery to the original shape [73]. Second (and very relevant to the thesis subject), bistable FMM is capable of changing its flexural modulus, indicating a rapid switch between two, possibly very different, stiffness settings.

It is even possible to switch from high stiffness states to *near- or fully-zero stiffness* states. It is crucial to note that achieving a fully-zero stiffness response in an elastic structure is only possible when the strain energy redistributes effectively within the structure. This requires a precise balance between the energy released due to negative stiffness and the energy absorbed by positive stiffness [63], termed *static balancing*. Although no FMM exists with fully-zero stiffness characteristics, some FMM structures exist that achieve near-zero stiffness through static-balancing. An example is the monolithic binary stiffness switch by Kuppens et al.[13], which achieves static balancing by adding an elastic structure with negative stiffness in parallel with the functional part that has positive stiffness, see Figure 2.5.

Originally viewed as a undesirable feature, buckling instability exploitation in FMM has been a topic of many research. Some examples that utilize buckling instabilities to achieve multiple stable states are: 1) The *m-bit* by Chen et al.[74], which uses magnetic actuation to switch independently and reversibly between two stable states to range between stiffness and strength. 2) The *monostable mechanical metamaterial with snap-through instabilities composed of multiple magnetic systems* by Tan et al. [72], which was optimized for energy storage and has (minimal) stiffness differences between states. 3) The *monolithic binary stiffness switches* by Kuppens et al. [13], which utilizes negative stiffness to create a near-zero stiffness state and a high stiffness state. 4) The *chiral cylindrical tube* proposed by Wang et al. [75], which enables different stiffness modes by twisting the structure between stable points. 5) The *multistable domed unit cells in a flat plane* by Udani and Arrieta. [76], that use several bistable halve domes in a flat patch to switch between configurations based on the state of the domes. 6) The *bistable, auxetic shape memory elements* by Berwind et al. [58], which has a separate bistable element inside of the compliant unit cell. 7) The *perforated shellular metamaterial class* designed by Shi et al. [77], that exhibit bistability due to elliptical perforation of the shell.

2.3. Potential of Flexible Mechanical Metamaterials in Variable Stiffness Actuators

This section evaluates whether flexible mechanical metamaterials (FMMs) address existing limitations of variable stiffness actuators (VSAs) as identified in Section 2.1. Key limitations include the increased size, weight, and inertia of VSAs compared to traditional stiff actuators. Giraud et al. [15] proposed integrating rigid mechanical structures into an integrated cellular FMM to overcome these challenges.

2.3.1. Assessment of FMMs in VSAs

FMMs vary significantly depending on the intended application. Some can achieve a completely rigid setting, while others cannot [6]. This section highlights features of FMMs beneficial for VSAs, focusing on 1) their capability to mitigate VSA limitations, 2) percentage stiffness change, and 3) potential unintended loss of functionality.

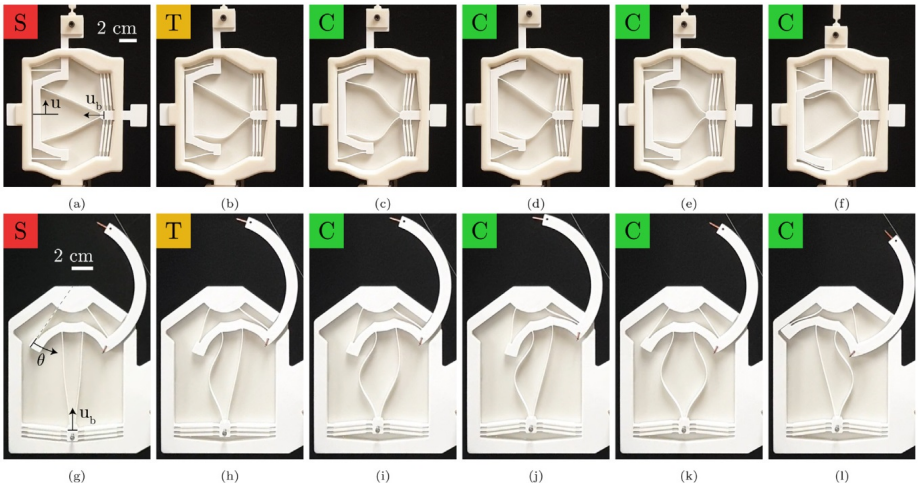

Figure 2.5: Kuppens et al.[13]. show two different configurations, one for a linear device (a-f) and one for a rotary device (g-l). There are three states: a solid and rigid setup marked by the color red (S), a wobbly transition state with the bistable switch flipping shown in yellow (T), and a solid yet flexible arrangement denoted by the color green (C).

Addressing VSA Limitations

Although many novel variable stiffness joints have been developed, most have not been successfully used in applications such as robot arms. This is due to their complex stiffness tuning mechanisms, bulky sizes, non-ideal stiffness curves, and slow response times in stiffness tuning [11]. Integrating complex mechanical components into a monolithic structure, as pioneered by Giraud et al. [15], reduces size, weight, and inertia while minimizing friction and wear, making it easier to achieve a compact and lightweight design [52]. However, this approach is limited by the operational lifespan of compliant mechanisms due to gradual plastic deformation [53]. While some VSAs suffer from application-dependent limitations like inability to design stiffness curves, these cannot be fully addressed using single cell FMMs. Multistable metamaterial that have multiple bistable unit cells, however, allow shifting between several preset stiffness curves, offering a partial solution. Multistability in FMMs also helps overcome the continuous energy requirement of some VSAs by maintaining multiple equilibrium states, though switching between these states requires energy.

Percentage Stiffness Change

FMMs are evaluated based on their stiffness range because this is relevant for many different VSA applications. Since this assessment of FMMs is application-independent, comparing absolute stiffness magnitudes has little meaning. It makes more sense to compare the *percentage stiffness change* in FMMs. This metric can be evaluated without actuator design, as it gives clear insight into the capabilities of the compliant element itself. It should be noted that stiffness is a structural property, this means that the stiffness is dependent on both the geometry of the structure as on the material from which the stiffness is measured. This means that the percentage stiffness change could be significantly different when the material or the arrangement of unit cells is changed [65]. However, the percentage stiffness change still offers insight into the potential of the metamaterial. Quite some recent research focuses on stiffness adaptation in FMMs, revealing that most designed FMMs exhibit significant percentage stiffness changes. This underscores the potential application of FMMs in VSAs. The stiffness range for various FMM unit cells can be found in Table 2.2. Table 2.2 shows the possible percentage decrease in the state of art of FMM.

Potential Loss in Functionality

While FMMs offer integration advantages and potentially enhance VSA functionalities, they must match or exceed the functionalities of traditional VSAs to be viable.Quantifying the loss of functionality is challenging due to the diverse functionalities of VSAs based on their specific use-cases. The only common feature among most traditional VSAs, which seems to be some what application-independent, is their ability to achieve *near- or fully-zero stiffness*, often attributed to internal mechanisms rather than the compliant structure itself. This feature is a crucial safety mechanism for some application, and often found in VSAs

Table 2.2: Percentage stiffness ranges (diff.) of some recently designed FMM. The type of deformation (def.) investigated in the researched is displayed as a B, C, T or Te, representing bending, compression, torsion and tension, respectively.

	[52]	[64]	[78]	[79]	[73]	[13]	[76]	[80]	[71]	[63]	[65]
Diff.	88%	99%	100%	100%	90%	100%	88%	34%	87%	100%	97%
Def.	B	C	C	C	C	C/T	Te	C	B	C	C

that have continuous stiffness modulation and have an application in human-robot interaction. However, in VSA that utilize discrete stiffness switches, such as the DVSA by Hussain et al. [11], this feature might be less feasible.

Some multistable FMMs, such as those by Kuppens et al. [13], achieve near-zero stiffness through static balancing, but rapid changes in stiffness due to load thresholds might be undesirable depending on the application. Some existing FMM eliminate undesired snap-through by utilizing anisotropic multistability to ensure that forces coaxial to the load-bearing axis can hardly trigger snap-through [80]. Sengupta and Li show that careful design can prevent unwanted snap-through and that anisotropic multistable designs allowed controlled stiffness changes.

3

Research Objective and Methodology

3.1. Problem Definition

Traditional robotic actuators lack the versatility that human hands have and are less suited to interact with soft or fragile objects because of it. Alleviating this issue requires inherent adaptable compliance in the actuator, thus many VSAs were developed. However, these VSAs suffer form common limitations such as increased size, weight, inertia, mechanical complexity and slow response time. In addition, many designs require a continuous energy supply to main a desired stiffness.

In recent years, there has been an increasing interest in mechanical metamaterials within the field of mechanical engineering. This has led to the development of advanced materials that combine multiple functions into compact and durable designs. However, the use of these materials in VSGs and VSAs in general is still largely unexplored. In particular, there is a notable absence of VSAs that use bistability—a property allowing materials to switch between two stable states—to efficiently change the actuator's stiffness. This ability could greatly enhance VSA performance, making the actuator lighter and smaller than traditional models, and very energy-efficient in maintaining stiffness. The application of bistable FMM as compliant elements in VSAs will allow for the design of VSAs with discreet stiffness states, that do not require energy to maintain these stiffness states. Despite this potential, no VSA currently exists that uses buckling instability to switch between two distinct states with different internal geometric arrangements, thereby changing the structure's inherent stiffness.

3.2. Research Objective

This thesis aims to address this gap by designing a novel VSG that leverages bistable mechanical metamaterials, enabling rapid switching between two preset inherent torsional stiffnesses due to geometric reorientation of internal structures. These stiffness settings will be structurally stable and will not require energy to maintain. The focus of the research will be on the characterization and optimization of an existing metamaterial for use in a VSG, as well as investigating the feasibility of using bistable FMM in VSAs. By conceptualizing a bistable VSG (B-VSG), the thesis will showcase the potential benefits of integrating these light-weight metamaterials into VSAs, specifically in robotic hands. This approach ensures that the project remains grounded in practical applications, making the outcomes directly relevant to industries where advanced actuation technologies are in demand.

The research objective can be summarized by the following research question:

Research Question

How can **bistability** be exploited to design a **lightweight variable stiffness gripper** that is **energy-efficient while maintaining stiffness**?"

Part II

Actuator Design and Findings

4

Design of Metamaterial

As stated in Chapter 3, the aim of the master thesis is to develop a novel gripper that has two different inherent torsional stiffnesses. This unique feature is due to the underlying bistable metamaterial, which has a different torsional stiffness depending on the state of the structure. The bistable mechanical metamaterial forms the foundation and novelty of the actuator, and should therefore be thoroughly characterized. Given that this research was conducted with limited time, the research was limited to a specific unit cell. This chapter will dive into the metamaterial design and the identification of relevant characteristics of the unit cell (the repetitive building block of the metamaterial).

4.1. Relevant Factors and Background

Although preliminary experiments have confirmed the bistability of the unit cell, its torsional stiffness characteristics and the main factors affecting this stiffness have not been thoroughly investigated. Before diving deep into optimizing the metamaterial for application in the VSG, it is crucial to understand some foundational concepts and explain the reasoning behind the experiments.

4.1.1. Torsional Stiffness Optimization

As explained in Chapter 2, stiffness is a structural property, it depends on the geometry and material of a structure. Changing either of these independent parameters can drastically change the overall stiffness of the structure. A stiffer material that is uniform over the structure will cause the structure to be stiffer, but might hinder bistability, yet making certain sections from a stiffer material might increase stiffness without affecting the bistability characteristics.

When using a torsional spring to transmit force to an object, the magnitude force that is transmitted depends on the stiffness of the torsional spring. Higher stiffness means that a higher force can be transmitted. If the spring is infinitely stiff, this means that the force that is transmitted via the spring is equal to the force applied to the spring by the object supplying the load. Under torsional load, the stiffness function in Equation 2.1 slightly changes. Instead of the axial force, the torque becomes relevant. The torque (τ) is dependent on the deflection angle (ϕ). The k is the tangent torsional stiffness (which becomes $k(\phi)$ for nonlinear springs) and is defined as the derivative of external torque with respect to passive deflection:

$$k(\phi) = \frac{\delta\tau(\phi)}{\delta\phi} \tag{4.1}$$

and the elastic energy stored under torsion is:

$$U(\phi) = \int_{\phi}^{0} \tau(\phi) d\phi, \tag{4.2}$$

where U is the elastic energy stored under torsion.

4.1.2. Bistability

In mechanical stability, a division can be made between simple stable structures, monostable (or self-recovering snapping) structures and bistable (or snapping) structures [70]. The difference between

self-recovering snapping and bistable snapping lies in the strain energy of the system. In bistable elements, the strain energy-displacement curve has a second (local) minimum (the elastic energy well), self-recovering snapping structures lack this local minimum. For this reason, self-recovering snapping structures require energy to maintain the snapped through state, whereas bistable elements only require energy to switch between states.

Bistability indicates that two stable state exist [70]. When the exerted force is larger than the critical buckling load (F_c) the bistable unit cells the force will quickly dip to zero and exhibit a negative force peak, displaying negative stiffness [73]. The point when the force-displacement curve crosses the zero-force line is the point went the strain energy is at its maximum. After the negative force peak, the negative force increases to zero, showing the positive stiffness again and decreasing strain energy. The second stable state of the bistable unit is the point at which the elastic energy is in a local minimum. Indicating that energy is needed to deform from this position. An example of a force-displacements curve and energy-displacement curve for bistable elastic material is illustrated in Figure 2.3

Snap-through is possible when a structure exhibits *negative stiffness* due to deformation. Metamaterials that have negative stiffness features have excellent application in many fields, including energy trapping, cyclic energy absorption and stiffness adaptation [73][80]. In general, the deformation along the applied load direction increases linearly or non-linearly with the load. In metamaterials that have negative stiffness characteristics, an increase in deformation beyond a critical point results in a load drop, usually with snap-through behavior. This snap-though behaviour of material can be divided in snap-through enabling material or self-recovering material, corresponding with bistability and monostability, respectively [73]. In many of the existing multistable mechanical metamaterials, achieving multistable mechanisms involves adjusting the geometric parameters of structures made from a single material. This adjustment aims to generate stiffness mismatches between snapping and supporting (relatively stiffer/thicker) segments [81]. In the case of the unit cell that is under investigation in this research, these stiffness mismatches between snapping and supporting sections would be expressed by ratio $t2/t1$ (see Figure 4.1).

To snap between two stable states, the force acting on a bistable element has to overcome its energy barrier. The energy barrier is defined as the difference in strain energy between local maximum and minimum, these correspond to U_{max} and U_1 in Figure 2.3, respectively. This energy barrier depends on structural forms, geometrical sizes, and material properties. Recently, strain mismatch in composite metamaterials, in contract to structures from a single material, has been investigated to help overcome this energy barrier. Wu et al. [82] suggest that a combination of strain mismatch resulting from material heterogeneity and the use of snap-through bistability strategies holds promise in enhancing the diversity and practical utility of shape transformations. Unlike metamaterials made from a single material, composite metamaterials provide design flexibility, allowing for the creation of more complex functions and smaller structures [83].

4.2. Introduction into the Unit Cell

The purpose of the metamaterial is to be able to switch between two stable states, where each state has a different torsional stiffness. The flexural modulus of bistable elements changes depending on the state in which the elements exist. The shift in flexural modulus causes a stiffness change. This stiffness change can be exploited in a VSA with a discrete stiffness range.

The unit cell examined in this thesis is inspired by the work of Yang and Ma [84]. They propose a innovative two-dimensional (2D) mechanical metamaterial composed of opposing or parallel snapping curved (U-shaped) segments utilizing an elastic snap-through instability mechanism. When subjected to uniaxial loading, these metamaterials experience significant deformation due to a stiffness mismatch between the snapping components (prone to buckling instabilities) and the relatively stiffer and thinner supporting components. By adjusting the geometric parameters, such as the relative thickness of the snapping and supporting segments and the amplitude of the snapping curved segments, nonlinear mechanical responses including self-recovering snapping and multi-stability can be achieved. The 2D structure proposed by Yang and Ma, along with its geometric parameters, is shown in Figure 4.1.

The metamaterial proposed by Yang and Ma is already parameterized by several geometric constraints. The curved features are shaped using a mathematical or trigonometric function ($y = b/2cos(x/a); [0, a]$) to ensure a smooth snap-through transition and maintain symmetrical, stable forms before and after significant

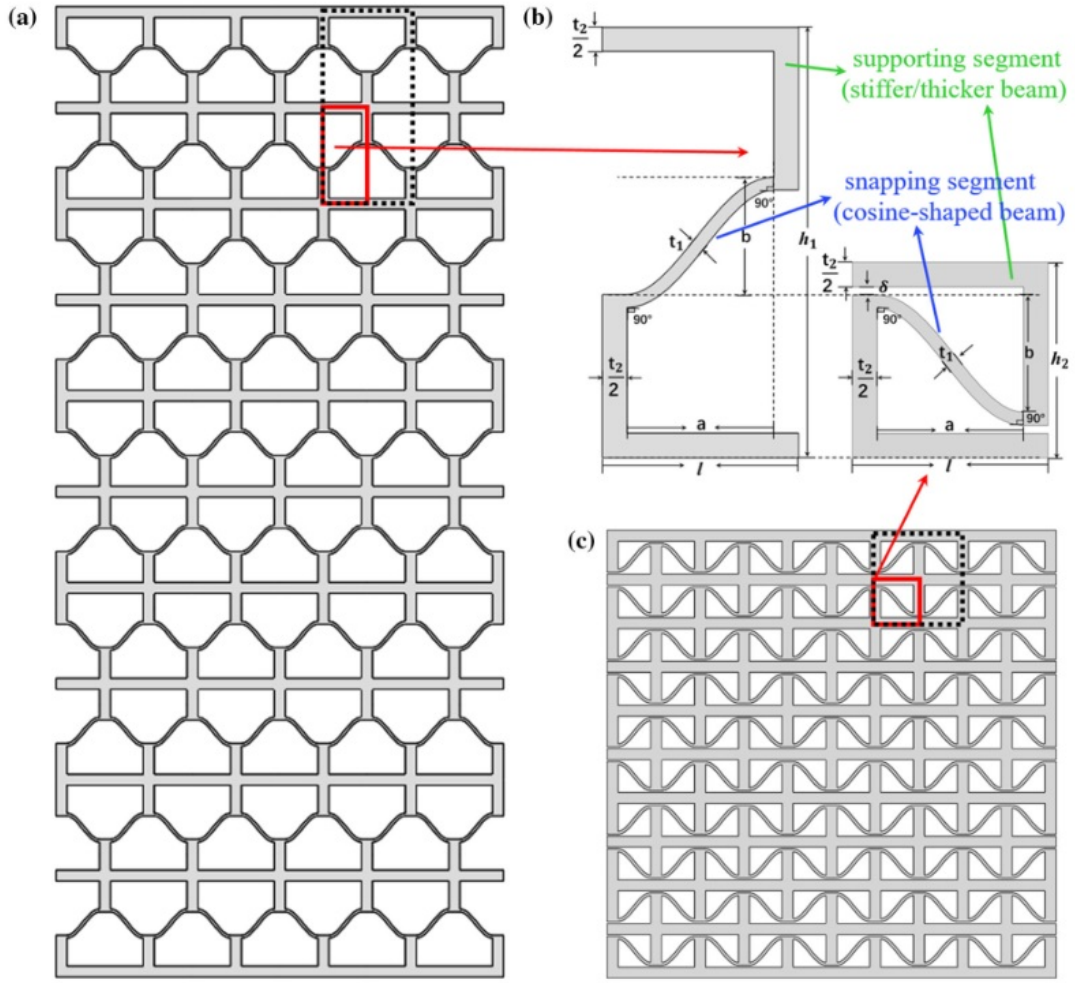

Figure 4.1: Planer mechanical metamaterial containing snapping segments, as proposed by Yang and Ma [84]

deformation. To simplify the number of independent geometric parameters, Yang and Ma defined the geometric parameters in Figure 4.1 as follows: d is set to $\frac{1}{24}l$, $t1$ is $\frac{1}{12}l$, and a is $\frac{3}{4}l$. These values help streamline the design by reducing the complexity of the parameters involved.

Based on the geometry illustrated in Figure 4.1, Yang and Ma designed a cylindrical FMM unit cell in a follow-up research [81], which can be observed in Figure 4.3. This unit cell gets its bistable characteristics from the cosine-shaped beam supported by relatively thinker vertical support beams to impose strain mismatch (see Figure 4.2), similar to the unit cell in Figure 4.1. The deformation under load in the cosine-shaped segment is greater than in the vertical beams supporting this cosine segment. The strain mismatch causes the cosine-shaped beam to snap under load, changing the flexural modulus of the structure.

Yang and Ma found that the stability of this mechanical metamaterial, which features parallel cosine-shaped snapping segments, depends on the thickness ratio between the snapping segments and the supporting segments ($t2/t1$). In addition, the amplitude of the snapping curved segments relative to their length are crucial (b/l). These factors determine whether the metamaterial shows simple stability, monostability or bistability.

Previous research into the cylindrical metamaterial has been limited to axial deformation [81], aimed to investigate the buckling instabilities that make this metamaterial bistable. However, this research will focus on the characterization of this metamaterial under torsional load. This has not yet been investigated, but is crucial information in order to utilize the structure in a VSG that has variable torsional stiffness. The hypothesis is that the torsional stiffness of the unit cell changes depending on the stable state in which the

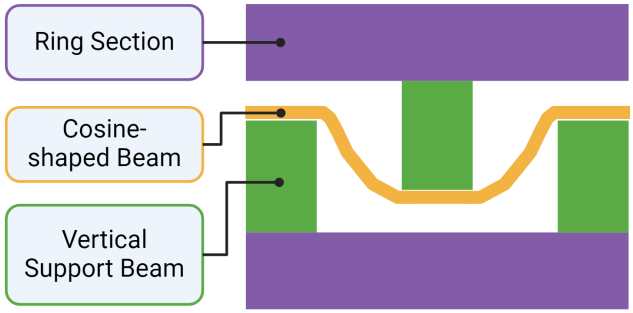

Figure 4.2: Explanation of names used for different sections of the unit cell.

structure resides, see Figure 4.3 for an illustration. The change in stiffness is caused due to geometric reorientation of the beams in the metamaterial. The torsional stiffness of the cylindrical design depends on the deflection of internal bending beams. Changing the state of the cylindrical cell changes the flexural modulus of these internal elements, effectively changing the torsional stiffness of the structure. When this phenomenon is characterized and used as a compliant element in a VSA, the VSA would be classified under *changing physical properties*, a class that currently has minimal designs.

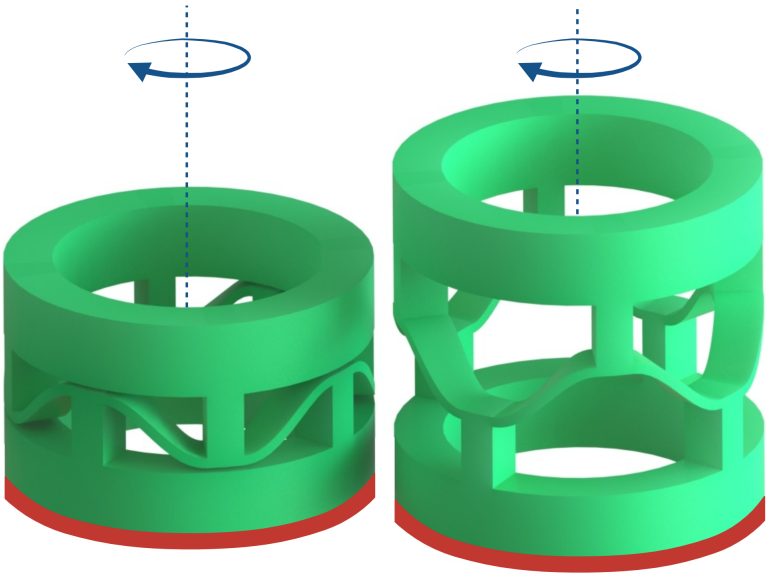

Figure 4.3: The cylindrical unit cell design used in this research. The torsional stiffness of the unit cell in both states will be investigated. The red side of the unit cell is fixed, while the opposite side is rotated. Left: Closed state of the unit cell. Right: Open state of the unit cell

For the planar metamaterial, the stability regions have been characterized in previous research, as can be seen in Figure 4.4. However, the stability regions for the cylindrical structure that is the subject of this research are not yet known. Since this research explores the phenomenon of changing torsional stiffness depending on the stable state of a metamaterial, is it crucial to ensure that parametric ratios b/l and $t2/t1$ remain in the bistable region of stability landscape. For the purpose of this research, the specific boundaries of the bistability region are less relevant, as long as the structure remains bistable. From preliminary experimentation, the observation was made that the sloped border (real blue line) between monostable and bistable in Figure 4.4 translates in the positive $t2/t1$ direction, when the planar unit cell is projected onto a cylindrical surface. However, the specific border has not yet been investigated.

A major difference between the planar structure by Yang and Ma and the cylindrical structure by Yang and Ma is the physical assembly of the unit cells. In the example of the planar structure, the U-shaped beams are actually manufactured as a flat structure and manually forced in the cosine shape during assembly of the unit cell. This assembly process causes stresses to exist in either open or closed state, since the rest state of the U-shaped section is actually flat. On the other hand, the cylindrical structure is manufactured as either open or closed. This manufacturing process causes different prestresses in the unit cell than manually forcing a flat structure in a cosine shape. This difference is likely related to the change in stability.

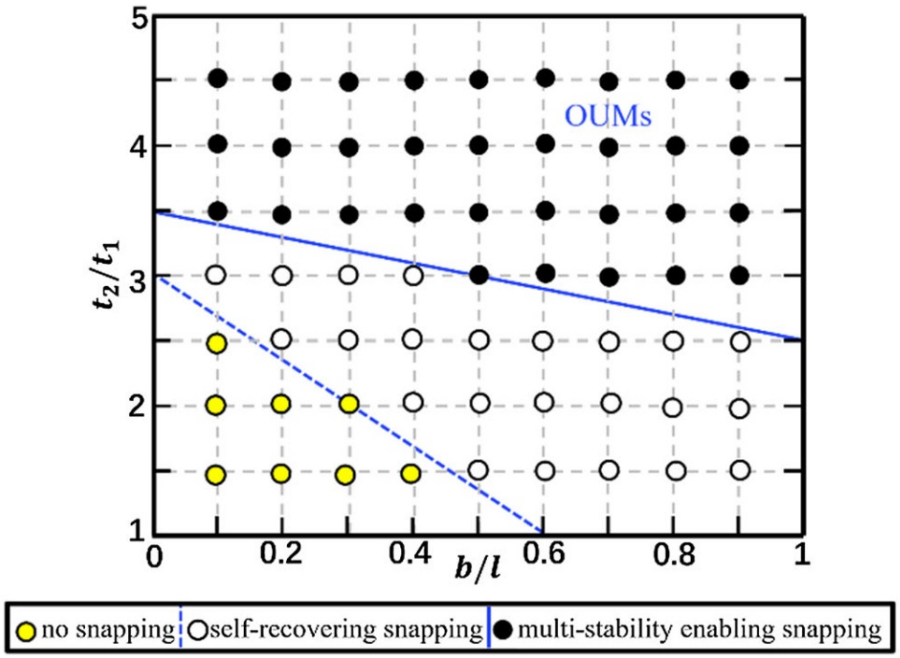

Figure 4.4: The stability region as presented by Yang and Ma [84]. The yellow dots represent measured data points that lie in the region that showed simple stability characteristics. The white dots represent measured data points that lie in the region that showed monostability characteristics. The black dots represent measured data points that lie in the region that showed simple stability characteristics. The real and dashed blue lines indicate the borders between the regions.

Axial-torsional Coupling

For the experiments, it is evident that the unit cell exhibits coupling behaviour between angular displacement and axial displacement. Whenever torsion is applied to the structure, the structure deforms axially also. The direction of the axial deformation depends on the state of the cell. This coupling between load can be caused by (a combination of) several different effects: 1) The unit cell behaves as an anisotropic structure. Meaning that the relation between applied force and resulting displacement are dependent on the direction of the load. 2) The complex structure of the unit cell. 3) The auxetic behaviour of the unit cell. When the vertical support beams of the structure are infinitely stiff, the Poisson ratio will be zero. However, due flexion of the vertical beams in the normal direction to the cylindrical surface of the unit cell when the structure is snapped from closed to open, the Poisson ratio is slightly negative. The Poisson ratio is depending on the compliance of the vertical support beams.

Because of this coupling, it is crucial to investigate the effects it might have on the stability in both states of the bistable cell. The stability of the bistable cell is a crucial factor for application in a VSA. The actuator should operate without changing stiffness unreliably and only when intended. In particular, the structure should not snap due to load on the end effector, as the VSA should not change its stiffness due to external stimuli. Because of this it is important to make the structure as stable as possible in both states.

4.3. Characterization of the Bistable Cell

As explained there are two very relevant factors when applying metamaterial in a VSG, torsional stiffness and bistability. Torsional stiffness is relevant because the difference in torsional stiffness between the two stable states is the fundamental principle by which the VSG will operate, and without bistability this effect will not be present. Additionally, without controlled snap-through, the VSM (the metamaterial), will not be suited for application in a VSG.

In the analysis of the bistable cell, the torsional stiffness should be characterized and the stability should be analysed. The torsional stiffness is dependent on the geometry and material in the bistable cell. Therefore, the characterization should focus on changing these systematically to investigate the effects. The coupling between axial and angular deformation is caused by the internal structure of the unit cell, which will not be changed in the scope of this research. However, the prestress in the structure caused by manufacturing of the unit cell seems to have an effect on the force required for snap-through. This indicates that the stability can be influenced by different manufacturing methods.

The characterization of the unit cell is performed with three questions in mind:

- How does changing certain geometric ratios of the unit cell affect the (percentage) torsional stiffness difference between the open and closed state of the unit cell?
- How does changing the material of certain sections of the unit cell affect the (percentage) torsional stiffness difference between the open and closed state of the unit cell?
- How does the manufacturing state influence the bistability of the unit cell?

The stiffness difference and percentage stiffness difference are both very relevant metrics for the design of the VSG because these metrics give insight in different topics. As previously explained in Chapter 2, the percentage stiffness difference ($\Delta\%k$) gives insight into the application potential of a VSA. By changing the material of the entire unit cell, it can become stiffer, but the $\Delta\%k$ remains the same. The $\Delta\%k$ shows a material-independent effect for a structure that is made from uniform material. However, this research limits itself to the use of PLA and two different thermoplastic elastomers (TPEs), therefore potentially limiting the stiffness increase that changing the material can cause. Therefore, it is also important to consider the absolute value of stiffness difference to make a qualitative statement regarding the application possibilities. While the stiffness difference (Δk) and $\Delta\%k$ are very important metrics, it is crucial that the bistability of the unit cell is not lost due to optimizing for the stiffness difference. Different simulations and experiments are performed with the mentioned characterization goals in mind.

5

Design of the Bistable Variable Stiffness Gripper (B-VSG)

In this chapter, a novel variable stiffness gripper using bistable metamaterials (B-VSG) is introduced. The design centers around the innovative application of bistable unit cells, which fundamentally alter the actuator's stiffness properties. This allows the robotic gripper to switch between distinct stiffness states, enhancing its adaptability and functionality in varying operational contexts. The metamaterial serves both as a compliant element and an integrated VSM, positioning the B-VSG as a cutting-edge solution in robotic manipulation.

5.1. Working Principle and Application Considerations

Before diving into a design for such an actuator, it is important to zoom in on the fundamental mechanism that underlies the stiffness change (i.e. the bistable unit cell) and address some design challenges. As formulated in the research question, this research aims to design a novel type of VSG using bistable metamaterial. This metamaterial is used as a complaint element and integrated VSM for application in the robot gripper.

Using a bistable VSM (i.e. the bistable metamaterial) in the VSG results in a discreet VSG design, where the gripper has two or more distinct inherent stiffnesses it can switch between. The change in inherent stiffness of the actuator, by switching between stable states of the metamaterial, should be sufficiently large to ensure practical application. In addition, the stiffness difference should be comparable to existing VSAs that are based on a similar principle or were designed for a similar purpose. From the literature review in Chapter 2, it is clear that VSA performance is application-dependent and comparing between designs is difficult. Therefore, the performance of the B-VSG should be compared to VSAs that are designed with similar purposes in mind and are based on a similar principle. Two examples from literature are the D-VSA by Hussain et al.[11], which is a VSA that uses a clutching mechanism and was designed to improve the response time of VSAs, and the F-VSA by Giraud et al.[15], which uses preloading of metamaterial to modulate the inherent stiffness of the actuator and was aimed to solve size, weight and inertia limitations. Although the D-VSA and F-VSA are not grippers, the designs were both developed to solve the limitations that are addressed in this research also, and share commonalities with a VSG design based on bistable metamaterial.

For this actuator to utilize a bistable structure, the structure should be able to snap freely. However, when the bistable unit cell snaps from its open state to its closed state (and vise versa), the total length of the metamaterial changes, A varying length due to the bistability increases the complexity of the actuator, and limits the application possibilities greatly. Therefore, the metamaterial should remain at a constant length during stiffness change.

In order to ensure constant length, multiple bistable cells are used in series. The outer surfaces of the metamaterial can be connected to an end effector or fixed object, and one of the middle sections can be snapped back and forth. This results in a metamaterial that has bistable unit cells with inverse states. As can be viewed in the example structure in Figure 5.1.

The transmission, compliant elements and clutching mechanism, that are part of the VSM, are all integrated in the metamaterial, essentially forming a certain number of virtual torsional springs that can

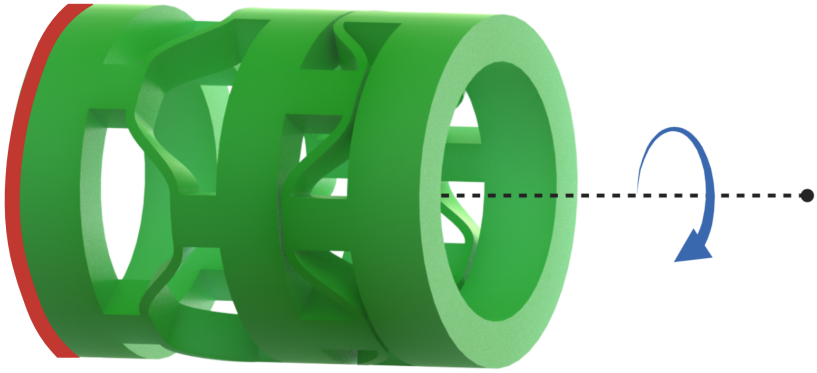

Figure 5.1: Example of a multi-cell metamaterial, where certain cells are in the open state and certain cells are in the closed state. The total length of the structure is constant. The red side of the metamaterial is fixed, while the opposite side is rotated.

be involved or excluded by snap-through. When the metamaterial snaps from one state to another, the geometry changes. This changing geometry results in a change in the flexural modulus of the internal sections. Since the overall torsional stiffness depends on the flexural modulus of these section, the overall torsional stiffness changes also. In this chapter, several different aspects of the VSG design will be discussed in detail.

5.2. Design Considerations

This section systematically addresses the design considerations for developing a Bistable Variable Stiffness Gripper (B-VSG), utilizing bistable metamaterials. Initially, the design process evaluates the fundamental unit—the metamaterial—whose properties critically influence the actuator's stiffness variability. The effects of serially stacked unit cells on the overall stiffness characteristics is explored, emphasizing the need for maintaining a constant structural length during operation to ensure practical applicability and seamless integration into robotic systems. Additionally, several actuator configurations and multiple requirements for the actuation unit that modulates the inherent stiffness are discussed.

5.2.1. Design Requirements, Specifications and Constraints

As mentioned in Chapter 2, VSA performance and designs are highly dependent on the indented application. Because the B-VSG is not designed with a specific application in mind, the requirement are less specific. Based on the working principle and application considerations, several design requirements, specifications and constraints are formulated:

Requirements

- The VSG should be able to switch between two different stiffness settings using snap-through of the metamaterial.
- The VSG should require no energy to maintain a stiffness setting.
- The change in inherent stiffness of the actuator, by switching between stable states of the metamaterial, should be sufficiently large to ensure practical application.
- The stiffness difference should be comparable to existing VSAs that are based on a similar principle or were designed for a similar purpose.

Specifications

- The metamaterial in the VSG is based on the cylindrical metamaterial by Yang and Ma [81].
- The structure should be able to snap freely to realise rapid stiffness change.

Constraints

- The total length of the metamaterial in the VSG should remain constant.
- The transmission, compliant elements, and clutching mechanism, that are part of the VSM, are all integrated in the metamaterial to reduce size, weight, and mechanical trading complexity.

5.2.2. Metamaterial Design

Given the fact that the number of cells should be at least equal to two for the structure to be bistable with constant length, the first step in optimizing the design is to establish the constraint of the number of unit cells in the metamaterial. In this case, a single cylindrical bistable structure is regarded as a single unit cell.

The difference in stiffness for a single bistable unit cell is equal to the magnitude of the difference between the stiffness in the open state and the difference in the closed state, expressed in Equation 5.2a. When the structure is expanded to two bistable cells stacked in series, the expression for the stiffness difference changes. The equation for the overall stiffness of two torsional springs connected in series is given in Equation 5.1.

Using Equation 5.1, the stiffness difference for a metamaterial that has two bistable cells and two different states is expressed in Equation 5.2b. The geometric parameter b (see Figure 4.1) of both cells has to be equal in order to achieve a bistable structure when the two outer edges are fixed. This geometric interdependency of both unit cells greatly limits the achievable stiffness difference.

$$\sum k = \frac{1}{\frac{1}{k_1} + \frac{1}{k_2}} \tag{5.1}$$

Further increasing the number of cells to a total of three results in a stiffness difference observable in Equation 5.2c. To ensure the bistability of the structure, the geometric parameter b (the amplitude of the cosine-shaped section) of one of the cells has to be equal to the sum of b of the other two cells. The two smaller cells have an coupled state, meaning that they are either both open or both closed. A big advantage of this structure is that the geometries within the structure differ greatly, this can be exploited to increase the stiffness difference.

$$\Delta k_{i=1} = |k_O - k_C| \tag{5.2a}$$

$$\Delta k_{i=2} = \left| \frac{1}{\frac{1}{k_{1,O}} + \frac{1}{k_{2,C}}} - \frac{1}{\frac{1}{k_{1,C}} + \frac{1}{k_{2,O}}} \right| \tag{5.2b}$$

$$\Delta k_{i=3} = \left| \frac{1}{\frac{1}{k_{1,O}} + \frac{1}{k_{2,C}} + \frac{1}{k_{3,C}}} - \frac{1}{\frac{1}{k_{1,C}} + \frac{1}{k_{2,O}} + \frac{1}{k_{3,O}}} \right|, \tag{5.2c}$$

where i describes the number of bistable cells, and O and C describe the state of the cell (Open or Closed). k_1, k_2, and k_3 shows the index of the bistable cell in the metamaterial.

From Equations 5.2, it should be noted that the largest stiffness difference is achieved when only a single bistable cell is used. However, using a single bistable cell is not feasible given the constraint of constant length of the structure.

Important to consider is that when the stacked unit cells have the same stiffnesses (i.e. $k_{1,O} = k_{2,O}$ and $k_{1,C} = k_{2,C}$), the stiffness difference between the two open states is equal to zero. This is shown by the expression in Equation 5.3. Because of this, the selected metamaterial for the actuator is the metamaterial made from three stacked bistable unit cells.

$$\Delta k_{i=2} = \left| \frac{1}{\frac{1}{k_{1,O}}} + \frac{1}{\frac{1}{k_{2,C}}} - \frac{1}{\frac{1}{k_{1,C}} + \frac{1}{k_{2,O}}} \right| \tag{5.3a}$$

$$\Delta k_{i=2} = 0 \tag{5.3b}$$

As mentioned before, the three-celled metamaterial has to have two cells whose summed amplitude of the cosine-shaped sections (b_s) is equal to the amplitude of the cosine-shaped section of the third cell (b_l) and have coupled state in order to maintain bistability. The stiffness difference of the three-celled structure will be less then the stiffness difference of a single bistable cell. However, the stiffness difference of the single bistable cell can be approached by making certain cells in the three-celled structure more rigid. For the sake of simplicity, the two coupled cells will be assumed to have equal stiffness in open and closed state and have equal b. This results in a stiffness difference expressed in Equation 5.4. Two possible examples of the metamaterial are illustrated in Figure 5.2.

$$\Delta k_{i=3} = \left| \frac{1}{\frac{1}{k_{1,O}} + 2\frac{1}{k_{2,C}}} - \frac{1}{\frac{1}{k_{1,C}} + 2\frac{1}{k_{2,O}}} \right| \tag{5.4}$$

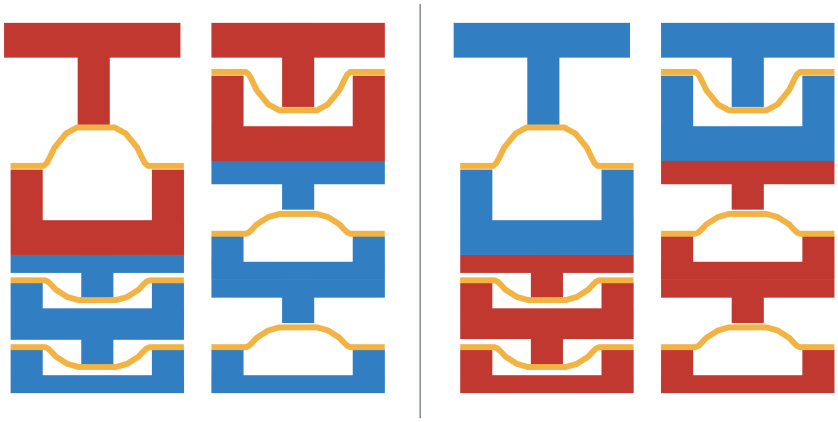

Figure 5.2: Two possible configurations of the three-celled metamaterial, where blue indicates stiffer cells and red indicates compliant cells. Left: The larger cell is compliant and the smaller cells are stiff. Right: The larger cell is stiff and the smaller cells are compliant

In Equations 5.5, the limits of the stiffness difference are investigated. The limits are systematically investigated by increasing certain stiffnesses to infinity, effectively making these states infinitely rigid, and decreasing certain stiffnesses to zero, effectively making these states infinitely compliant. With this analysis, both the effects of increasing the stiffness difference between two states of a single cell as well as the effects of increasing the stiffness between cells is under investigation. These limits show that the theoretical maximum stiffness difference in the three-celled structure is equal to the stiffness difference of a single bistable cell (see Equation 5.2a), and occurs when the stiffnesses of the two equal cells in the structure approach infinity. From Equation 5.5e, it can be concluded that the both the compliant and stiff state of the two equal bistable cells in the structure should be as stiff as possible.

$$\lim_{k_{1,O}\to 0} \lim_{k_{1,C}\to 0} \Delta k_{i=3} = 0 \tag{5.5a}$$

$$\lim_{k_{1,O}\to \infty} \lim_{k_{1,C}\to \infty} \Delta k_{i=3} = \frac{1}{2} \left| k_{2,O} - k_{2,C} \right| \tag{5.5b}$$

$$\lim_{k_{1,O}\to 0} \lim_{k_{1,C}\to 0} \Delta k_{i=3} = \frac{k_{2,C}}{2} \tag{5.5c}$$

$$\lim_{k_{2,O}\to 0} \lim_{k_{2,C}\to 0} \Delta k_{i=3} = 0 \tag{5.5d}$$

$$\lim_{k_{2,O}\to \infty} \lim_{k_{2,C}\to \infty} \Delta k_{i=3} = \left| k_{1,O} - k_{1,C} \right| \tag{5.5e}$$

$$\lim_{k_{2,O}\to \infty} \lim_{k_{2,C}\to 0} \Delta k_{i=3} = k_{1,C} \tag{5.5f}$$

5.2.3. Actuator Configuration

In Chapter 2, existing VSAs were classified based on the arrangement of essential components in the actuator. This classification is selected, because the focus of the thesis lies on the application of a novel compliant element, the bistable metamaterial, in a VSG. As previously explained, this classification holds two classes: the series approach and the antagonistic approach.

The antagonistic approach is based on the principle behind muscles, where activating flexor or extensor muscles separately changes the angle of a joint, and activating them simultaneously increases the stiffness of the joint. VSAs belonging to this class are based on preloading nonlinear springs and the stiffness change is coupled to the position of the end effector.

The stiffness changing mechanisms behind the VSA under development in this research is not based on preloading nonlinear springs, but rather belongs to the class of changing physical properties. A class that belongs to the ”series approach” according to the classification in Chapter 2.

However, the internal configuration of the actuation units and metamaterial can be in parallel or in series. To prevent confusion, lets classify the following actuator configuration based on the internal arrangement of the actuation units and the metamaterial. The two possible arrangements are: the *parallel configuration* and the *series configuration*.

In order to fully understand these two configurations, it is important to clearly define series and parallel configurations. Following the generally acknowledged definition of series and parallel in mechanical systems [85], a configuration is categorized as series if the movement of the output link is a result of combining the movements of two elements. Alternatively, a configuration is classified as parallel if the torque on the output link is the combined sum of the torques from the two elements.

Parallel configuration

An inherent advantage of parallel configurations is improved stability. However, in choosing the configuration, there exists a trade-off between range of motion and number of actuation units. In the parallel configuration, there exist two possible configuration. A schematic of these configurations is shown in Figure 5.3.

- **Motor in parallel to metamaterial**: The actuation unit (motor) that drives the rotation of the end effector is in parallel to the metamaterial and connected to the end effector via another metamaterial. This configuration requires two actuation units in total, one to drive the rotation of the end effector and one to switch between stiffness states of the metamaterials. A downside of this configuration is the limited range of motion. The metamaterial is rigidly connected at one end, limiting the total range of motion of the end effector to the internal range of motion of the metamaterial.
- **Two motors in parallel**: Two actuation units (motor) are connected in parallel to the end effector via metamaterials. The position of the end effector is dependent on the movement of both actuation unit, whose rotation should be equal but opposite. This configuration requires three actuation units in total, two to move the end effector and one to switch the stiffness of the metamaterials. An advantages of this configuration is a larger range of motion of the end effector. A notable downside of this configuration in the large number of actuation units required to control this VSA.

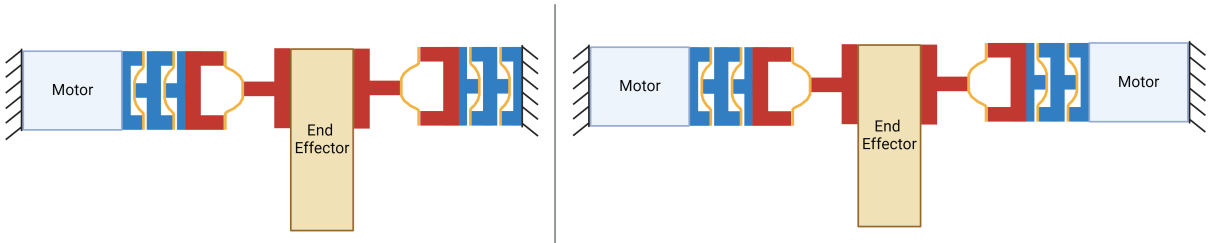

a) Servomotor in parallel to metamaterial

b) Two servomotors in parallel

Figure 5.3: Schematic drawing for two different parallel actuator configurations.

Series approach
In the series approach, the actuation unit (motor) that drives the rotation of the end effector will be connected to the end effector via the metamaterial. This metamaterial is in series to the actuation unit that drives the end effector. In the series approach, two actuation units are required, one to control the position of the end effector and one to control the stiffness state of the metamaterial. The range of motion of the end effector is limited by the range of motion of the motor. Advantages of the series configuration over the parallel configurations are the small number of required actuation unit and the large range of motion. A schematic drawing of the series configuration can be observed in Figure 5.4.

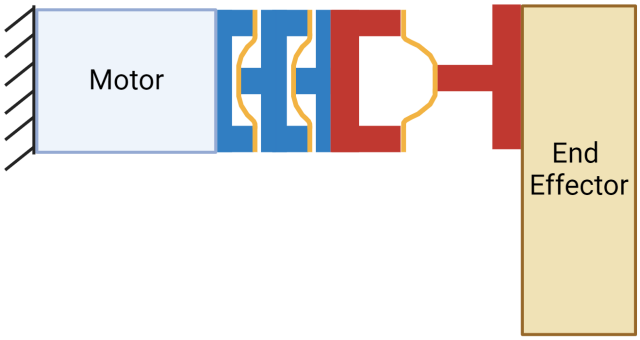

Figure 5.4: Schematic drawing of actuator in series configuration.

Choice of Actuator Configuration in the VSG
After evaluating both the parallel and series configurations, the *series configuration* is chosen for its simplicity and enhanced flexibility. This setup requires just two actuation units: one to manage the position of the end effector and another to adjust the metamaterial stiffness. This is fewer than required for the parallel configurations, simplifying the design and reducing maintenance and costs.

The series configuration allows full use of the motor's range of motion, providing greater flexibility, especially useful in applications like robotic hands or grippers (such as the B-VSG). This straightforward configuration reduces mechanical complexity, making it a reliable and efficient choice. The deduces mechanical complexity is also in accordance with the design requirements. Consequently, the series configuration is preferred for its simpler design, improved motion range, and operational efficiency.

5.2.4. Actuation Units
As mentioned, two different types of actuation units need to be present in the metamaterial, one to change the position of the end effector and one to change the stiffness. The actuation unit used to change the position of the end effector has to be a motor. The requirements of this motor highly depends on the application of the VSA. Some application require more torque, others require a low energy consumption.

In general, requirements are difficult to set when there is no application in mind. Because of this, there are no real requirements to the motor that drives the end effector, besides it having enough power to deform the compliant element. In addition, the motor should be as small as possible and have as low a mass as possible, not to counteract the advantages of the metamaterial. Since the motor that drives the end effector is not novel, it will not be considered further during the design process.

The actuation mechanism to change the stiffness of the metamaterial is part of the novelty of this research and will be considered during the design process because of this reason. Main requirements of the actuation unit that controls the stiffness are:

- **Force Requirement**: The actuation unit should be able to generate enough force to induce a snap-through of the metamaterial.
- **Back-drivability**: The structure should be able to snap-through and snap-back. The actuation

unit should be back-drivable in the sense that the snapping section should be moved in opposite directions.

- **Rapid movement**: One of the advantages of utilizing a structure with negative stiffness characteristics is it capability to switch rapidly between stable states. If the actuation method is not able to move rapidly as well, this advantage of the bistable mechanism will be lost.
- **Small size**: An advantage of using metamaterial as a compliant element is its inherent possibility to make integrated structures. This drastically reduces the size of a mechanisms when compared to traditional mechanisms. The actuation unit should be small, not to counteract the size advantage of the metamaterial
- **Low mass**: The integrated structure of the metamaterial reduces the weight also. Therefore, the actuation unit responsible for the stiffness change should be light weight.

After careful consideration **pneumatic actuation** is selected because of its fast response time, low specific weight and high power rate (torque-squared to inertia ratio) [86]. Other advantages of pneumatic actuation are its low cost, ease of implementation and easy fabrication (molding and 3D printing) [87].

Since the purpose of the pneumatic actuator is to induce snap-through in the metamaterial, which requires linear motion, the pneumatic actuator needs to be a *linear pneumatic actuator*. Different designs of linear pneumatic actuators exists. For instance, a soft pneumatic actuator can be fabricated, see Figure B.7a, that acts like a linearly expanding balloon using a custom mold design and silicone such as Ecoflex (see Figure B.7b). Another example is a *linear piston air pump*, which can be manufactured using AM techniques.

For this research it is decided to use an off-the-shelf miniature piston. This is decided because the miniature piston is freely available and cheap, also the novelty of the VSA does not lies in the piston design, but rather in the use of bistable metamaterial. The piston is internally connected to the metamaterial, see Figure 5.5.

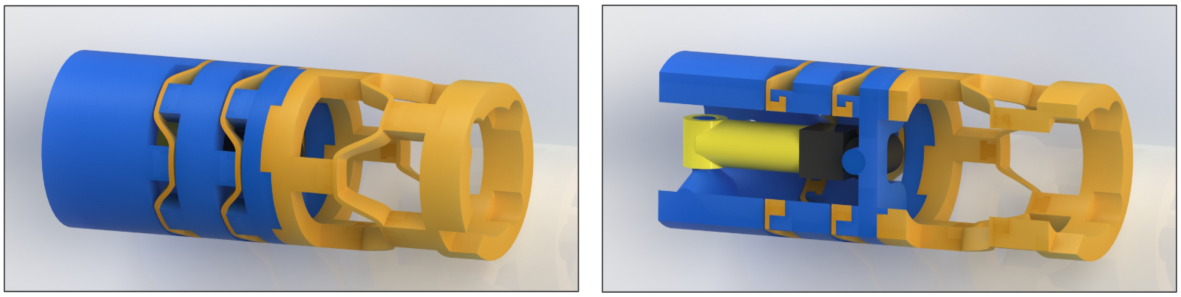

Figure 5.5: The three-cell metamaterial with the internally mounted linear pneumatic actuator.

5.3. Bistable Variable Stiffness Gripper Concepts

As explained, two types of actuation units should be present in the B-VSG, one actuation unit to modulate the stiffness and one actuation unit to control the position of the end-effector. The stroke length of the piston should be equal to twice the amplitude of the cosine-shaped beam (or $2b$) in order for the mechanism to be bistable. Since this research does not focus on designing a custom piston, the stroke length of the piston will form a constraint on the design of the metamaterial. Because the amplitude of the cosine-shaped beam is dependent on the stroke length of the piston, the stiffness change in the actuator could be less than optimal.

Given the fact that the developed B-VSG functions as a demonstrator of the application of bistable metamaterials in robotic hand design. Two different design concepts will be showcased.

5.3.1. Concept 1: The Actuated Design

The first concept will show a bistable gripper with a single metamaterial which inherent stiffness is modulated using the pneumatic actuator. This concept is named the *actuated design*. This concept is meant to

showcase the practicality and reliability of the actuation mechanism. In this concept, the amplitude of the cosine-shaped beam is dependent on the stroke length of a selected off-the-shelve piston. Additionally, some performance measurements will be conducted on this prototype. The first concept is illustrated in Figure 5.6a. The actuated design will serve as a *proof-of-concept* of the pneumatic actuation method.

5.3.2. Concept 2: The Unactuated Design

In the second design, see Figure 5.6b, the pneumatic actuator is omitted to improve the design freedom and a second moving end-effector is incorporated in the design. This concept is named the *unactuated design*. These choices were made to potentially increase the stiffness change in the actuator. This concept will be developed further and mounted to a robot arm to showcase application potential.

In the second design, there will be space reserved for (future) custom pneumatic actuators, which can modulate the stiffness. Ideally, these pistons will be integrated in the design of the metamaterial. The stroke length of these pistons will be dependent on the chosen amplitude of the cosine-shaped beam, instead of forming a design constraint on the metamaterial geometry. This B-VSG will form a stepping stone for further development of the actuator.

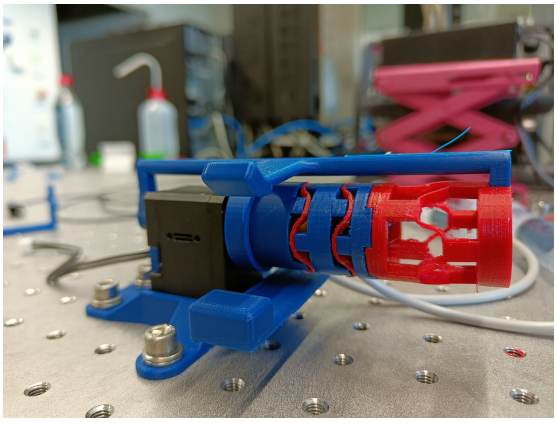

(a) Gripper design with actuation unit to change the stiffness

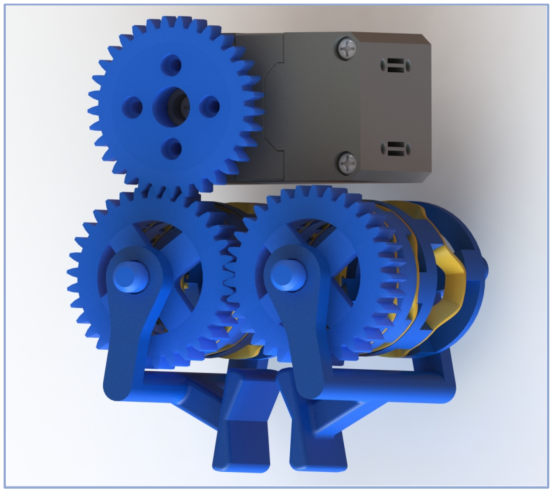

(b) Gripper design with two metamaterials and without actuated stiffness modulation

Figure 5.6: Two different concepts for the B-VSG

5.3.3. Commonalities between the Concepts

Both design concepts are based on a similar principle and therefore share some commonalities in the designs. In both designs, the used actuator configuration in the gripper is that of a *series configuration*. The servomotor is attached to the metamaterial, which in turn is attached to the end effector. Additionally, both concepts are *angular grippers*. Another commonality between the two design concepts is that the position of the end effector is controlled using the servomotor. The input for the system is a goal angle, where the end effector is moved to using a constant velocity.

5.3.4. Differences between the Concepts

The actuated design concept serves as a proof-of-concept of a simplified bistable variable stiffness gripper that uses pneumatic actuation to modulate its inherent stiffness. It aims to explore a method of actuating the stiffness changing in the metamaterial. On the other hand, the unactuated concept is less constrained and disregards the pneumatic actuator, but focuses more on optimizing the metamaterial and improving application. There are two notable design differences between the actuated and unactuated design concept:

- **Control of Stiffness**: The stiffness in the actuated concept is controlled using a miniature off-the-shelve piston. Figure 5.5 shows how the piston interacts with the structure. The two outer edges of the metamaterial are constrained, and only the internal structure is free to deform or move. Two

syringes were connected to the piston, one to each of the in- /outlets of the piston, see Figure B.11. Effectively snapping the structure from one state to the other by applying pressure to the piston. This control strategy simplifies the stiffness control to controlling a single linear pneumatic actuator. However, in this concept the stroke length of the piston dictates the amplitude of the cosine-shaped beam and Therefore constraints the design. In the unactuated concept, the stiffness actuation unit is omitted. This alleviates the design constraint introduced by the fixed stroke length of the piston.

- **Number of Metamaterials in the Design**: In the unactuated design, there are two moving end-effector, each with a separate metamaterial that acts as its VSM. This allows for a higher difference in stiffness acted on the object that is gripped, because both arms can be either compliant or stiffer. This is in contrast to the actuated design concept, which has one moving compliant (or slightly stiffer) gripper finger complemented by a rigid, stationary gripper finger.

5.4. Final Design of B-VSG

As explained in Section 5.3, the *unactuated design* concept will be developed further into a final design, which aims to showcase the possibilities of bistable metamaterials in versatile robotic hand design. This design has been chosen because it allows for optimization of the VSM by disregarding the actuation unit for stiffness regulation, as a custom pneumatic actuator can be easily implemented in future work.

The basic design of the B-VSA is visible in Figure 5.7. The angular gripper fingers from the previous design, see Figure 5.6b, have been replaced by a *parallel gripper design*. This alteration is made to improve the grasping of the gripper on different objects. The parallel grasping is realised by using a parallelogram structure in the gripper arm design, which ensures that contact surface of the gripper finger is always vertical. The range of the parallel gripper design is 35mm, meaning that the maximum width of the objects the gripper can grasp is equal to 35mm.

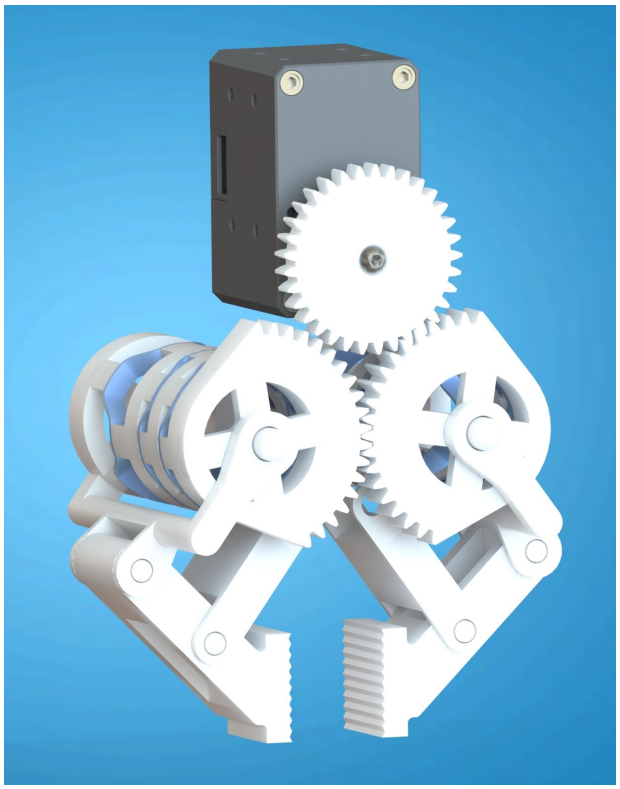

Figure 5.7: Basic design of parallel variable stiffness gripper.

The variable stiffness of the actuator is realized by using a bistable metamaterial. Essentially, the metamaterial integrates two different virtual torsional springs, a clutching mechanisms and transmission into a single structure. By snapping the metamaterial through and back, the inherent torsional stiffness of the actuator rapidly changes. Because the metamaterial is structurally bistable, the actuator does not

require energy to maintain either of the two states. This results no energy requirement to main the inherent torsional stiffness of the actuator in either of the two stiffness settings. Because this actuator relies on rapid stiffness change between two different stiffnesses, the actuator has a discreet stiffness profile.

The metamaterial that forms the VSM inside of the gripper is created using pressure-fitting mechanical interlocks, where different material sections are joint together. The cosine-shaped sections are fabricated from FilaFlexible40 at a 40% infill, the vertical support beams and ring sections are made from generic PLA at an infill of 90%. The metamaterial is created from three stacked bistable cells, where two cell have a coupled state (they are both open or both closed). The summed amplitudes of the cosine shaped beams of the coupled cells are equal to the amplitude of the cosine-shaped beam of the third cell ($2b_s = b_l$). The geometric ratios are as follow: $t2/t1$ is equal to 6 in all bistable unit cells that made up the three-celled metamaterial, $b_l/l = 0.625$ and $b_s = \frac{b_l}{2}$. Inside of the metamaterial, there is enough space for future placement of custom pneumatic actuators, which will function similar to the actuated prototype. The metamaterial used in the B-VSG is illustrated in Figure 5.8

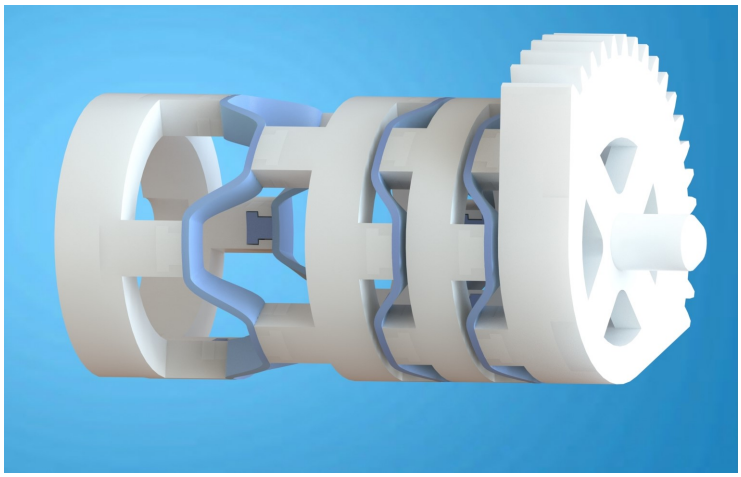

Figure 5.8: Metamaterial used as the variable stiffness mechanism in the B-VSG. The white sections are made from PLA and the blue sections are fabricated using FilaFlexible40.

Assembly of the B-VSG is straightforward thanks to snap-fit connections, allowing quick and tool-free assembly right after printing. Its rotating components are designed to operate freely without the need for bearings, simplifying the manufacturing and assembly process. Only the actuation unit, which positions the end effectors, requires a single Allen wrench for internal mounting.

The gearing system aimed to connect a servomotor (Dynamixel XM430-W210-R) to the end-effectors is carefully designed for the B-VSG. The reference diameter of the gear that is connected to the servomotor is 33mm, and the reference diameter of the gears connected to the metamaterial are 42mm. This gear ratio is not selected because of velocity or torque requirements, but rather because these reference diameters allowed for the smallest actuator design. Additionally, the gear design includes a built-in safety feature. When the gripper fingers are fully extended, the gears linked to the metamaterial reach a point where they cannot be turned any further by the gear connected to the servomotor. If the servomotor mistakenly attempts to continue rotating the metamaterial beyond this point, the flexibility built into the metamaterial and the custom gear design serves as a mechanical stop. This means the gears stay locked in their maximum open position. This safety mechanism prevents the servomotor from accidentally causing damage by over-rotating the gripper arms.

The B-VSG is designed to be mounted to a robot arm, as can been seen in Figure 5.9, which ensures its practical application. The B-VSG is able to grasp objects with a soft or harder grip, by changing the torsional stiffness of its compliant element. The gripper fingers of the B-VSG are aligned with the central axis of the flange of the robot arm.

The B-VSG is specifically designed to be small and light-weight, properties that are often limitations in the current state-of-the-art of VSAs but very important factors in robotic hand design. All components of the actuators, besides the servomotor, are made using PLA or FilaFlexible, making the overall design very

light-weight. The housing of the B-VSG has a honeycomb pattern to reduce the weight of the gripper. The total mass of the B-VSG, including servomotor, is 189 grams (weight of servomotor is 86 grams). The maximum height (closed grippers), width (open grippers) and length of the actuator are 138mm by 105mm by 78mm.

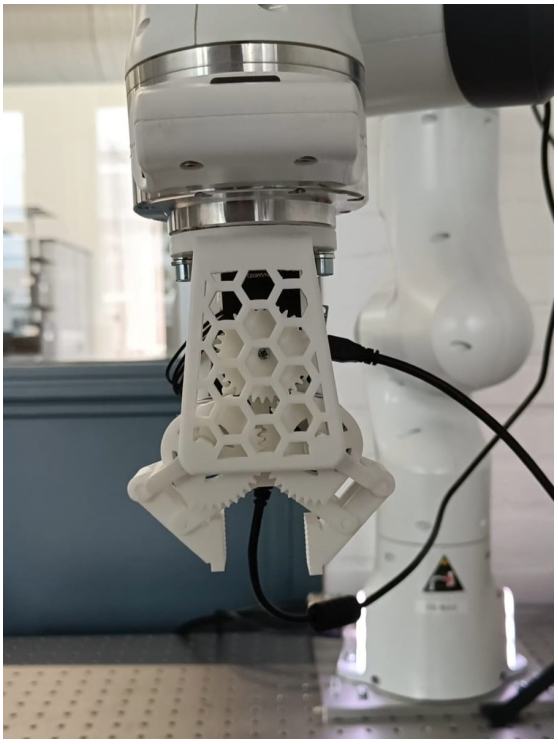

(a) Final B-VSG design attached to a robot arm.

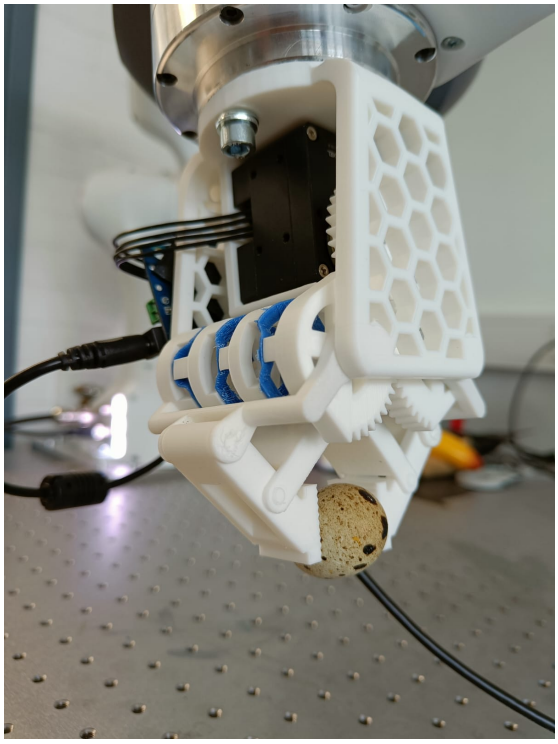

(b) B-VSG holding an lapwing egg without damaging it, showcasing its inherent compliance.

Figure 5.9: The final design of the B-VSG

6

Materials and Methodology

This chapter outlines the methodology employed to address the primary research questions presented in Chapter 4 and the design process described in Chapter 5. The focus of this study is the development of a VSG utilizing bistable mechanical metamaterials (B-VSG). These materials can alternate between two distinct torsional stiffness states and are optimized for use in a novel, energy-efficient actuator characterized by lightweight construction and adjustable stiffness properties.

FEAs are central to this research, facilitating a detailed modeling of the metamaterials' mechanical behaviors and enabling precise measurements of stiffness alterations. These analyses help in validating the computational models through empirical data acquired from real-world tests. Systematic simulations via FEA identify critical factors influencing torsional stiffness and delineate the impact of various design parameters on this property.

Prototyping is integral to the validation process, where additive manufacturing techniques are employed to produce samples for physical testing. These tests ensure the prototypes' behaviors are consistent with predictions from computational models, thereby confirming the models' accuracy and providing data to refine the metamaterials' design for optimal torsional stiffness. Additionally, a physical model is used to characterize the dynamic behaviour of a single bistable cell, essential for future control of the VSG.

Further refinement of the metamaterials is achieved by optimizing the unit cell initially designed by Yang and Ma [81]. The improved design forms the basis of the final VSG, evaluated for its capacity to undergo significant stiffness alterations while maintaining energy efficiency. The obtained data from the mechanical characterization of the bistable cell will be used to design a three-celled metamaterial that will be used as a complaint element and integrated VSM in the gripper.

Data visualization and analysis are performed using custom Python scripts, focusing primarily on the linear elastic behavior of the materials. Linear regression is applied to interpret the data, assuming that non-linearities do not significantly affect the results.

The research, however, faces certain limitations including the inability to alter the base geometry of the unit cell, adherence to the initial designs by Yang and Ma, and potential discrepancies between theoretical predictions and actual prototype performances due to material imperfections.

This chapter discusses manufacturing of the V-BSG and four experimental approaches: 1) Computational simulations through FEAs, 2) Empirical validation of the FEAs, 3) Stability analysis of the bistable cell, and 4) Analysis of the dynamic behavior of the bistable cell. Prior to these experiments, preparatory steps include the creation of a digital model of the bistable cells and the metamaterial using SOLIDWORKS, setting the stage for subsequent experimental and computational investigations.

6.1. Parametric Design in SOLIDWORKS

During the initial phase of this research, SOLIDWORKS is used as a computer-aided design (CAD) tool to support FEA and later to conceptualize the demonstrator. Before proceeding with CAD modeling, it is essential to address the specific requirements of the intended FEA. The FEA aims to assess the torsional stiffness in both the open and closed states of the structure to determine the difference in stiffness between these states. Given the complexity and time-consuming nature of simulating nonlinear snapping behaviors, separate files depicting the structure in both states are created to facilitate this analysis.

Table 6.1: Constant parameters and parametric expressions in the unit cell design.

Parameter	Value [mm]	Description
l	10	Width of snapping cell
t_1	$1/12 * l$	Thickness of the cosine-shaped section
δ	$1/24 * l$	Gap between supporting segments
h_2	$t_2 + 2\delta + t1 + b$	Total height of the structure in closed state
h_1	$3b + t_1 + 2\delta + t_2$	Total height of the structure in open state
d	4	Wall thickness of cylindrical unit cell
D	$l/\sin(\frac{1}{8}\pi) + d$	Diameter of the cylindrical unit cell

The design process begins with projecting a 2D sketch of the planar structure, as conceptualized by Yang and Ma [84], onto a cylindrical surface. This projection is facilitated by linking the geometric parameters of the sketch to an external file containing all parameter expressions (referenced in Table 6.1). This linkage ensured consistent and accurate model dimensions. The cylindrical surface is then accurately trimmed using the 2D sketch as a template. The resultant surface is thickened to 4 mm, providing the structure with its three-dimensional shape, see Figure 4.3. The model is further refined by mirroring the 3D structure and arranging it in a circular pattern to form a complete cylinder.

A crucial step in the setup is to ensure that the snapping cell fits precisely around the cylinder. For this research, the number of unit cells in the cylindrical bistable cell is set to four pairs of mirrored bistable unit cells. This configuration is chosen to guarantee symmetrical and consistent behavior during the snap-through process. This precision is achieved by applying a specific formula for chord length, detailed in Equation 6.1, which matched the chord length a to width l from the snapping cell, as illustrated in Figure 4.1.

$$l = a = 2R \sin \alpha/2, \tag{6.1}$$

where l is the width of a snapping section, a represents the chord length, R is the radius of the cylinder, and α is the central angle of a single unit cell in the cylindrical bistable structure.

After the unit cell is configured, various structures were generated by altering the linked parameters in the external file according to the simulation needs and controlled via a Python script (see Appendix C). In addition to a CAD model of the bistable cell, a parametric model of the three-celled metamaterial is also created using the previously described method. The final SOLIDWORKS models were saved as ASCII files, efficiently preparing them for subsequent use in the FEA and thus smoothing the transition from design to analysis.

Different structures were generated in SOLIDWORKS using different geometric ratios as input. The intervals between geometric changes are 0.5 for the ratio t_2/t_1 and 0.1 for the ratio b/l. The data points observed in Figure 6.3 were used as input for the FEA for the analysis for the bistable cell. These specific data points will be explained in Section 6.3.3.

6.2. Manufacturing of the Metamaterial

As established Chapter 2, material effects the stiffness of the metamaterial greatly. Since different materials require different manufacturing techniques, it is important to consider manufacturing possibilities and limitations before doing computational or experimental analysis. As stated in Chapter 3, the thesis will limit itself to rapid prototyping techniques and well-known materials given the time-constrained nature of this project. In the initial phase of this research, the material is limited to *Ninjatek Cheetah TPU Shore 95A* (flexible) and *Generic PLA* (rigid). Both these materials are thermoplastic and are therefore highly suited for use in additive manufacturing, which is a preferred manufacturing method for rapid prototyping In addition, material properties of these materials are well-known and the materials are widely used in academic research. A downside of using TPU and PLA is that these materials do not chemically bond and, because of this, are unsuited for multi-material AM techniques and will require mechanical joining methods. In the last stadium of this research, *Filatech FilaFlexible40 Shore 40D* is used as a replacement

of the Ninjatek Cheetah TPU. The replacement of Cheetah TPU by FilaFlexible40 happened in the final prototyping phase, after conducting all experiments. The primary reason is the unavailability of Cheetah TPU and the similarities between the two TPEs. Although the chemical composition of FilaFlexible40 is unknown, the shore hardness is quite similar to Cheetah TPU. Even though a similar shore hardness does not directly result in a similar Young's modulus, is does indicate similar elastic properties. This research used single-material fused decomposition modeling, a common AM technique, to manufacture the prototypes.

Rapid Prototyping and Material Selection
This research will use rapid prototyping techniques and well-known materials due to the time constraints of the research. As mentioned, the materials are limited to Ninjatek Cheetah TPU Shore 95A[1] (replaced by Filatech FilaFlexible40[2] in the last phase of the thesis) and Generic PLA. Both these materials are thermoplastic and well-suited for use in additive manufacturing, which is ideal for rapid prototyping. Additionally, the material properties of these materials are well-documented and they are widely used in academic research.

Since this research is limited to the use of PLA and TPU, the infill of PLA will be adjusted to emulate different Young's Moduli. According to research by Rismalia et al. [88], different infill percentages and infill patterns of PLA have a limited effect on the Young's modulus of the metamaterial. The research by Rismalia et al. suggests that testing structures made from different infill of PLA should result in different torsional stiffnesses and show a trend similar to the simulations that use different materials.

The 3D printers used for AM during this thesis are: the Prusa MK4 (replaced by a Prusa MK3S in the last stadium of the research) to manufacture parts made from flexible material (TPE) and the Bambulabs X1 Carbon to manufacture parts made from PLA. Both the Prusa MK4 (or MK3S) and Bambulabs X1 Carbon are single-material 3D printers that use fused deposition modeling (FDM).

The reasons for using two separate 3D printers are: 1) The Bambulabs X1 Carbon is able to printer faster and higher quality PLA parts. 2) The Prusa printers fabricate better quality flexible material. 3) Using two printers simultaneously speeds up prototyping.

6.2.1. Fused Deposition Modeling (FDM)
FDM is one of the most widely used AM technologies, commonly referred to as 3D printing. FDM has gained popularity due to its simplicity, cost-effectiveness, and the ability to use a variety of thermoplastic materials [89]. The FDM process involves the deposition of material layer by layer to build a three-dimensional object. The primary components of an FDM system include the printer head, the build platform, liquefier, gantry and the material feed mechanism [90]. The process starts with a digital model of the object, which is sliced into thin cross-sectional layers using specialized software, termed *slicing software*. The FDM printer then follows these instructions to create the object layer by layer.

The material used in FDM is typically a thermoplastic filament, which is fed into the printer head. The printer head, or *extruder*, heats the filament to its melting point and extrudes it through a nozzle onto the build platform. Depending on the type of FDM printer, the extruder and build plate move in different direction to create the shape of each layer. This process is repeated until the entire object is formed [89].

FDM uses a variety of thermoplastic materials, most commonly acrylonitrile butadiene styrene (ABS), polylactic acid (PLA), polyethylene (PE), polypropylene (PP), nylon/polyamide (PA), and polycarbonates (PC) [89]. Each material offers different properties such as strength, flexibility, and heat resistance, making FDM suitable for a wide range of applications from prototyping to functional parts. FDM offers several advantages when compared to other manufacturing techniques, including ease of use, low cost, and the ability to produce parts with high accuracy and repeatability. However, it also has limitations such as size, surface finish, and accuracy [91]. However, for this research the advantages outweigh the disadvantages and therefore FDM is selected as the primary manufacturing method.

6.2.2. Multimaterial Design
A downside of using PLA and TPU in single-material FDM is the necessity to use mechanical interlocks to manually assemble a multimaterial structure. If multimaterial FDM is available, the TPU and PLA can

[1] https://ninjatek.com/shop/cheetah/

[2] https://fila-tech.store/product/filaflexible40/

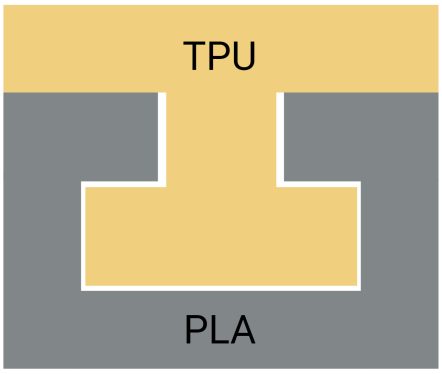

Figure 6.1: Mechanical interlock used to join multimaterial sections together

be layered such that they are manufactured in interlocked state, ensuring the joint even though the two materials do not bond chemically. Since only single-material FDM printers are used during this research, the multimaterial sections were manually assembled using mechanical interlocks and pressure fitted. Ribeiro et al.[92] compared different types of interface geometries to join TPU and PLA. The interface geometry used in this research was found to have the highest Young's modulus, highest ultimate stress and largest strain at break in the research conducted by Ribeiro et al. The mechanical interlock chosen can be observed in Figure 6.1.

In an effort to improve the customizability of the unit cell, a mold is designed. This allows for a wider use of materials and enables the use of better mechanical interlocks. Sections of the unit cell can be manufactured from PLA using FDM and inserted into the mold. Next, the cavities in the mold can be filled using some liquid(ized) polymer. Once the polymer is cured, the mold can be opened and the cylindrical unit cell can be taken out. The mold design for this manufacturing method can be observed in Figure B.8.

After conducting several experiments, it became evident that improving the injection molding method and mold design to a usable level for the research would be too time-consuming. Since the mechanical interlocking method using PLA and TPU seems to perform sufficiently well, it is decided to ultimately discontinue further development of the mold design, mainly because of time constraints. However the method does show promise for future development.

6.3. Finite Element Analysis (FEA) Methodology

The study focused on evaluating the mechanical properties of structures using FEA through two primary analyses: material properties and geometric ratios. This approach is designed to understand the effects of variations in material and geometry on the structure's behavior.

6.3.1. Simulation Setup

All simulations are performed using *Abaqus/Implicit* to take advantage of its capabilities for modeling static deformation. In the literature, many of the research into mechanical metamaterials utilized Abaqus for the performed FEAs, some examples are the work of Wang et al.[75], the work by Lele et al.[69], the work by Florijn et al.[93] and the work by Chen et al.[73]. Since Abaqus is widely used in literature and its integration with Python makes it user friendly, Abaqus is chosen as the finite element software for this master thesis. Abaqus has two different solvers used for structural analysis of components: Abaqus/Implicit and Abaqus/Explicit.

Harewood and McHugh [94] explain that Abaqus/Implicit is traditionally preferred for quasi-static problems because of its accuracy and stability. In the implicit solver, Abaqus selects an initial guess for each increment, assuming an incrementally linear material response based on the tangent stiffness from the previous increment. For linear elastic materials, this would yield the correct solution directly. For non-linear problems, this provides a good initial guess for small increments. However, the implicit solver can face numerical difficulties in converging to a correct solution during analyses involving large element

deformations, highly non-linear plasticity, or surface contact. Since the simulations were performed over a small displacement and the bistable unit cell is almost linear elastic under torsion, the Abaqus/Implicit solver is used.

According to Srirekha and Bashetty [95], FEA involves three main steps. First, in pre-processing, a geometrical model is created using CAD, material properties are defined, and boundary conditions are set. The structure is divided into a mesh of finite elements. Second, during the processing or solution phase, computational algorithms calculate how each element responds to external forces based on the material properties and boundary conditions. This involves solving equations that describe the behavior of each element. Finally, in post-processing, the results—such as stress, strain, and displacement—are visualized and analyzed to understand the structure's performance and to make necessary design modifications.

The structural model, imported from SOLIDWORKS, is partitioned to manage different materials effectively and to refine the mesh, which is set at a mesh size of 0.5 mm to yield accurate results within a reasonable calculation time. Although the flexible material used in the simulations typically requires the use of a hyperelastic model (such as Mooney-Rivlin, Neo-Hookean, or Ogden), the linear approach allowed for the simpler C3D8R (8-node linear brick) element types, instead of hybrid mesh types that are necessary to model hyperelastic materials.

Although three-dimensional solid structures have no rotational degrees of freedom in Abaqus, this can be managed by applying moments or rotations to reference points instead and *coupling* these reference points to solid structures. Boundary conditions were managed by kinematically coupling the upper and lower surfaces of the structure to two reference points aligned with the central axis. One reference point is fixed in all directions (*Encastre constraint*), and the other is subjected to a small angular displacement ($\pi/40$ radians along the Y-axis with an angular velocity of $\pi/40$ rad/s) to maintain primarily elastic deformations, see Figure 6.2. The angular displacement and reaction moment of the rotated and fixed reference points were outputted. The angular displacement of the rotated reference point and the reaction moment of the fixed reference point were plotted against each other to create the torque-angle response of the structure. This response is used to determine the torsional stiffness from the slopes of these curves.

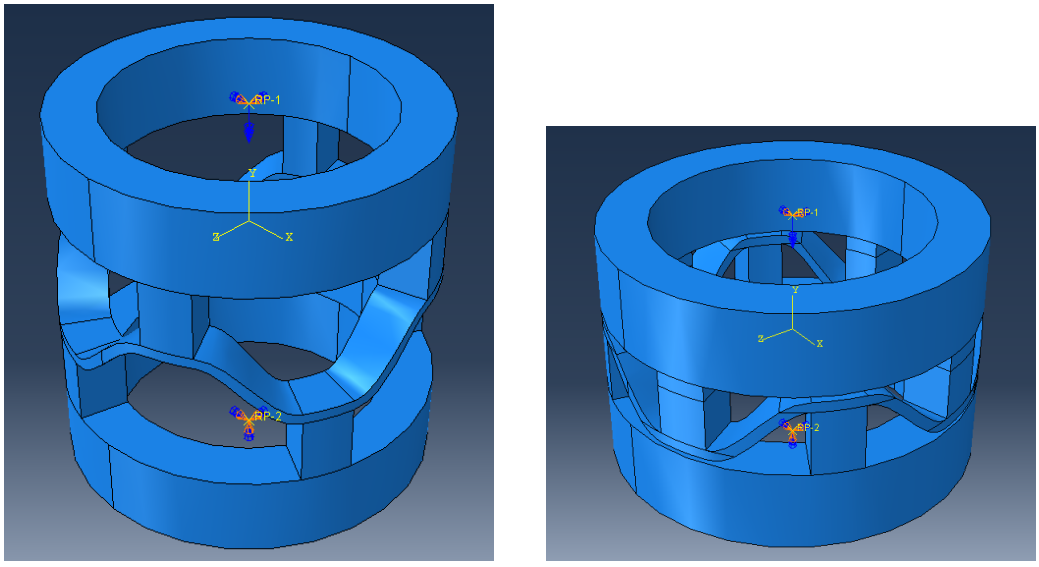

(a) Boundary conditions in Abaqus for unit cell in open state.

(b) Boundary conditions in Abaqus for unit cell in closed state.

Figure 6.2: Boundary conditions in the FEA in Abaqus, where a rotation is applied to RP1 and RP2 is fixed.

6.3.2. Analysis of Material Properties

The first part of the analysis concentrated on the impact of varying material properties within the sections of the structure with constant geoemtry over all simulations, illustrated in Figure 4.2. The geometric ratios were set to: $t_2/t_1 = 6$ mm and $b/l = 0.6$ mm, see Table 6.1. The materials used included a consistent

application of Ninjatek Cheetah TPU Shore 95A (with an approximated Young's modulus of 26 MPa [96] and a Poisson ratio of 0.25 [97]) alongside a range of arbitrary linear elastic materials, with Young's moduli varying from 5 MPa to 25.6 GPa. This part of the study is organized into two configurations and a uniform simulation:

1. The first configuration used TPU only for the cosine-shaped beam, while other sections were made from the arbitrary linear elastic material.
2. The second configuration used TPU for both the cosine beam and vertical support beams, with the remaining parts made from the arbitrary material.
3. In the uniform simulation, the material composition of the unit cell will be uniform and the Young's Modulus of the entire structure will be changed.

These configurations were iteratively simulated to examine how different distributions of materials affect structural behavior, especially focusing on torsional stiffness and deformation.

6.3.3. Analysis of Geometric Ratios

The second set of simulations explored how changes in geometric ratios influenced the structure's mechanical properties. Here, the entire structure is made from Ninjatek Cheetah TPU Shore 95A. Given the complex geometry that is present in the selected unit cell, see Figure 4.1 and Table 6.1, there are many geometry parameters that can be changed. A few examples and their effects are:

- δ can be increased or decreased, not only affecting the length of the vertical support beams, but also possible influencing dry friction effects in the closed state of the structure.
- $t1$ can be changed, where a thicker cosine beams might result in a stiffer structure.
- b can be altered, where a larger b results is a taller structure and likely decreases stiffness

The above mentioned examples and their suspected influence are only a select few of the many geometric parameters that can be changed. Changing this many independent geometric parameters would results in a complex multivariable optimization, which would result in an extensive, over-complicated forward-design of the metamaterial and is therefore not preferred. Instead of weighing all independent parameters, this research will focus on changing some geometric ratios by fixing certain parameters and changing the complementing parameters systematically. In previous research by Yang and Ma [84], the influence of the ratios of $t2/t1$ and b/l on the bistability of the structure were investigated (see Figure 4.4). Since it is known that these ratios have a clear influence on the bistability of the structure and this influence is already defined for the planar structure, this research will focus on changing these ratios as well.

The geometric ratios, t_2/t_1 and b/l, were varied within the specified region established in Figure 6.3. The limits of this region are derived from the bistability region for the planar metamaterial proposed by Yang and Ma, see Figure 4.4, and extended to the limits of the geometry. Data points below the green line are known to lack bistable characteristics. Other geometries outside of the data set contained unsolvable constraints and were not possible to generate. This analysis aimed to isolate the geometric effects from the material properties to understand how changes in shape and size influence the structure.

6.3.4. Comparative Analysis Across Structural Configurations

The methodology also covers both open and closed versions of the structures, allowing for a comparison of torsional stiffness between these variants. This comparative analysis is key in identifying the relation between (percentage) stiffness difference and relevant attributes such as geometric ratios and material properties.

After simulating the percentage stiffness difference ($\Delta\%k$) and the stiffness difference (Δk) for every data point, a stiffness landscape is created using linear interpolation between the data points. Such a stiffness landscape is created for both the open and closed state of the unit cell. These landscapes are used to further calculate the $\Delta\%k$ and the Δk within the boundaries of the data points.

6.4. Experimental Setting

Four types of experiments are performed in the experimental setting. These experiments require physical prototypes, which are fabricated with FDM as previously discussed. The validation of the FEA and stability

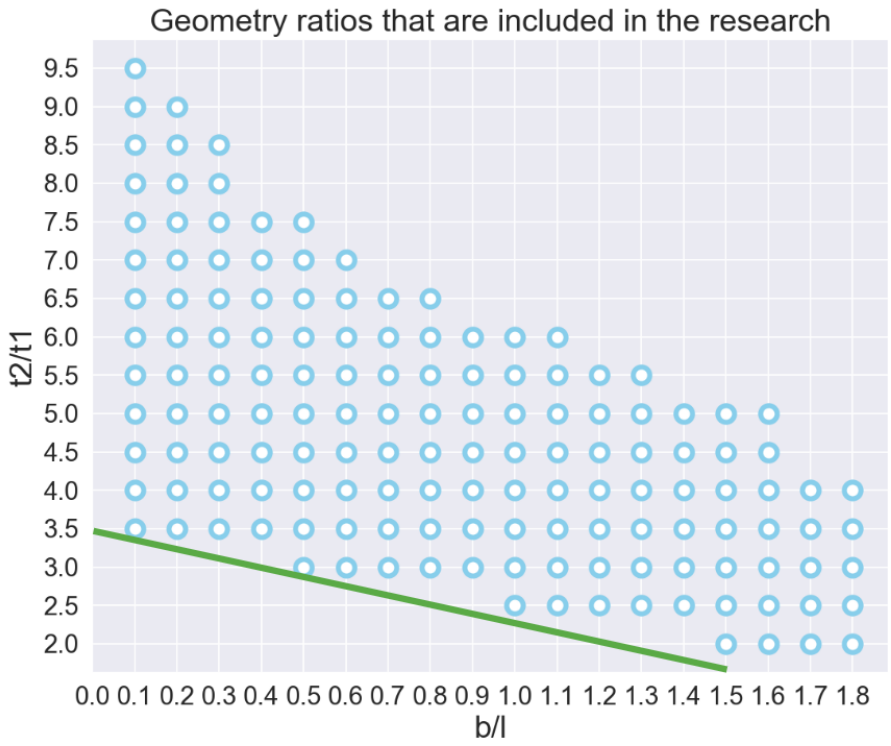

Figure 6.3: Data points that were investigated in the analysis of the influence of geometric ratios t_2/t_1 and b/l on the torsional stiffness. The green line indicates the border of the bistability region for the planar metamaterial, as explained by Yang and Ma [84].

analysis of the bistable cell were performed using a ZwickRoell biaxial tensile torsion test machine using position control, see Figure B.5. The reaction force or reaction moment (depending on the experiment) is measured using a load cell. The dynamic behaviour analysis is performed by connecting a bistable cell to a servomotor (Dynamixel XM430-W210-R) and capturing video footage of the movement using a high speed camera. Additionally, the grip forces of the two prototypes are measured.

6.4.1. Method of Validating the Finite Element Analyses

Prototypes will be produced using AM and tested to see if their behavior aligns with the computational models. The samples are placed in the biaxial testing machine and twisted with a controlled displacement of $10°/min$ over an angular displacement of 10°. The position-controlled measurements were performed in a cycle of three measurements to minimize noise in the measurements. The torque and angle measurements are plotted against each other. The torque-angle data is divided into six sections, by sectioning the data at the peaks and valleys. The sections with positive slopes are extracted. After this, a line is fitted to the extracted data and the slope is calculated. The slope of the linear curve is equal to the effective torsional stiffness of the structure. This validation will provide the data needed to refine the structure for torsional stiffness.

6.4.2. Method of Analyzing the Stability of a Bistable Cell

As explained in Section 4.2, there exists a coupling between rotation and axial displacement in the bistable cell. The coupling between angular and axial displacement is most impactful when the structure is in the open state. When the structure is only slightly bistable, torsion can result in unintended snap-through to the closed state, when critical force in the axial direction is reached. This effect is less significant in the closed state of the structure. In the closed state, the vertical support beams limit the range of motion of the structure, and the critical force in the axial direction cannot be reached by torsional load.

The hypothesis suggests that the von Mises stress varies between states (asymmetric von Mises stress) when the unit cell is manufacturing in either one of the buckling states, but appears more balanced

(symmetric von Mises stress) when the beam is initially flat and later shaped into a curve. This assymmetry in von Mises stresses might affect the amount of force needed to change the cell from open to closed and vice versa, known as the *critical force*. To test this, all possible manufacturing states were physically created and tested in the ZwickRoell biaxial testing machine, see Figure B.5. The examined manufacturing states, see Figure 6.4, are:

- The unit cell is printed in the **open** state.
- The unit cell is printed in the **closed** state.
- The unit cell is printed in three separate sections; notably, the cosine-shaped section is first printed **flat**, then manually shaped into a curve using mechanical locks and pressure fitting.

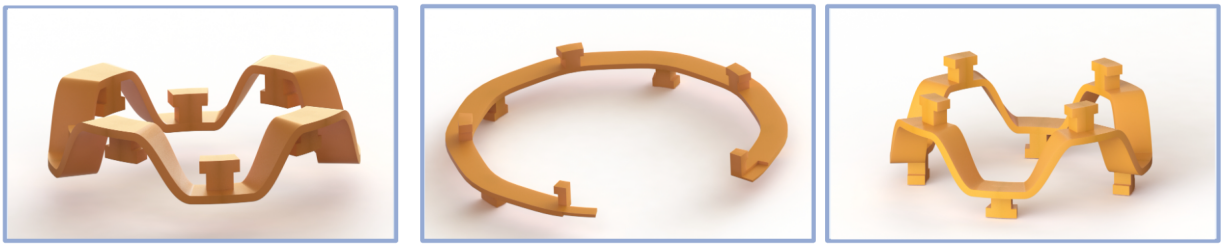

a) Printed closed b) Printed flat c) Printed open

Figure 6.4: Different states of printing the cosine-shaped beam. For the open and closed states, visible in a) and c), the unit cell is printed as one part if the material is uniform. The flat manufacturing state, visible in b), is always printed separately and manually forced in the cosine shape during assembly.

6.4.3. Dynamic Behaviour and Modeling

All of the previously described experiments are performed under static conditions and are not necessarily valid under dynamic conditions. It is important to know the dynamic behaviour of the structure in order to develop a control system for the final VSA design. This section does not investigate the behaviour of the final VSG, but shows a method of investigating the dynamic response of a single unit cell.

To investigate the dynamic behaviour of the bistable structure, a set of experiments is conducted. A single bistable structure is mounted on a servomotor (Dynamixel XM430-W210-R), enabling precise control over its angular displacement. The ring section of the bistable cells were fabricated from 40% infill PLA, all other sections were manufactured using 40% infill TPU. To simulate the influence of inertia, a mass of 0.85 gram is attached to the structure using a lever arm with the length of 33.2 millimeter. This configuration is chosen to enhance the dynamic response of the system.

The structure is rotated to a specified angular displacement, and its movement is captured using a high-speed camera operating at 300 frames per second (FPS). Following the initial displacement, the bistable structure is snapped to its alternate stable state, and the experiment is repeated under identical conditions. For the experimental setup, see Figure B.4.

Motion tracking software (Tracker[3]) is utilized to monitor a marker placed on the rotating structure, providing precise measurements of the structure's rotational dynamics. The high-speed video recordings revealed distinct oscillations of the mass around the displaced angle.

A dynamic model is used to simulate the dynamic behaviour of the mass attached to the bistable structure when the mass has been rotated from 0 to 180 degrees. Important to note is that the model needs to have an nonzero initial velocity.

Using the information obtained from the experiment, an initial guess for the stiffness of the structure is made. In addition, an initial guess for the damping is made. Finally, an initial angular velocity of 90 °/s is used as initial condition for the model, since this seemed to fit the measurements best. It should be noted that the angular velocity of the initial rotation of the system is around 500 °/s, but the servomotor seems

[3] `https://physlets.org/tracker/`

to gradually slow down when it approaches a rotation of 180 °. The angular velocity is chosen based on the initial angular velocity that the experimental data has after a rotation of 180 °. After this, k and c were systematically changed to find the best fit.

Since the motor torque is almost equal to the moment induced by the gravitational forces acting on the mass in the final position, the gravitational forces and motor torque acting on the mass when the structure has been rotated to its final position are neglected. The equation of motion that is used in the dynamic model is showed in Equation 6.2:

$$J\ddot{\theta} + c\dot{\theta} + k\theta = \tau_{external} = 0, \tag{6.2}$$

where J is the polar moment of inertia, c is the damping coefficient, k is the stiffness, θ is the angle between the position of the mass and the reference position, and $\tau_{external}$ is the sum of the external torques, which is assumed zero at the moment the model begins.

For the model, the mass is assumed to be a point mass with mass M and at a distance R from the center of rotation. The polar moment of inertia J of a point mass about a point is defined in Equation 6.3a. Since this system only has a single point mass, the formula for the polar moment of inertia simplifies to Equation 6.3b.

$$J = \sum M_i R_i^2 \tag{6.3a}$$

$$J = MR^2 \tag{6.3b}$$

From the equation of motion in Equation 6.2, the transfer function of the system can be derived, as can be seen in Equations 6.4. Once the values for k and c are estimated, the poles of the transfer function can also be estimated using Equation 6.4f. The location of the poles is important predict the response characteristics of the system.

$$\mathcal{L}\{J\ddot{\theta} + c\dot{\theta} + k\theta\} = \mathcal{L}\{\tau_{external}\} \tag{6.4a}$$

$$Js^2\Theta(s) + cs\Theta(s) + k\Theta(s) = \mathcal{T}_{external}(s) \tag{6.4b}$$

$$(Js^2 + cs + k)\Theta(s) = \mathcal{T}_{external}(s) \tag{6.4c}$$

$$\Theta(s) = \frac{\mathcal{T}_{external}(s)}{Js^2 + cs + k} \tag{6.4d}$$

$$G(s) = \frac{\Theta(s)}{\mathcal{T}_{external}(s)} = \frac{1}{Js^2 + cs + k} \tag{6.4e}$$

$$s = \frac{-c \pm \sqrt{c^2 - 4Jk}}{2J} \tag{6.4f}$$

6.4.4. Grip Force and Stiffness Measurements of Prototypes

Analyzing the performance of the different prototypes requires measuring the grip force with which the gripper grasps an object. Measuring the grip force of the assembled actuated gripper in both the compliant and stiff settings provides insights into its performance and possible applications. To measure this grip force, a load cell is used. A load cell is a sensor that converts force into an electrical signal.

Two different setups were used, based on the available lab equipment. The grip force of the actuated prototype is measured using a load cell and an Arduino Uno. The measurements were read using the Serial Output of the Arduino. For the unactuated prototype, the grip force is measured using a Futek LSB200 Load Cell and viewed using LabVIEW.

In both cases, the prototype is measured in both the compliant and stiff states of the actuator. Using low-velocity position-controlled motion, the metamaterial in both states is subjected to the same angular deformation. A higher force measurement indicates a stiffer state. It is important to note that the grip force is measured for one end effector per prototype.

For the actuated prototype, the torsional stiffness of the metamaterial is also measured using a biaxial testing machine. Three load cycles were performed on the compliant state, followed by three load cycles on the stiff state. The stiffness is determined in a similar manner to previous tests on the biaxial testing machine.

6.5. Gripper Design and Interaction

The stiffness actuation mechanism chosen for the actuated design is the Mould King M00011 Atmospheric Pressure Piston Yellow With 2 Inlets, which is responsible for the snapping action that modulates the stiffness of the metamaterial. This piston features dual inlets, allowing for both extension and retraction of the piston shaft using pressure, which improves the ability to achieve higher critical forces within the metamaterial. It also has a stroke length of 15 mm, which determines the allowable b values for the unit cells in the metamaterial.

The movement of the gripper fingers is controlled by a Dynamixel XM430-W210-R servomotor. The gripper is designed for use with the Franka Emika Panda, a 7-axis robot arm with an 850 mm reach, ideal for precise and extended-range tasks. The servomotor is separately controlled using a Python interface. The servomotor is connected to a U2D2 Board, which is in turn connected to a computer.

7

Results

This chapter shows thorough mechanical characterization and dynamic behavior analysis of the bistable metamaterial through both simulations and experimental methods. It starts with a detailed FEA to explore how changes in geometric ratios and material properties (Young's modulus) affect the torsional response of these materials in different states, open and closed. This part of the study lays the groundwork for understanding how these materials behave under various mechanical stresses.

Moving from theory to practice, the chapter covers experiment results designed to test the predictions made by the simulations, aiming to solidify the understanding of how these materials perform under real-world conditions. It includes dynamic tests to analyze how the metamaterial behaves when used in practical applications. The behaviour is subsequently modeled using the equation of motion presented in Chapter 6.

By integrating findings from both simulations and experiments, this chapter enhances the understanding of the mechanical properties of the bistable metamaterial and aims to maximize the torsional stiffness difference between the two states of the material. The findings results in the design of a novel VSG.

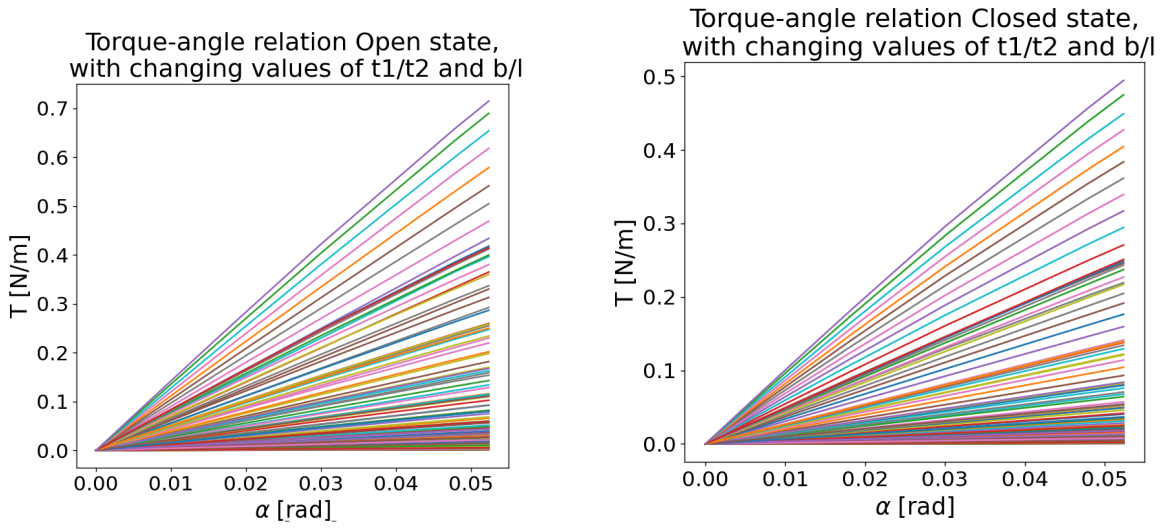

(a) Torque-angle data for unit cell in open state

(b) Torque-angle data for unit cell in closed state

Figure 7.1: Torque-angle data obtained from the FEA

7.1. Simulation Results

This section presents the results of the FEA focused on understanding how geometric ratios influence the torsional stiffness of bistable metamaterials. The results from this section aim to answer the following questions (see Chapter 4):

- How does changing certain geometric ratios of the unit cell affect the (percentage) torsional stiffness difference between the open and closed state of the unit cell?
- How does changing the material of certain sections of the unit cell affect the (percentage) torsional stiffness difference between the open and closed state of the unit cell?

After setting up the model as previously described, the relationship between applied torque and angular displacement for small rotations is thoroughly analyzed. Two different types of FEA will be discussed in this section. The first being a FEA meant to investigate the influence of varying selected geometric ratio's on the Δk and $\Delta\%k$. The second FEA is focused on characterizing the effect of changing material properties, particularly the Young's modulus, of selected sections of the bistable cell on the torsional stiffness.

7.1.1. Finite Element Analysis: Geometric Ratios

After setting up the model as explained in Section 6.3, the relation between applied torque and angular displacement (for small rotations) is outputted from the simulation. From Figure 7.1, it can be observed from the torque-angle data that is obtained from the simulation that the relation is almost linear elastic. The torsional stiffness of the structures can be derived by taking the slope of the extracted torque-angle data.

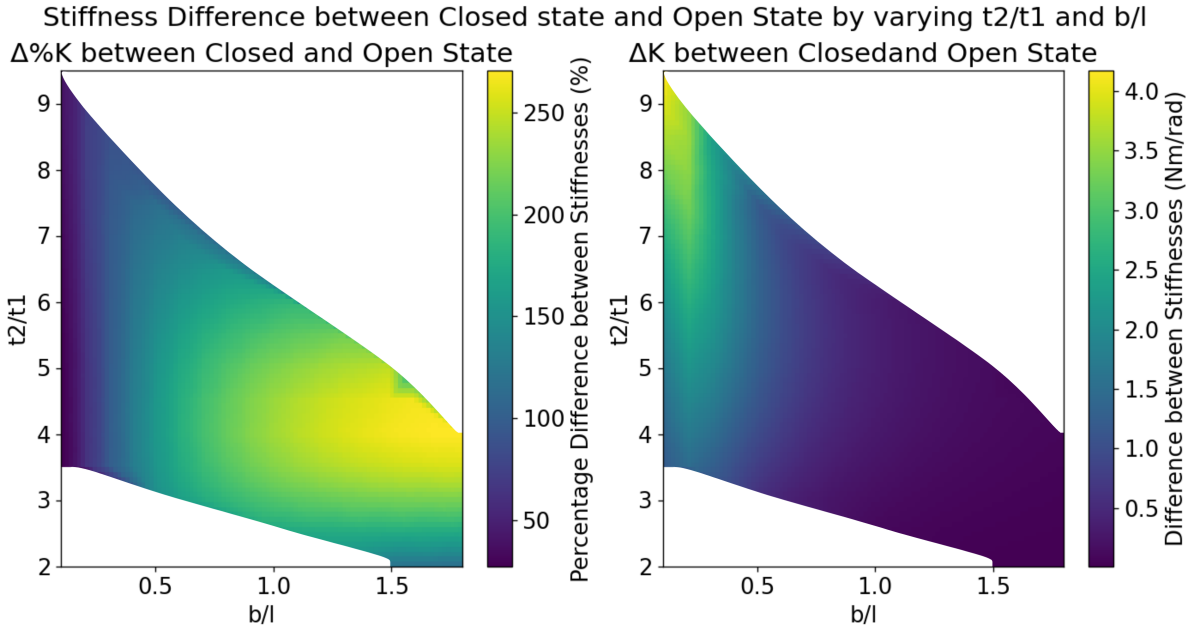

Figure 7.2: Heat maps indicating the $\Delta\%k$ (left) and the Δk (right) between the open and closed state of the unit cell for varying geometric ratios $t2/t1$ and b/l, where the color indicates the stiffness difference or $\Delta\%k$, respectively.

The stiffnesses were extracted for the open and closed state for all investigated data points. After this, the Δk (i.e. the torsional stiffness difference between the open and closed bistable cell) and $\Delta\%k$ (i.e. the percentage increase in torsional stiffness from the compliant state to the stiffer state) is calculated. Since these values are dependent on two ratios ($t2/t1$ and b/l), the best way to represent these results is using a heat map, where the color indicates the stiffness value in the Z direction. The heat map showing the $\Delta\%k$ and the Δk between the open and closed state of the unit cell for varying geometric ratios $t2/t1$ and b/l is shown in Figure 7.2. Due to the linear interpolation used to derive the stiffness values in between the data points, the representation at the edges of the region is incorrect. To address this, the edges are smoothed during post-processing. The 3D plots illustrating the influence of $t2/t1$ and b/l on the stiffness of the closed and open state of the bistable cell are depicted in Figure B.3.

7.1.2. Finite Element Analysis: Material Properties

As mentioned in Section 6.3.2, three different computational analyses focused on changing material properties are performed. In the first simulation, only the cosine-shaped beam is made from linear

approximated Cheetah TPU and the vertical support beams and the ring are made from a linear elastic material with changing Young's Modulus. The second simulation investigated a structure where the cosine-shaped beam and vertical support beam are both made from linear approximated Cheetah TPU, and only the ring sections are made from the linear elastic material with changing Young's Modulus. The distinction between sections in the bistable cell can be viewed in Figure 4.2. The results from these simulations can be observed in Figure 7.3, which shows the $\Delta\%k$ and the Δk between the open and closed state of the materials, for different tests. The names of the different structural elements in the unit cell are illustrated in Figure 4.2.

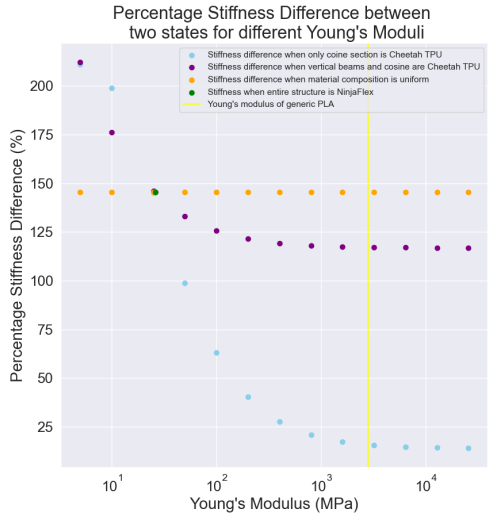

(a) Effects of changing Young's Modulus of certain sections of the unit cell on the $\Delta\%k$ between the Open state and the Closed state

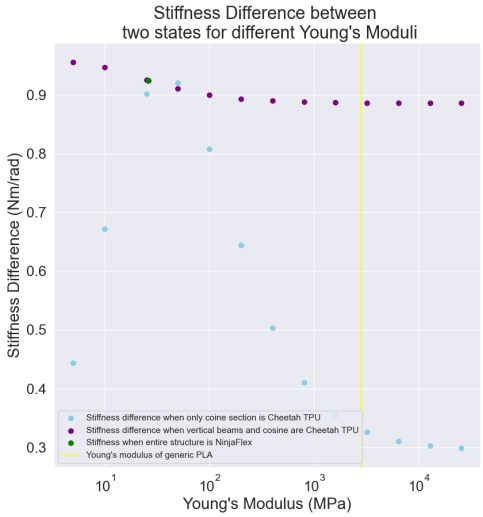

(b) Effects of changing Young's Modulus of certain sections of the unit cell on the Δk between the Open state and the Closed state

Figure 7.3: Boundary conditions in the FEA in Abaqus, where a rotation is applied to RP1 and RP2 is fixed.

7.1.3. Finite Element Analysis: Geometric Ratios of Three-celled Metamaterial

In Section 7.1.1, the effects of changing the geometric ratios of $t2/t1$ and b/l are investigated by keeping $t1$ and l constant and systematically changing the values of $t2$ and b. The characterization showed that (percentage) stiffness difference is affected by both b/l and $t2/t1$.

From Figure 7.2, it is evident that there is a trade-off between maximizing $\Delta\%k$ and maximizing Δk for a single bistable cell. This is problematic, because ideally the structure should have a high $\Delta\%k$ in addition to a high Δk. Finding the optimum between the $\Delta\%k$ and the Δk is not straightforward. Since the simulations in Section 7.1.1 were performed for a single bistable unit cell, the results might not be proportional to a three-celled metamaterial.

In order to find the optimum between $\Delta\%k$ and Δk, a new FEA is performed on the three-celled metamaterial using Abaqus. The settings for the FEA are equal to the settings specified in Chapter 6.3. In the FEA, only the value for b of the largest unit cell is varied. The b for the smaller two unit cells (b_s) were constrained to be equal to 0.5 times b of the larger unit cell (b_l). The ratio $t2/t1$ for both the larger and smaller cells is set to be equal to 4. All other parameters are equal to previous simulations and can be found in Table 6.1.

The reason for varying only b and not the ratio $t2/t1$ is based on the insights provided by Equations 5.5 and the observations from Section 7.1 about how the geometric ratio $t2/t1$ affects the stiffness difference. Equation 5.5e shows that the two smaller cells in the structure should be as stiff as possible, this means that the $t2/t1$ ratio for these cells should be as large as possible. Increasingly, the $t2/t1$ does not effect the $\Delta\%k$ significantly for low values of b. However, the $t2/t1$ for the larger cell should be as low as possible

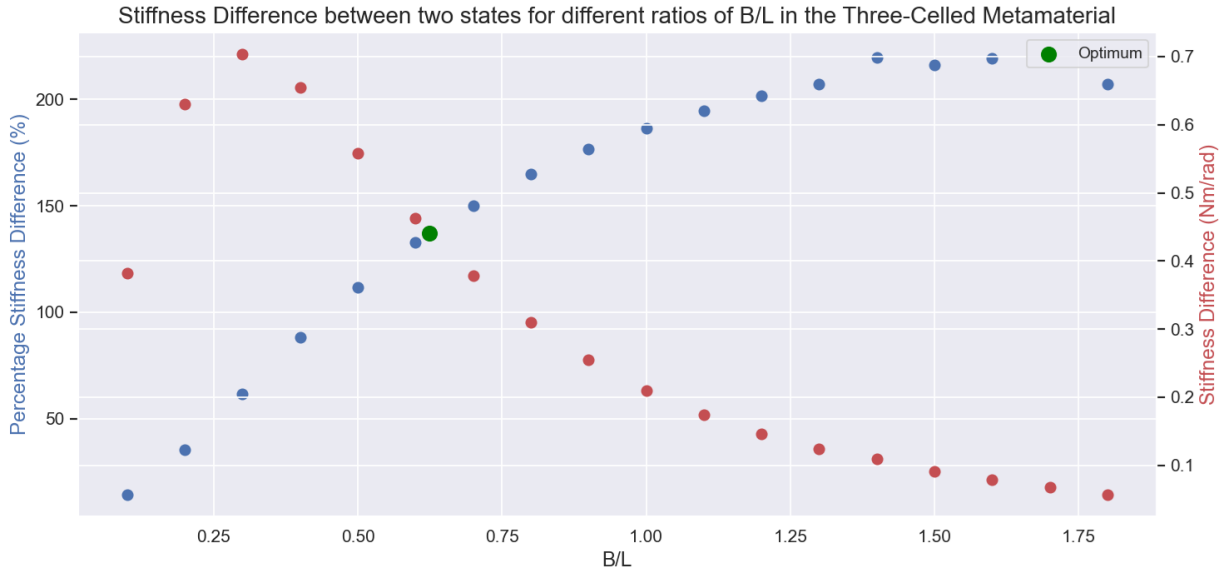

Figure 7.4: Torsional stiffness results from a FEA of the three-celled metamaterial for changing values of b/l

(although still ensuring bistability), to increase the $\Delta\%k$. A low $t2/t1$ ratio in structures with a large b does not significantly effect the Δk.

The simulation results were processed similarly to the results in Section 7.1 and the stiffness differences between the two state of the metamaterial are shown in Figure 7.4. The material used in the simulation is determined to be the best choice based on previous simulations discussed in Section 7.1.2 and the findings from Equations 5.5. Consequently, the larger unit cell is uniformly composed of TPU, while the smaller unit cells are constructed partly from PLA, specifically in the ring sections and vertical support beams. The optimal balance between $\Delta\%k$ and Δk occurs at $b_l \approx 0.625$, leading to a value of b for the smaller cells at approximately $b_s \approx 0.313$.

7.2. Experimental Results and Validation

Ensuring the practical validity of the previous findings and further paving the path towards the final application of the structure in a VSG, several experiments were performed. This chapter will give a detailed presentation of experimental findings. First, a dynamic test will be presented where motion analysis gives insight into the stiffness and damping change of the structure. Second, the bistability of the structure will be shown for different manufacturing configurations. Lastly, the validity of simulations performed in Abaqus are analysed by comparing experimental results to the simulation results.

7.2.1. Dynamic Behaviour of the Bistable Structure and Modeling

Understanding the dynamic behaviour of the bistable cell is crucial to realise precise control of the actuator. After performing the measurements as described in Chapter 6, the measurements from both stable states of the structure were plotted in Figure 7.5, showing the different oscillatory behaviours. The actual difference in stiffness and damping can only be defined when the system is analysed numerically using a dynamic model.

The model and experimental results are shown in Figure 7.6. From the model, the stiffnesses and damping coefficients that closest resembled the experimental data are: $k_c = 0.95Nm$ and $c_c = 0.002Nms/rad$ and $k_s = 2.3Nm$ and $c_s = 0.01Nms/rad$.

7.2.2. Stability Analysis

As previously discussed, unit cells are fabricated using FDM and are printed in what is considered a resting or equilibrium state. The way a unit cell is initially shaped during printing determines the stresses it faces during use, which can affect the overall stability of the structure. This section aims to answer the following

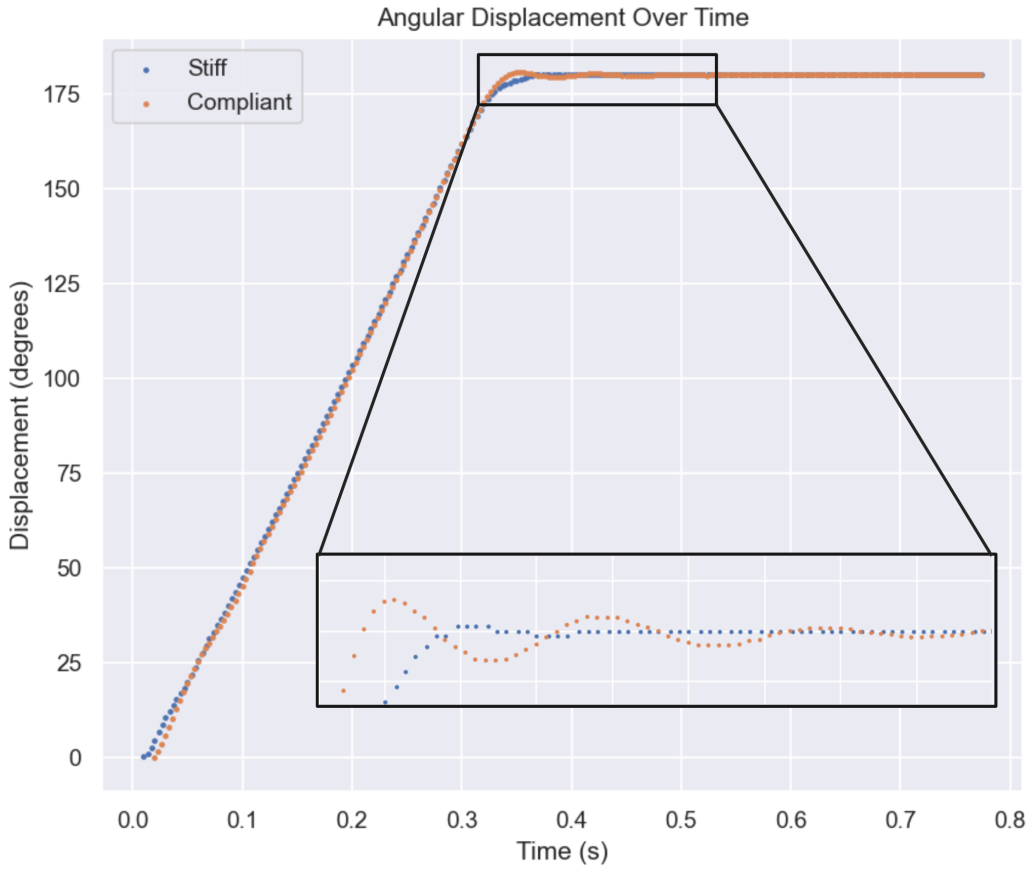

Figure 7.5: Movement of the rotating structure with a mounted mass, zoomed in on the oscillations of the system in the compliant state and the stiffer state

question (formulated in Chapter 4): How does the manufacturing state influence the bistability of the unit cell?

To prevent sudden and unwanted changes in stiffness (caused by unintended snap-through) it is crucial to ensure the stability of both the open and closed states of the cell. In this study, the stability of various manufacturing states of the cosine-shaped beam is evaluated, covering the configurations illustrated in Figure 6.4. The results for the stability analysis are depicted in Figure 7.7.

7.2.3. Experimental Validation of Finite Element Analysis

Validation of the computational model is crucial in order to be able to use the results from the performed FEAs in the design process of real-life prototypes. This validation can be done by fabricating different structures that are simulated and examine these in the physical world. Validating the relations observed from the FEA is done by testing the torsional stiffness of a small amount of physical samples, and check the correlation with the predicted value from the simulations. This underlines the advantages of FEA over physical tests. Physically testing the torsional stiffness is done using a biaxial testing machine, where a specified rotation with a set angular velocity is applied to the structure. The biaxial testing machine is able to measure the applied torque on the structure by measuring the reaction moment on the base of the structure, similar to the Abaqus simulation.

Material Properties Analysis

As explained in Section 6.3, three different types of simulations were performed:

1. Rotation applied to a structure where only the cosine-shaped beam is made from TPU, while other sections are made from the arbitrary linear elastic material.

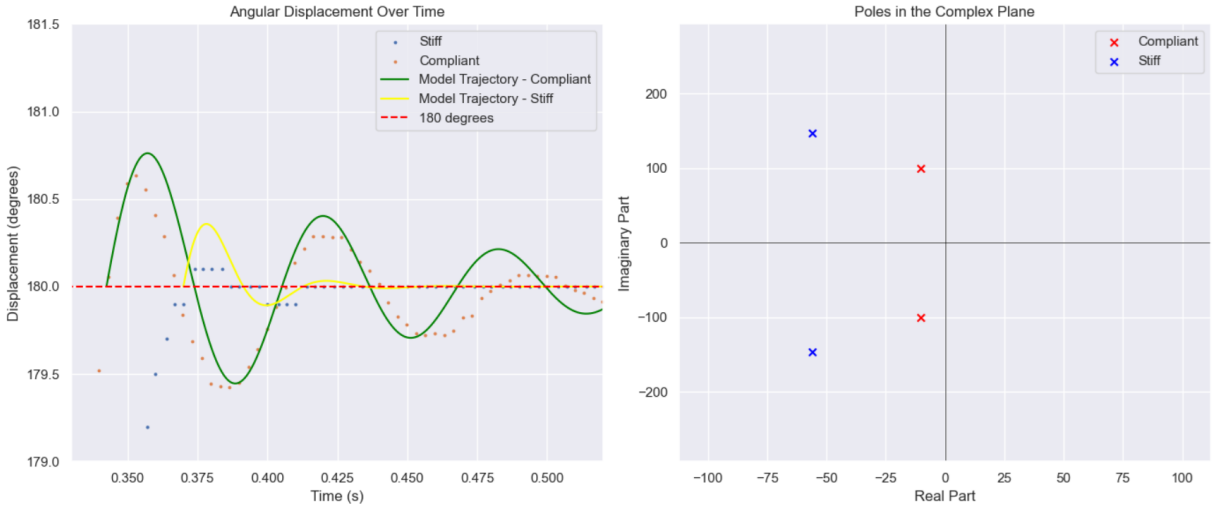

Figure 7.6: The model of the dynamic behaviour of a specific unit cell and the corresponding experimental results. In addition, the poles of the transfer function in the left half of complex plane.

2. Rotation applied to a structure where both the cosine-shaped beam and vertical support beams are made from TPU, and the remaining parts are made from the arbitrary material.
3. Rotation applied to a structure where the material composition of the unit cell is uniform and the Young's Modulus of the entire structure will be changed.

Sample	k_s (Nm)	k_c (Nm)	$\Delta\%k$ (%)
Uniform TPU	0.835	0.530	57.5
Ring sections are 15% PLA	0.868	0.558	55.5
Ring sections are 40% PLA	0.833	0.477	74.7
Ring sections are 90% PLA	0.820	0.550	49.1
Ring and vertical beam sections are 15% PLA	1.806	0.876	106.1
Ring and vertical beam sections are 40% PLA	1.848	0.917	101.5
Ring and vertical beam sections are 40% PLA	1.764	0.826	113.8

Table 7.1: Experimentally obtained stiffness data from samples with different material sections.

The experimentally obtained data and the linear curve fitted to this data can be observed in Figure B.9. This figure shows a clear difference between the open and closed state of each structure. The slopes obtained from these figures are compared to their respective stiffness. The data from the experimental setting are shown in Table 7.1. In Figure 7.8, a comparison is made between the experimentally obtained results and the expected results from the FEA that simulated changing the Young's modulus of certain sections of the unit cell.

Geometric Ratio Analysis

As explained in Section 4.1, the influence of changing two geometric ratios is determined by systemic analysis of different combinations of these geometric ratios. The simulation results can be validated by manufacturing several structures with different combinations of the geometric ratios. All structures are uniformly manufactured from Cheetah 95A TPU using FDM.

The experimentally obtained data and the linear curve fitted to these data can be observed in Figure B.10. This figure shows a clear difference between the open and closed state of each structure. The slopes obtained from these figures are compared to their respective stiffness. The data from the experimental setting are shown in Table 7.2. In Figure 7.9, a comparison is made between the experimentally obtained results and the expected results from the simulation.

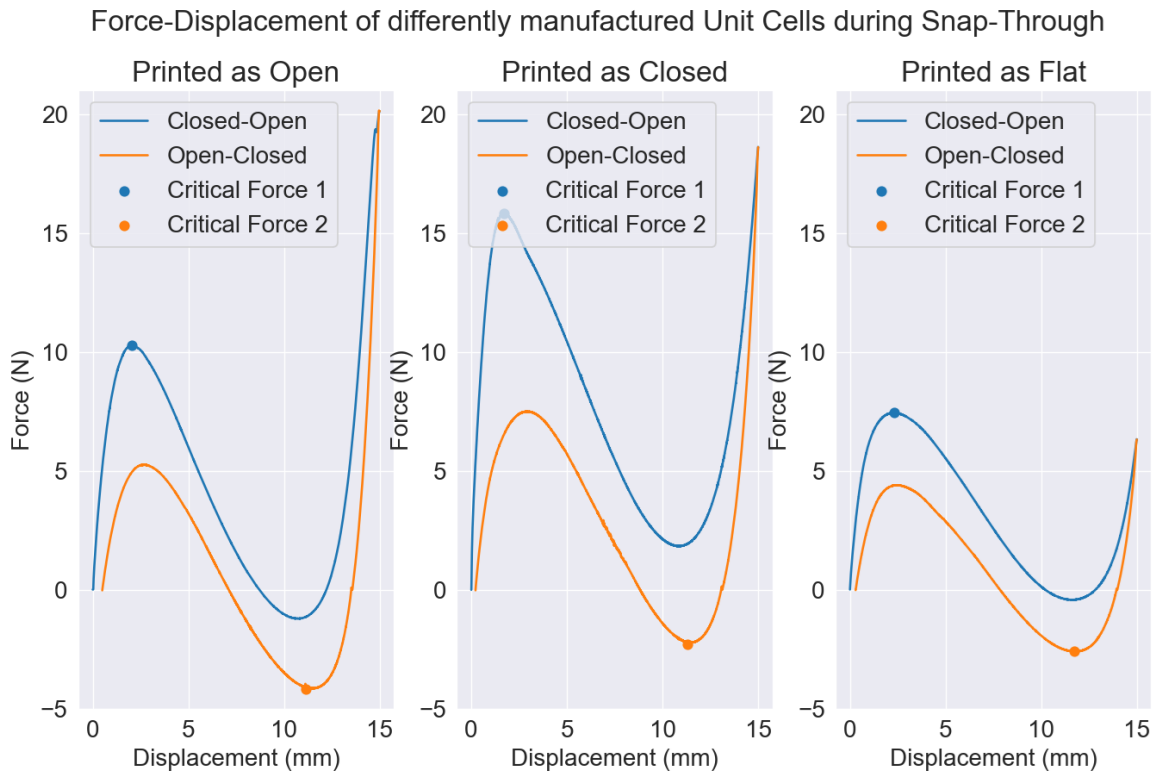

Figure 7.7: Snap-though behaviour of differently manufactured unit cells, where left is manufactured in open configuration, middle is manufactured in closed configuration and left is assembled manually by forcing a flat beam into a cosine shape

Sample	k_c (Nm)	k_s (Nm)	$\Delta\%k$ (%)
$t2/t1 = 7$ & b/l = 0.8	0.947	0.765	23.7
$t2/t1 = 6$ & b/l = 0.8	0.915	0.686	33.4
$t2/t1 = 6.5$ & b/l = 0.3	4.168	2.990	39.4
$t2/t1 = 8$ & b/l = 0.3	4.382	3.677	19.2

Table 7.2: Experimentally obtained stiffness data from samples with different geometric ratios.

7.3. Performance of the Bistable Variable Stiffness Gripper (B-VSG)

The final design of the B-VSG is tested while mounted on the robot arm. The grip force of one of the two end effector is measured using the load cell. The results for the grip force in the compliant and stiffer state can be observed in Figure 7.10.

The results show an increase in measured force when the metamaterial is deformed, a peak force and relaxation of the TPU when the final deformation has been reached, followed by a final decrease of the grip force when the gripper finger rotates back to its initial position. The difference in grip force for a single end effector between the compliant and stiff state is approximately 0.2 Newton.

7.3.1. Actuated Bistable Variable Stiffness Gripper (B-VSG) Performance

The fabricated metamaterial for the actuated gripper, which is based on the stated design choices, is placed in the biaxial testing machine to measure the torsional stiffness in the compliant state and the stiffer state. The results from the experiments are illustrated in Figure 7.11. The torsional stiffnesses for both states of the metamaterial, and the $\Delta\%k$ and Δk are shown in Table 7.3

The grip force is measured for the compliant state and for the stiffer state of the metamaterial. The

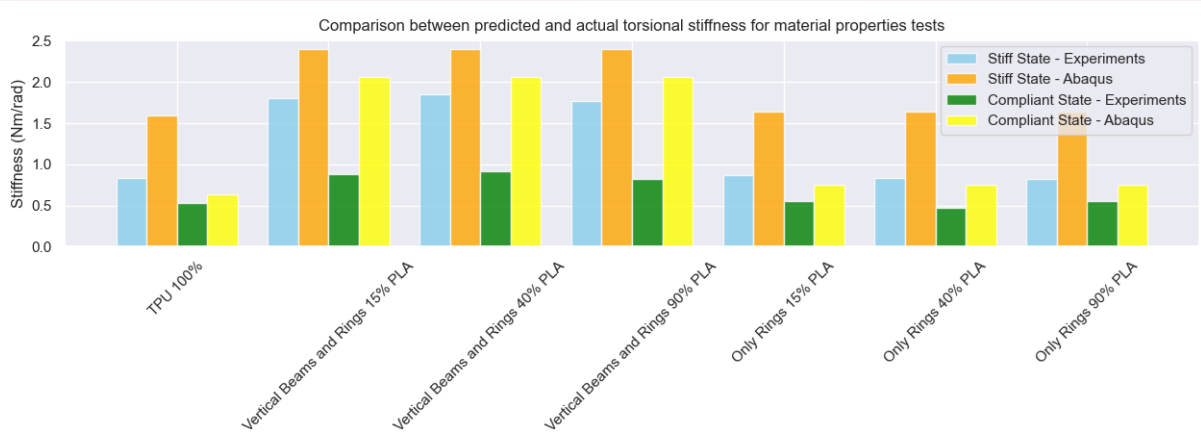

Figure 7.8: Comparison between obtained torsional stiffness from linearized experimental data and predicted torsional stiffness from simulations in Abaqus for changing the Young's modulus of selected sections.

k_c	0.429 Nm/rad
k_s	0.602 Nm/rad
$\Delta\%k$	40.2%
Δk	0.173 Nm/rad

Table 7.3: Stiffness and (Percentage) Stiffness Difference in the Metamaterial

results are illustrated in Figure 7.12. The final design of the actuated gripper is visible in Figure 5.6a. The difference in grip force between the compliant and stiff state is approximately 0.6 Newton.

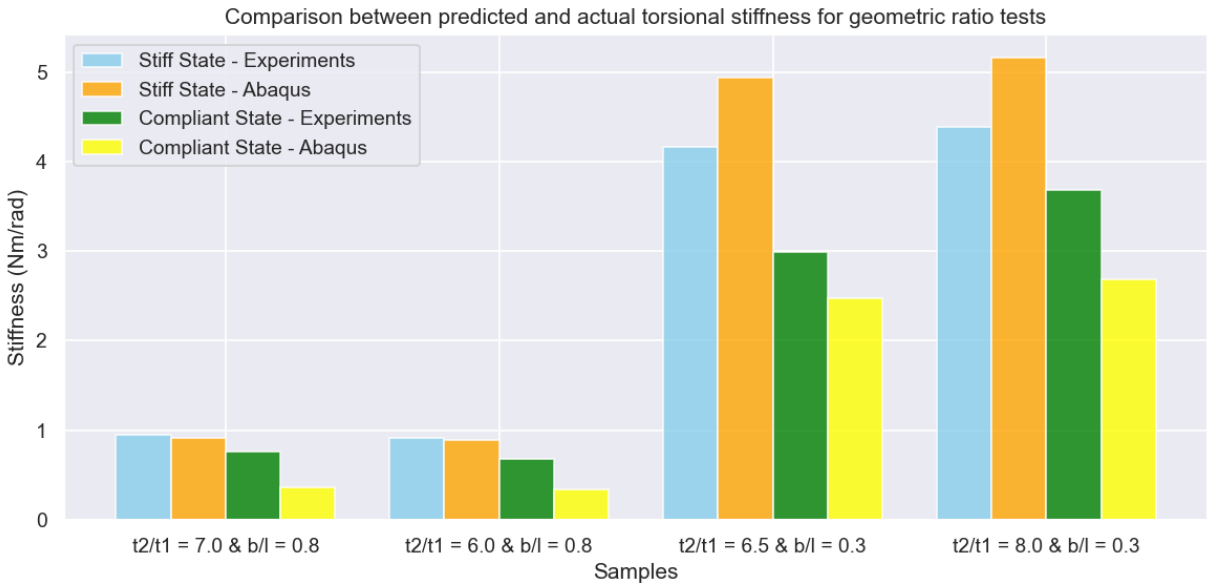

Figure 7.9: Comparison between obtained torsional stiffness from linearized experimental data and predicted torsional stiffness from simulations in Abaqus for changing geometric ratios

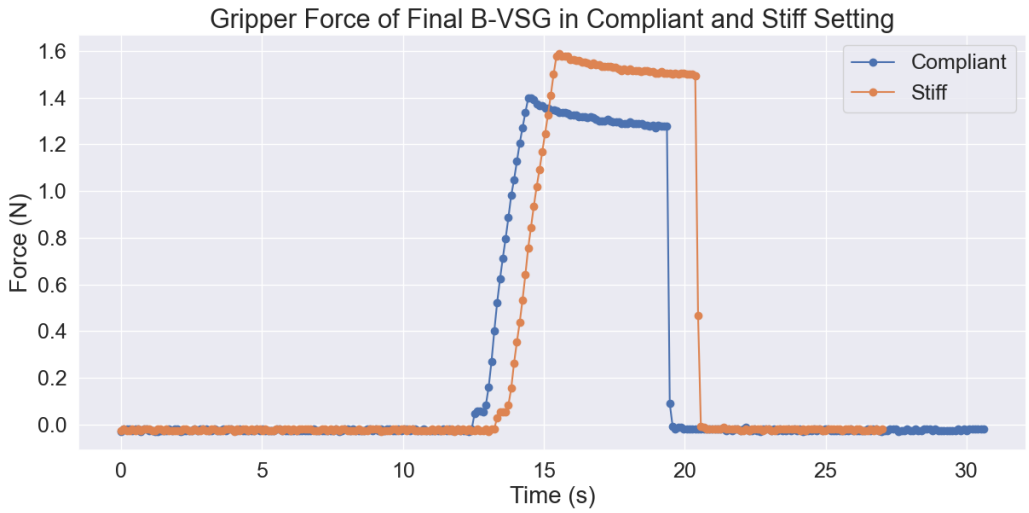

Figure 7.10: Grip force measurements on the gripper design, in compliant state and in stiffer state.

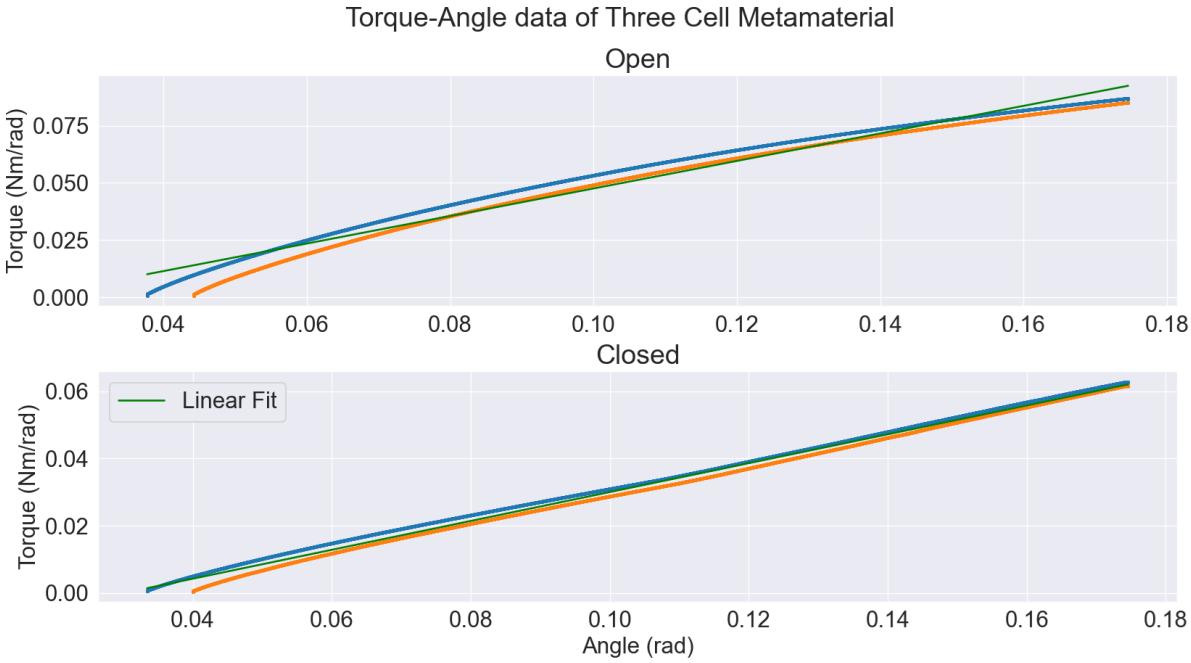

Figure 7.11: Experimentally derived torque-angle data for the three-celled metamaterial used in the actuated gripper proof-of-concept, for the compliant state and the stiff state

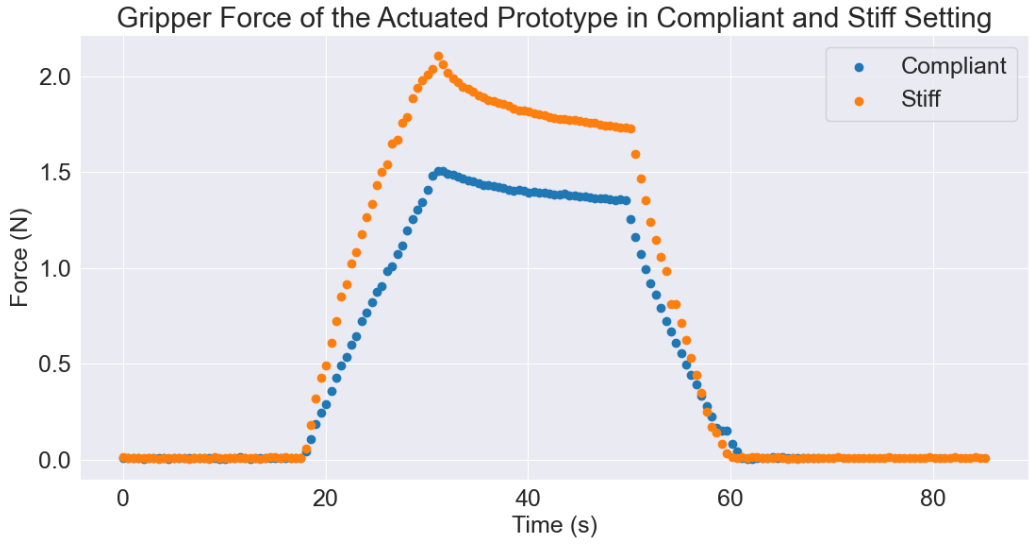

Figure 7.12: Grip force measurements on the actuated gripper design, in compliant state and in stiffer state.

8

Discussion

This chapter evaluates the experiments conducted and the results obtained. By comparing theoretical models with experimental outcomes, it aims to validate the accuracy of FEAs and identify any performance discrepancies affecting practical applications. The chapter also explores the stability and dynamics of the metamaterial, analyzing how design choices influence performance. It provides a detailed examination of the limitations and potential improvements of the final designs, offering insights into the entire design process and the challenges encountered. Additionally, reflections on the thesis process analyze the research approach, highlighting key learning points.

The main goal of this chapter is to integrate theoretical insights with experimental data to improve the design of the VSG and the application of bistable metamaterials. It seeks to advance the field by proposing design optimizations and exploring their implications for technology and engineering.

8.1. Comprehensive Evaluation of Experimental Data in the Bistable Metamaterial Design

This section examines the results from FEAs alongside experimental data, focusing on the development of bistable variable stiffness actuators using metamaterials. The analysis explores the dynamic behaviour of bistable structures, the stability of the structures based on manufacturing, and how different geometric ratios and materials influence the metamaterial stiffness, comparing simulated models to real-world results. This comparison identifies inconsistencies and provides insights into the effectiveness of the designs. The objective is to bridge the gap between theory and practice, ensuring that the models accurately predict how these metamaterials perform. The analysis not only tests assumptions but also aims to refine the approach to designing these complex structures.

8.1.1. Analysis of Geometric Ratios on Stiffness Difference Through Finite Element Modeling

Depending on both b/l and $t2/t1$, the stiffness ranges between 14.25 Nm/rad and 0.02 Nm/rad in the open state of the bistable structure, and between 10.08 Nm/rad and 0.01 Nm/rad in the closed state of the bistable structure. From Figure B.3 it can be clearly observed that the FEA predicts that both b/l and $t2/t1$ have a clear effect on the stiffness. As seen in Figure **??**, $t2/t1$ is predicted to have a significant influence on the Δk for small values of b/l, and on the $\Delta\%k$ for large values of b/l. The highest $\Delta\%k$ is predicted where both b/l and $t2/t1$ are large.

In the large b/l region, the Δk is very small in both the compliant and stiff settings. This results in a minimal difference between the stiffnesses, at a minimum of 0.01 Nm/rad, but a significant $\Delta\%k$, reaching a maximum of 270.4%, because the torsional stiffness in the compliant setting is nearly zero. Conversely, in the small b/l region, the stiffness is relatively high in both the compliant and stiff states, leading to a small $\Delta\%k$ of a minimum of 27.7% and a large Δk of up to 4.2 Nm/rad. There appears to be a trade-off between a large Δk and a large $\Delta\%k$. Depending on the application, the geometric ratios should be carefully considered to balance between percentage increase and absolute difference in stiffness.

The FEA results show that the Δk of the structure decreases most significantly by increased b/l and $t2/t1$. In contrast, increasing $t2/t1$ and decreasing b/l result in a unit cell that has a large Δk, but has

a small $\Delta\%k$ and is relatively stiff in both the open and closed states. Four different hypothesis can be formulated based on the FEA results:

- Increasing b/l increases $\Delta\%k$
- Increasing $t2/t1$ for large b/l increases $\Delta\%k$
- Increasing $t2/t1$ for small b/l increases Δk
- Increasing b/l decreases Δk.

8.1.2. Analysis of Material Properties on Stiffness Difference Through Finite Element Modeling

From the simulation where only the cosine-shaped section is constantly made from TPU and all other sections are changed, see Figure 7.3, it is evident that the stiffness differences between the two states of the unit cell converge to a minimum difference. This can be explained (primarily) by the increasing stiffness of the vertical support beams. When the Young's modulus of the vertical support beams is low, they flex (bend) during deformation, but when the Young's modulus is sufficiently high, only the cosine-shaped beam deforms. This is illustrated in Figure 8.1. The fact that $\Delta\%k$ and Δk do not go to zero when the Young's Modulus of the vertical beams increase further, but rather converge to $\approx 20\%$ and ≈ 0.3 Nm/rad, has to do with the changing geometry of the structure during snap-through.

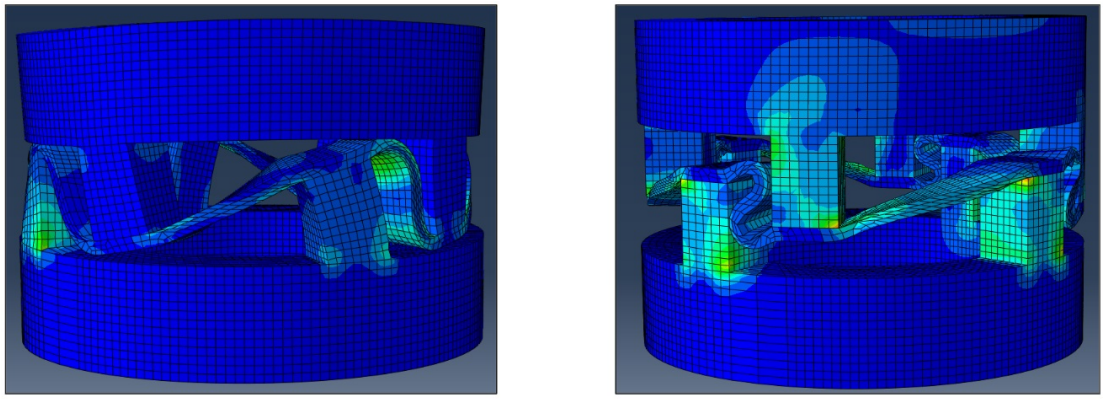

Figure 8.1: Deformation of the unit cell under angular displacement, when the ring sections and vertical support beams have a low Young's Modulus (left) and high Young's Modulus (right)

Changing the geometry changes the stress distribution in the structure during loading. When the structure is closed, the *web-flange junction* ("arm pit" where the vertical support beam and cosine-shaped beam meet) of the structure acts as a flexure hinge during angular displacement, this hinge reduces the force required to rotate the structure. When a rotation is applied to the open structure, on the other hand, there is no flexure hinge. The stresses are concentrated above the web-flange junction and at the corners of the base of the vertical support beam. The specific stress distribution is dependent on many factors, including the difference in moment of inertia of the vertical support beam and the cosine-shaped section and the material used in both sections, since both these factors can cause a *strain mismatch*.

The simulation where only the ring section is changed, see Figure 7.3, shows that changing the ring sections has an effect similar to changing the Young's modulus of both the ring sections and vertical support beams. However, the effect of changing only the material properties on the ring sections is much smaller. This can be explained by the fact that the ring section-the section which material properties are changed during this simulation-is only subjected to local moments at the junctions between the vertical support beams and the ring section and is not further loaded due to rotation. The deformation, and resistance to this deformation, happens primarily in the vertical support beams and the cosine-shaped section, keeping these constant results in small changes in the overall stiffness difference.

The third simulation, see Figure 7.3, shows the stiffness difference when the material is uniform throughout the structure, meaning there is no strain mismatch that is caused by different material properties,

only by changing geometries. The $\Delta\%k$ is constant regardless of the Young's modulus, because the only difference in stiffness between the open and closed state is due to the changing orientation of structural components, which is constant for all simulations. The forces required to realise the simulated rotation, and thus the overall stiffnesses, increase dramatically since the entire structure becomes stiffer, however the $\Delta\%k$ between the two torsional stiffness remains constant. This is interesting, because it suggests that the percentage change in stiffness is indeed material independent, provided the structure is uniformly made from linear elastic material.

An interesting observation from Figure 7.3a is that the geometric $\Delta\%k$, solely caused by changing the orientation of structural sections, is different when the material is uniform and when the material of certain sections is changed. This geometric $\Delta\%k$ is shown by the value of $\Delta\%k$ that the individual curves converge to. The suggested hypothesis is that these various geometric $\Delta\%k$ are different from each other because of different strain mismatches in the structures. Although the strain mismatch caused by the changing geometries is constant for all three simulations, in the first and second simulation there are strain mismatches caused by material inconsistencies in the structure also. These strain mismatches caused by material inconsistencies result in different stiffness value that the simulations converge to.

The yellow line in Figure 7.3 indicates the Young's Modulus of generic PLA [88], the material that will be used during physical tests. The results from the computational model suggest that by using PLA as a material in the vertical support beams and the ring segments, the $\Delta\%k$ between the two cells can be greatly decreased.

Evident from all three simulations is that the overall stiffness of the unit cell seems to be increasing when the Young's modulus of certain (or all) sections is increased. This can be explained by an increase in the flexural modulus of the sections that have an increased Young's modulus, effecting the Δk of the unit cell.

Based on the FEA results, three different hypothesis can be formulated:

- Increasing the Young's modulus of the ring sections and vertical support beams, decreases $\Delta\%k$ and Δk, where the vertical support beam has the largest effect.
- Decreasing the Young's modulus of the ring sections and vertical support beams, increases $\Delta\%k$.
- Increasing the Young's modulus of sections of the unit cell increases the overall stiffness.

8.1.3. Validation of the Finite Element Analyses

From the FEA, several hypotheses are formulated regarding the $\Delta\%k$ and Δk. In this section the conclusions drawn from the FEA will be compared to the results obtained from the experiments.

- **Increasing b/l increases $\Delta\%k$**: This is rejected based on the results of the experiments. This is most likely caused due to dry friction, which causes the closed cells with large b/l to be much stiffer than expected.
- **Increasing $t2/t1$ for large b/l increases $\Delta\%k$**: Based on the conducted experiments, this cannot be confirmed or rejected. The largest b/l that is used in the experiment is not sufficiently large to test the hypothesis. The results seem to be valid, since there is a small, expected decrease in $\Delta\%k$ when increasing $t2/t1$ for $b/l = 0.8$.
- **Increasing $t2/t1$ for small b/l increases Δk**: This does not seem to be in accordance with the experimental results, likely because of differences between the physical structures and the simulated structures.
- **Increasing b/l decreases the overall stiffness**: This is supported by the experimental results. The stiffness of structures with $b/l = 0.8$ are consistently smaller than the stiffnesses for $b/l = 0.3$.
- **Increasing the Young's Modulus of the ring sections and vertical support beam, decreases $\Delta\%k$ and Δk, where the vertical support beam has the largest effect**: This not supported by the experimental results, likely because of differences between the physical structures and the simulated structures.
- **Decreasing the Young's modulus of the ring sections and vertical support beams, increases $\Delta\%k$**: This hypothesis has not been properly tested. It is only possible to use a smaller Young's modulus in the experimental setting by decreasing the infill of the TPU. However, this resulted in very fragile structures and was therefore not feasible to test.

- **Increasing the Young's modulus of sections of the unit cell increases the overall stiffness**: This is largely supported by the experiments, as there is a clear increase between the experiments using a uniform TPU unit cell and the experiments that used PLA for the vertical support beams.

According to the hypothesis that the Young's modulus of the PLA parts should increase with an increasing infill percentage [88] (see Chapter 3) and the FEA results, the structure should become more stiff with a larger infill of PLA. However, this is not the case. This could be caused by discrepancies between the FEM and the physical structure. Another explanation for the lack of effect by changing the infill could be because the uncertainty during the experimentation is larger than the uncertainty on the data presented in the research by Rismalia et al.[88].

Interesting to note, the difference between the FEA results and the experimental results are much greater in the uniform TPU unit cell in Figure 7.8, than in the uniform TPU cells in Figure 7.9. This underscores the effect of the mechanical interlock. The results in Figure 7.9 are from structures where the TPU is fused and the results in Figure 7.8 shows a uniform TPU unit cell with mechanical interlocks. The increased discrepancy in the latter shows the negative effect of the interlocks.

In Table 7.3, the experimentally obtained stiffnesses, $\Delta\%k$, and Δk for the three-celled metamaterial used in the actuated prototype are discussed. This metamaterial has also been subjected to FEA. This FEA is performed to find an optimum for the trade-off between $\Delta\%k$ and Δk. By examining the stiffness values from the FEA for the same geometric ratios as the physically tested structure, the accuracy of this model can be assessed. According to the FEA results, the stiffness in the compliant and stiffer state should be 0.56 Nm/rad and 0.22 Nm/rad, respectively. Resulting in a $\Delta\%k$ and Δk of 0.34 Nm/rad and an 154.5% increase. However, the experimental results show a lower (percentage) stiffness difference. Similar to the validation of the single bistable cell structures, there are discrepancies between the results from the experimental setting and the FEA results.

8.1.4. Discrepancies between the Finite Element Analysis and the Experimental Setting

In the simulation that examines stiffness changes caused by altering the Young's modulus of the vertical support beams and the ring section, there is a significant difference between the stiffness predicted by the model and the stiffness actually measured in the experimental setting. Explaining this discrepancy requires investigating the mechanical joints between the TPU and PLA sections. In the model, PLA and TPU are fused, and the structure behaves as a single homogeneous structure. However, in the physical experiments, PLA and TPU are not fused but rather connected using mechanical interlocks and pressure fitting. This causes TPU and PLA to delaminate when the structure is in the open state, as illustrated in Figure 8.2, decreasing the stiffness. The fact that the materials are not fused, poses a likely explanation why the real-life structures are more compliant than the homogeneous structure in the Abaqus model.

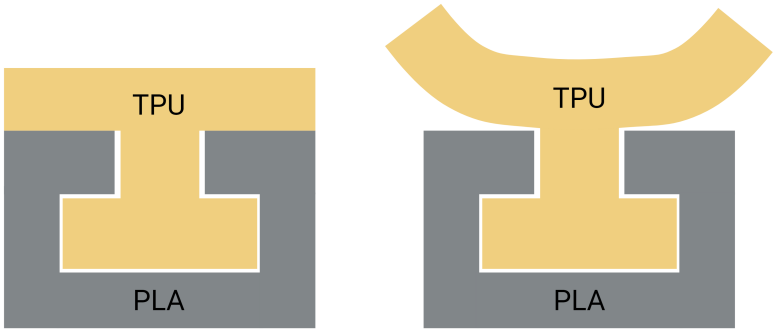

Figure 8.2: Left: TPU and PLA joint using the mechanical interlock when the TPU and PLA are laminated. Right: TPU and PLA joint using mechanical interlock when the TPU and PLA are delaminated during snap-through to the open state of the structure

Another mismatch between the simulation results and real-life experiments, are the discrepancies observed in the results for the geometry tests of the structure when it is in the closed state. The stiffness in real-world experiments is constantly higher. This is likely due to internal dry friction in the structure.

A possible solution for this is to increase δ of the unit cell to increase the distance between the vertical support beams and the ring sections.

There are many factor contributing to the observed discrepancies between the simulation results and the experimental results. Some examples of contributing factors that come into play in the physical experiments, but are absent in the FEA, are:

- Material inhomogeneity
- Assembly imperfections
- Friction between internal structures
- Manufacturing imperfections
- (Micro)fractures
- Inherent randomness
- Relaxation

8.1.5. Evaluating the Correlation Between Dynamic Modeling and Experimental Findings in the Bistable Structure

The oscillations in the two trajectories in Figure 7.5, corresponding to the bistable structure's two stable states, exhibiting different amplitudes and frequencies. This discrepancy suggests variations in the stiffness and damping coefficient between the two states. Such differences indicate that the mechanical properties of the bistable structure are state-dependent, affecting its dynamic response. The observed oscillations can be attributed to several interacting forces:

- **Inertia of the Mass**: The added mass significantly contributed to the system's inertia, affecting the angular momentum and oscillatory motion.
- **Gravitational Force**: The gravitational force acting on the mass influenced the oscillation amplitude and frequency, particularly when the structure is in a tilted position.
- **Spring-Damper Characteristics of the TPU**: The intrinsic spring-damper behaviour of the bistable structure played a crucial role in the damping and stiffness characteristics observed during oscillation.

A perfect fit between the dynamic model and experimentally obtained data is not found, see Figure 7.6. This could be caused due to several reasons. Most likely, the model is oversimplified. In the model, gravitational forces are neglected and the behaviour is simplified. The stiffness term in the model described in Section 6.4.3 is linear with respect to the displacement. However, the experimental results show a slight non-linearity. This non-linearity is not present in the model.

Although the specific stiffness and damping coefficients cannot be concluded from the model, it does give some insight in the order of magnitude of the stiffnesses and damping coefficients. In addition, it shows an observable difference for both the stiffness and the damping coefficient between the open state and the closed state of the bistable cell.

From the model, the stiffnesses and damping coefficients that closest resembled the experimental data are: $k_c = 0.95Nm$ and $c_c = 0.002Nms/rad$ and $k_s = 2.3Nm$ and $c_s = 0.01Nms/rad$. The derived stiffnesses are within expectation based on the results from the FEA. Using these values, the poles in the complex plane for the corresponding transfer function for Equation 6.2 can be found. The poles are shown in Figure 7.6. Given the oscillating behaviour and the poles that are complex conjugates, the structure behaves in both the stiff and compliant state as an *underdamped system*.

8.1.6. Analyzing Stability of Different Manufacturing States of the Bistable Structures

From the results in Figure 7.7, it becomes clear that when the unit cell is manufactured in either of the two states, the manufacturing state is more stable then the other state. If the cosine-shaped beam is manufactured flat and is forced into a cosine shape this results is a more symmetric force-displacement curve during snap-through. Meaning that the critical forces (F_c) necessary to snap between the equilibrium states are similar when snapping from closed to open and from open to closed. From the analysis, it is found:

- **Closed manufacturing state**: A lot of force is required to change from closed to open, but very little is needed to return to closed
- **Open manufacturing state**: Less force is required to snap from closed to open when compared to the unit cell manufactured in the closed state, however more force is required to snap back
- **Flat manufacturing state**: Both critical forces are lower, making it easier to switch between states.

From these observations, ensuring the stability in the open state is most crucial, since torsional load applied to the open structure is prone to unintended snap to the closed state. The stability under load in the closed state is reinforced by the vertical support beams hindering the range of motion. Therefore, the bistable structure should be manufactured in an *open state*, preventing unintended snap during torsional load (due to axial-torsional coupling) and increasing the reliability of the VSG overall.

Improving Stiffness Difference by Investigating Stability of the Bistable Cell
The specific stability region of the cylindrical bistable cell is unknown. It might be possible to improve the design slightly more by searching for the boundaries of the bistability region. The geometry analysis in Figure **??** shows that there is a notable effect of $t2/t1$ on the $\Delta\%k$ and Δk, depending on b/l. For small values of b/l the Δk can be decreased by lowering $t2/t1$. However, decreasing $t2/t1$ too far will result in a loss of bistability. Figure 4.4 shows the bistability region for the planar metamaterial. The stability regions of the cylindrical cell is not equal to the regions shown in Figure 4.4 and are influenced by the manufacturing as well. Similar to the planar metamaterial by Yang and Ma [84], the stability is still dependent on the ratio between $t2$ and $t1$, and between b and l. Improving the stiffness difference of the metamaterial, by decreasing the difference in the smaller bistable cells, is possible by approaching the boundaries of the bistability region.

8.1.7. Consistency of Experimental Results

When performing physical experiments on the 3D-printed structures using the ZwickRoell biaxial testing machine, the structures were loaded three times to average the slopes and to reduce measurement noise. However, the data showed inconsistencies. In particular, the first load cycle is different from the other load cycles and often strongly nonlinear. This is likely caused due to friction effects and relaxation of the material. In addition, the angular displacement at which the structure experienced zero torque is not constant over the load cycles. This is likely caused by relaxation of the polymer also. Another explanation is slip between the grippers of the biaxial testing machine and the samples, however this possibility is reduced by the use of a specially designed clamp to secure the samples in the gripper of the testing machine, see Figure B.5.

Due to these facts, measurements of the first load cycle were omitted from the analysis. However, when the structure is applied in an actuator, it can be expected that the first deformation after long rest is also nonlinear and might be different than expected. This influences the reliability of the actuator design, as the first load cycle could be different from the following load cycles.

8.2. Design Choices in the Bistable Variable Stiffness Gripper after Experimentation

Based on the findings from Sections 7.1 and 7.2, the gripper concepts are further developed. The gripper designs are aimed to maximize the difference in stiffness between the two stiffness settings of the grippers. Based on the analysis in Equations 5.5, the $\Delta\%k$ and the Δk of the bistable cell connected to the end effectors were maximized. While the $\Delta\%k$ and the Δk of the bistable cells connected to the servomotor were minimized. The grippers generate a lower grip force in the compliant setting and a higher grip force in the stiffer setting. The design choices for the actuated and unactuated prototype will be discussed in this section.

8.2.1. Geometric Ratio Selection in the Actuated and Unactuated Prototype

The geometric ratios investigated in this research are $t2/t1$ and b/l, as shown in Figure 4.1. Based on the simulation results, the optimum balance between $\Delta\%k$ and Δk is achieved when b_l (the amplitude of the cosine-shaped section of the larger cell) is set to 0.625 and b_s (the amplitude of the cosine-shaped section of the smaller cells) is set to $\frac{b_l}{2}$ to realize bistability of the constrained metamaterial.

As discussed, the amplitude of the cosine-shaped beam (or b) in the *actuated prototype* is dependent on the stroke length of the pneumatic actuator. In the actuated prototype, the stroke of the piston fixes the value for b_l. To realize controllable stiffness switching, the sum of the amplitudes of all cosine-shaped beams present in the metamaterial ($\sum b$) is equal to the stroke length of the piston (15mm). This results in $b_l = 7.5mm$ and $b_s = 3.25mm$.

The actuation unit that controls the stiffness modulation is omitted in the *unactuated prototype*. This alleviates the constraint that the stroke length of the piston imposes on the actuated design. Due to the increased design freedom in the unactuated design, the geometric ratios were set to the optimal values of $b_l/l = 0.625$ and $b_s = \frac{b_l}{2}$.

According to the FEA, for smaller cells, the thickness ratio $t2/t1$ should be minimized to reduce the stiffness difference between the states of the structures. In contrast, this ratio should be maximized in the larger cell to increase the (percentage) stiffness difference. However, lowering $t2/t1$ too much in cases where b/l is small will cause the structure to lose its bistability. To maintain bistability, the thickness ratios $t2/t1$ for both the large and smaller cells are uniformly set to 6. This precautionary measure is taken because if the ratio in the larger cell is decreased, the structure may only achieve monostability or simple stability. Since the exact region for bistability is unclear, a higher than optimal $t2/t1$ ratio is chosen for the smaller cells to ensure the bistability of the unit cells.

8.2.2. Material Selection in the Actuated and Unactuated Prototype

From Figure 7.3, it is clear that the biggest change is realised by changing the material of the vertical support beams. Following these results, to decrease the $\Delta\%k$ in the smaller two cells a stiff material should be used in the vertical support sections and the ring sections of the smaller cells. On the contrary, in the larger cell, a compliant material should be used to increase the $\Delta\%k$. Since this research is limited to the use of PLA and TPU (or FilaFlexible40), the stiffer sections of the structure should be made from PLA and the more compliant sections should be made from TPU.

Contrary to the FEA results, the experimental results in Figure 7.8 indicate that the $\Delta\%k$ and the Δk are actually largest when PLA is used in the vertical support beams. Using PLA in the vertical support beams also makes a bistable unit cell stiffer in both the open and closed state of the cell. This difference between the experimental results and the simulation results likely stem from discrepancies between the manually assembled unit cells using mechanical interlocks and the homogeneous model used in the simulation with fused boundaries between the TPU and PLA.

The material selection of the *actuated prototype*, see Figure 5.6a, is based on the simulation results solely, primarily due to the limited time for the research and the delayed possibility of experimental validation. The metamaterial design is aimed to maximize both the $\Delta\%k$ and the Δk. Thus, the material in the smaller cells is a combination of PLA and TPU, where the vertical support beams and ring sections are made from PLA. While the larger cell that is connected to the end effector is uniformly made from TPU. The actuated prototype serves as a proof-of-concept prototype for the VSM and the pneumatic stiffness actuation.

In contrast to the proof-of-concept actuated prototype, the *unactuated final design*, see Figure **??**, is finalized after the experimental validation of the FEA is performed. Therefore, the material selection is slightly different. Because of this the three-celled metamaterial, that forms the VSM of the unactuated final gripper, is constructed using PLA in the vertical support beams and ring sections, and FilaFlexible40 as material of the cosine-shaped beams. The different materials are connected using the mechanical interlocks shown in Figure 6.1.

The TPU (or FilaFlexible40) is printed at an infill of 40%. This is done because of two main reasons: 1) The cosine-shaped section is uneffected by increasing the infill further and a lower infill makes the cosine-shaped beam prone to defects. 2) The lower infill in the vertical support beam result in a larger $\Delta\%k$ and larger Δk, according to the simulations. Since a lower infill results in a lower effective Young's modulus of the flexible material. The PLA is printed at 90% infill to increase the Young's modulus of the vertical support beams and ring as much as possible. According to the simulation results, this results in a smaller $\Delta\%k$ and smaller Δk.

8.3. Assessing the Design and Performance of Bistable Variable Stiffness Gripper Development

This section examines the performance and design challenges faced in developing the B-VSG. It looks at the iterative design process, showing how experimental results and theoretical analysis have shaped the gripper prototypes. The discussion centers on mechanical reliability issues and possible improvements to boost performance. This evaluation covers the technical obstacles overcome and points out areas needing further refinement, stressing the need for ongoing optimization to enhance functionality and reliability.

8.3.1. Challenges and Enhancements for the Actuated Gripper Prototype

This subsection discusses the reliability issues and potential improvements for the actuated gripper prototype, particularly focusing on the stiffness actuation mechanism. It highlights the limitations faced with the existing prototype, primarily due to the unreliability of the linear pneumatic actuator used for adjusting stiffness. The section also outlines several design modifications aimed at enhancing the gripper's performance. These improvements draw on insights from both experimental results and finite element analysis to refine the prototype into a more effective and dependable device.

Reliability of Stiffness Actuation

The linear pneumatic actuator that is used to change the stiffness of the metamaterial in the actuated gripper prototype is quite unreliable. The choice for an off-the-shelf linear pneumatic actuator is substantiated by the low cost and availability of the piston, however the fixed stoke of the piston forms a geometric constraint on the metamaterial. The off-the-shelf piston has no known pressure rating, and it is not known how much pressure is needed to realise snap-through. When pressure is applied to the piston to open it and snap the metamaterial, this motion is repeatable and reliable. However, when the piston is closed to realise snap-back, the pressure required to achieve this is too high and small air leaks are audible. Therefore, snapping through and back is not reliable using the off-the-shelf miniature piston that is used in this research.

Improvements to the Actuated Prototype

The forces that the actuated gripper demonstrator is capable of generating are quite low and the difference is small. Some improvement to the gripper can be made to increase the stiffness difference of the demonstrator. First, the geometric constraint imposed by the stroke length of the piston can be omitted. Either by using a custom integrated piston, or by omitting the stiffness switching actuation unit from the design all together. When this constraint is alleviated, the found optimum value for b_l (visible in Figure 7.4) can be used in the design of the metamaterial. Another feature that can further improve the stiffness difference in the use of a second gripper arm. Using a single servo motor, two coupled gripper arms can be actuated. These improvement are considered in the design of the unactuated prototype and are implemented in the final unactuated gripper design.

Another improvement is reassigning material to specific sections in the metamaterial. The actuated gripper design is in accordance with the findings from the FEA, not with the experimental results. The reason for this is that the biaxial testing machine, used to do experimental validation, was available only after a significant portion of the research timeline. Because of this, the decision was made to trust the FEA results and design the gripper based on these results. However, the experimentation showed that making the vertical support sections and ring sections of the unit cell out of PLA will increase the stiffness difference and percentage stiffness difference, contrary to the FEA results. Changing the material in these sections to PLA will increase the overall stiffness difference of the VSA. These improvements are applied to the design of the unactuated prototype and are considered in the final B-VSG design.

8.3.2. Performance of Final Design of Bistable Variable Stiffness Gripper (B-VSG), Limitations and Possible Enhancements

The final design is influenced by an earlier version, the *unactuated prototype*, which includes two grippers. The force exerted by one of these grippers is measured and is shown in Figure 7.10. The measurement setup is detailed in Figure B.12. It is worth noting that these results are for a single gripper finger. Since the design incorporates two gripper fingers working together, the total gripping force is actually double. Therefore, the highest grip force measured for the B-VSG is 3.2 N, and the lowest is 2.8 N, marking an increase of about 14.3%.

However, these values are not the highest or lowest forces the gripper can achieve. Stronger forces may be observed when the metamaterial is rotated further. The forces that are measured at a fixed angle of deflection, maintained during tests in both the compliant and stiffer states of the material. If the friction is ignored, the percentage difference in grip force between the two states should stay consistent regardless of how much the metamaterial deflects, because the material acts like a linear torsional spring in both states.

Yet, friction is likely a significant factor in the mechanism, particularly because of the low forces shown in Figure 7.10. Comparing the actuated prototype to the final design, the (percentage) difference in percentage in the actuated prototype (see Figure 7.12) is larger than in the final design, contrary to what previous analyses predicted. The final design has more moving parts, resulting in higher dry friction in the gripper mechanism. This increased friction significantly impacts the measurements and suggests that reducing friction should be a focus in future improvements.

Inconsistent Flexible Material Usage
Throughout the experiments and analyses, Ninjatek Cheetah TPU is used. Cheetah TPU is well-documented in literature and thoroughly characterized, allowing its material properties to be used in the FEA. However, towards the end of the project, Filatech FilaFlexible40 became more available. Although most material properties of FilaFlexible40 are unknown, its shore hardness is similar to that of Cheetah TPU, making it seem like a suitable alternative. This change, however, introduced considerable uncertainty into the final stages of the research. The performance of the final B-VSG prototype is lower than the previously constructed actuated prototype, which is unexpected. This discrepancy could be due to various factors, including the use of FilaFlexible40 in this prototype. Since its material properties are unknown, it might not be suitable for the research. For future studies, it is recommended to use materials that are consistent and have well-known properties.

Stiffness Measurement of the Final B-VSG Design
In the actuated prototype, the stiffness of the metamaterial is tested using a biaxial testing machine, providing valuable insights into its effectiveness as a VSM. However, in the final B-VSG prototype, this testing machine is not available, so the stiffness differences could not be directly measured. Although the force at a constant displacement is recorded for both the compliant and stiffer states of the final B-VSG design, the exact deformation and thus the stiffness values remain unknown. It is evident that the stiffness varies, as shown by the higher forces in the stiffer state compared to the compliant state, but precise stiffness values could not be determined. Future studies should aim to more accurately measure the stiffness of the metamaterial used in the B-VSG.

Stiffness Switch under Constant Position
The proposed VSG is likely not optimal to use for applications that require stiffness switching under constant position, this means that it will not be able to change the stiffness of the gripper while grasping an object. Sections of the metamaterial are rotated under load. The rotation of the end effector is coupled to the rotation of the bistable cells in the metamaterial. The rotation of the bistable cells will likely change if they are snapped under deformation, this will result in a changing position of the end effector.

Even without load, an inherent feature of the stiffness switching that needs to be considered is the stepped snap-through of the three-celled metamaterial. The state of the two smaller bistable cells is coupled, meaning that the two cells are either both open or both closed. However, they do snap separately, and because of this the transition from compliant to stiff is stepped. One of the two cells will snap first and then the other will follow. This might results in a ”rocky” transition between the complaint state of the metamaterial and the stiff state of the metamaterial. The rocky transition could be disadvantages for applications where stiffness switches needs to be performed under constant and precise position.

Manufacturing and Assembly limitations
As explained previously, the materials that were mainly used in this research (PLA and TPU) are not suited for multi-material printing because the two materials do not adhere well. This necessitates printing different material sections separately and assembling these manually. This limited the minimum size of the metamaterial and decreases the FEA accuracy. A solution to this would be to research different materials, preferably a soft thermoplastic material and a rigid thermoplastic material, which chemically adhere. This would enable the use of multi-material printing and would allow for smaller metamaterial with a potentially

higher overall stiffness. An example would be to replace the PLA sections with ABS. ABS and TPU adhere at strengths comparable to commercial adhesives, depending on the order of AM [98]. This might pave a way to smaller metamaterial composites.

Stiffness Actuation
A major drawback of the B-VSG design is its lack of a dedicated actuation unit to regulate stiffness. Previously, the decision to exclude the off-the-shelf piston from the actuated prototype is discussed. In the final design of the metamaterial, there is potential to incorporate a custom pneumatic actuator similar to the one used in the actuated prototype. With advances in multi-material printing, it becomes feasible to print the entire metamaterial structure, including the piston, as a single unit. This integration demonstrates the capability to incorporate complex mechanical components seamlessly into the design of the metamaterial.

8.3.3. Grip Force Measurements on the Prototypes

In Figures 7.12 and 7.10 the grip force of both prototypes is visible. Both grippers show a similar force response when the gripper is moved to the load cell. As the gripper finger comes in contact with the load cell, the force gradually increases with further rotation because of deforming the metamaterial, which acts as a torsional spring. The force transmitted to the load cell (the grip force) is proportional to the rotation of the servomotor, as the metamaterial acts as a linear torsional spring.

Because the force that is exerted on the objects is dependent on the angular deflection of the metamaterial by the servomotor, the servomotor should have sufficient torque to deflect the metamaterial. In the final design however, the servomotor is not able to deflect the metamaterial much, resulting in a low grip force of the end effector. The angular deflection of the metamaterial under maximum torque of the servomotor is visible in Figure 8.3. Evident from the figures is that the deflection is minimal. For further development of the B-VSG, a servomotor with higher torque should be selected.

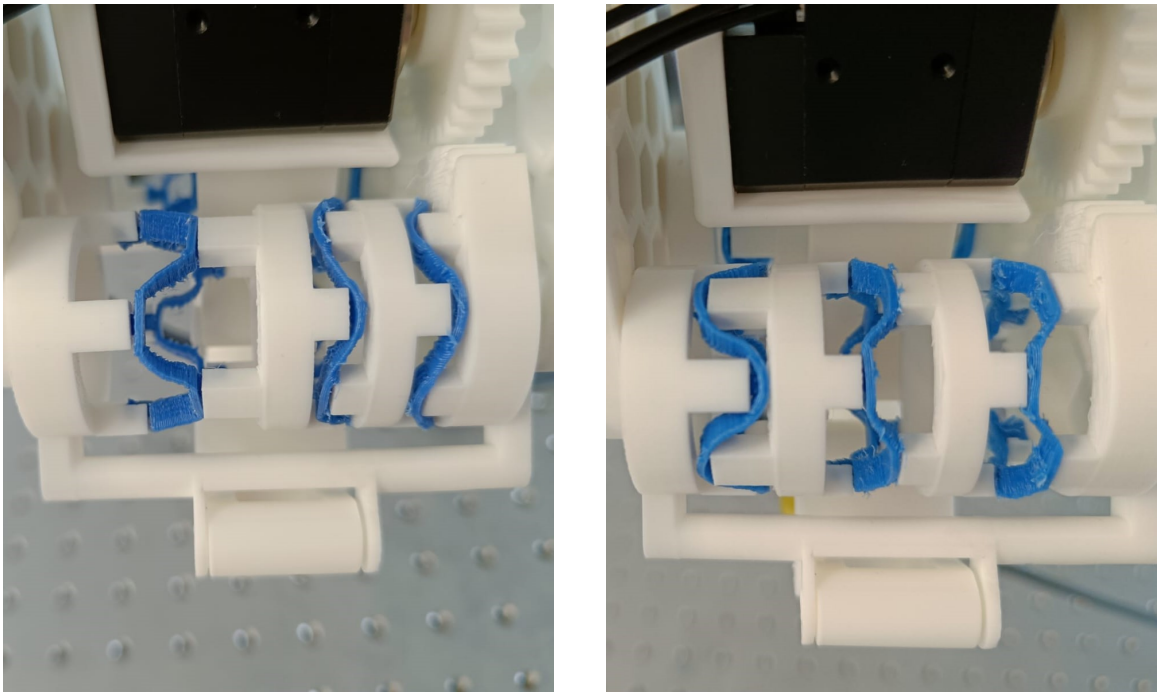

(a) Angular deflection of the metamaterial in the stiffer state under maximal torque

(b) Angular deflection of the metamaterial in the compliant state under maximal torque

Figure 8.3: Angular deflection of the metamaterial under maximal torsional load

8.3.4. Unit Cell Design Improvements

Even after extensive optimization, the achievable stiffness difference in a single bistable unit cell is small. This thesis is limited to optimizing an existing unit cell design. The design shows potential after optimization.

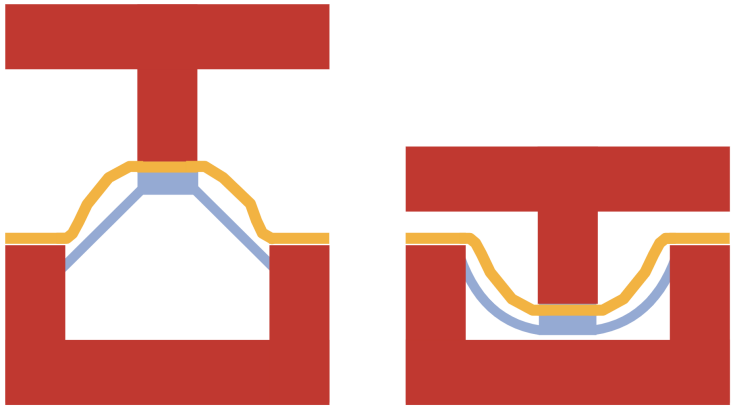

Figure 8.4: Possible improvement of the unit cell, where the grey sections are newly introduced to the existing structure to increase the torsional stiffness difference between the two states

However, further increasing the stiffness difference will require changing the inherent structure of the unit cell. A way of achieving a larger Δk would be to introduce a structure that increases the stiffness of the unit cell when the cell is snapped open, but does not affect the torsional stiffness significantly when snapped closed. Inspiration for such a structure can be found in the research by Kuppens et al.[13]. Kuppens et al. proposed a metamaterial that can engage and disengage preloading on a compliant structure by snapping between stable states, see Figure 2.5. A similar strategy can be applied to the bistable unit cell used in this research. The snap-through caused by axially loading the unit cell can be used to preload compliant structures, this will result in a more assymetric geometry between the two stable states, see Figure 8.4.

The introduced sections are unstressed when the system is in the closed state, and are loaded when the system is in the open state, resulting a significantly stiffer setup in the open state. Important considerations in this design are: 1) The linear approximation of the metamaterial might no longer be valid in the design depicted in Figure 8.4. 2) The elastic potential energy well needs to be deep enough that the structure remains bistable, even though the newly introduced sections try to close the structure because of their preloading. 3) The δ (the distance between the ring sections and vertical support beams) should be increased. Regardless of introducing new sections, increasing δ will decrease the dry friction in the closed state, thus likely decreasing stiffness in the closed state.

8.4. Comparative Analysis and Future Applications of the Novel Bistable Variable Stiffness Gripper

This section offers a detailed comparison of the newly developed bistable variable stiffness gripper (B-VSG) with existing VSAs, evaluating how the new model measures up against established designs. It discusses the novel features and advantages of the B-VSG, particularly in terms of its size, weight, complexity, and response time. Additionally, the discussion explores potential future applications for the B-VSG, considering necessary enhancements to enhance its practicality and broaden its range of uses. This analysis underscores the unique aspects of the B-VSG and outlines steps for further development to prepare it for real-world applications.

8.4.1. Comparison to the Current State of the Art

When comparing the novel B-VSG to the current state of the art, it should be compared to VSAs that are designed based on a similar principle. Therefore, the proposed design should be compared to: 1) The DVSA by Hussain et al.[11]. 2) The F-VSA by Giraud et al.[15]. Additionally, since the stiffness of the final B-VSG design could not be measured, the stiffnesses of the actuated prototype will be used for comparison.

The DVSA by Hussain et al.[11] closely resembles the design presented in this thesis, because both designs change their inherent stiffness in a discrete manner by changing the involved elastic elements. In addition, the DVSA is also designed to improve the response time of stiffness switching mechanisms in VSAs, similar to the VSA proposed in the current research. However, the DVSA does not aim to solve the known limitations of increased size, weight, inertia or mechanical complexity of the state of the art. In spite of the smaller scope with respect to solving prevalent limitation, the DVSA is a VSA that closed resembles the proposed design.

The F-VSA by Giraud et al.[15] resembles the proposed design because it aims to solve the limitations of increased size, weight, inertia and mechanical complexity of the state of the art by using mechanical metamaterial, similar to the proposed B-VSG. However, the F-VSA does not use bistable FMM and relies on preloading of certain unit cells in the FMM to achieve stiffness modulation. This strategy requires continues energy requirement to maintain stiffness and is generally slower than changing stiffness by rapid snap-through.

Firstly, a comparison with the DVSA by Hussain et al.[11] will be presented. Because the DVSA has three independent linear springs, it is capable of multiple distinct stiffness states. The DSVA has more stiffness states than the proposed design, that only has two (virtual) linear springs. Also, the effective stiffness of the DVSA is the sum of all involved torsional springs, since the springs are in parallel. In contrary to the current design, where the torsional springs are in series and the effective torsional stiffness is calculated using Equation 5.1. The difference between springs in parallel or in series affects the difference in stiffness greatly. This is visible in the four different stiffnesses of the DVSA, which are 6.2335 Nm, 29.0335 Nm, 34.5335 Nm and 57.3335 Nm. The corresponding maximum stiffness difference and maximum percentage stiffness difference in the DVSA are 51.1 Nm and $\approx 820\%$, respectively. Obviously, the (percentage) stiffness difference that the current state of the art is capable of, is far greater than the (percentage) stiffness difference that the proposed design is capable is, see Table 7.3.

However, the proposed B-VSG is lighter, smaller, and less mechanically complex because of the integrated structures in the metamaterial. Hussain et al.[11] do not provide the total mass of their actuator, but they report that the rotor weighs 1.35 kg, which is already much more than the total mass of the B-VSG. The DVSA is about 409 mm long and is made of many intricate mechanical parts, making it a very complex mechanism.

Second, a comparison of the proposed VSA with the F-VSA. The F-VSA by Giraud et al.[15] differs from the proposed design because the F-VSA has adaptable compliance in multiple directions, where the proposed design can only change its torsional stiffness about a single axis of rotation. In order to compare the stiffness fairly, both design will be compared based on the torsional stiffness. The maximum torsional stiffness that is presented in the work by Giraud et al.[15], is ≈ 1 Nm/rad, and the minimum is ≈ 0.7 Nm/rad. The corresponding maximum stiffness difference and maximum percentage stiffness difference in the F-VSA are 0.3 Nm/rad and 42.8%, respectively. Interesting to note is that the percentage stiffness difference of the F-VSA and the newly proposed design in this thesis are very similar, see Table 7.3.

Both designs aim to solve the weight, size and complexity challenges present in most existing VSAs, but the F-VSA does not aim to improve the response time or the energy efficiency of VSAs. Although Giraud et al. do not present the mass of their F-VSA design, it can be assumed to have a larger mass than the B-VSG presented in this research. Although no specific masses are discussed, the F-VSA by Giraud et al. requires eight linear actuators to regulate the stiffness, while the B-VSG only requires two linear actuators.

Overall, the novel VSA proposed in this research compared to the current state of art of VSAs that use FMM as a compliant element, but is still not comparable to more traditional VSAs. However, the integration of bistable FMM does have the potential to solve many of the limitations in the current state of the art. In particular, the integration of bistable metamaterial in a VSA design present a solution to the common limitations of size, weight, mechanical complexity and slow response time. The proposed B-VSG design weighs significantly less than comparable designs (186 grams), has a small size, has an integrated VSM that reduces mechanical complexity and has a quick response time thanks to its negative stiffness characteristics. Ultimately, the choice of actuator will largely depend on the intended application.

8.4.2. Improvements for Application and Application Potential

Even after careful research and optimization, the design of the B-VSG is not yet optimal or ready for real-world applications, because the achievable stiffness difference is lower than the current state of the art and the stiffness regulation in the final design is not actuated. Several improvements have been mentioned already: 1) Changing the unit cell design. 2) Integrating a custom pneumatic actuator in the design of the metamaterial to improve the stiffness actuation. 3) Improving the interface between the sections made from different material by using chemically adhering materials, this would result in physical structures that are more aligned with the FEA results. Making a qualitative statement about the stiffness difference and the stiffnesses of the metamaterial is challenging, since this very much dependent on the application of the actuator. However, it can be said that a wider stiffness range will make the VSA more suitable for different applications.

Another application that the metamaterial shows promising results for is that of a mechanical fuse. A mechanical fuse is a safety mechanisms that changes its compliance after a certain load threshold has been crossed. In the current research, the aim has been to make both the compliant state and stiff state of the metamaterial very stable, in order to prevent snap-through due to loading the VSG. However, when the stiff state is made to be barely stable, the coupling between angular and axial displacement can be utilized to induce snap-through when a specific torque is applied to the structure. This can be exploited as a safety mechanisms, rapidly decreasing stiffness when a certain torque threshold has been crossed. Such safety mechanisms are very important for safe human-robot interaction, for example in industrial robot arms.

8.5. Reflections on the Research Process and Project Management in Developing a Novel Variable Stiffness Gripper

The research process spanned over seven months, during which several crucial decisions were made. The thesis focused on developing a novel type of VSG using bistable metamaterials. While the journey had its challenges, it was a rewarding experience. The main goal was to demonstrate the feasibility of using buckling instabilities in FMM to create a novel VSG, rather than designing one for a specific practical application. This objective allowed for considerable flexibility in the research direction.

Given the scientific nature of this work, significant time was often spent exploring ideas or developing specific designs that ultimately proved impractical or too time-consuming. Reflecting on this, having a clearer research plan and goals from the onset would have been beneficial. Setting more defined boundaries early on could have kept the research more focused and prevented diversion into side projects driven more by personal interest than the thesis objectives.

Throughout this process, I had numerous learning opportunities. I sharpened existing skills and acquired new ones, such as using the finite element analysis software Abaqus. While these learning experiences were enjoyable and contributed to my professional growth, they also led to some inefficiencies due to the time required to master new tools. Additionally, a significant amount of time is spent on mechanical characterization, which is essential for designing the VSG. However, not all of this effort is necessary for the research. Being slightly less thorough in this area might have allowed more time for designing and analyzing the final actuator. Nevertheless, the detailed mechanical characterization of the bistable cell will be valuable for future research.

Despite the challenges, I thoroughly enjoyed the research. I appreciated being the manager of my project and conducting various experiments. Having access to all the necessary equipment and being able to use it independently was a significant advantage. I used the opportunity to satisfy my scientific curiosity by exploring different directions. Looking back, I am very pleased and happy with the research journey.

Part III

Concluding Matter

9

Conclusion and Outlook

This research successfully developed a novel type of bistable variable stiffness gripper (B-VSG) that incorporates bistable metamaterials into a variable stiffness actuator (VSA) for use in robotic systems. The B-VSG is notably lightweight at just 189 grams and simplifies mechanical complexity by combining several mechanical components (like compliant elements and a clutching mechanism) into a single 3D-printed structure.

The gripper exhibits a rapid change in stiffness, enabled by the inherent properties of the bistable metamaterial which requires no energy to maintain its stiffness state. This quick snap-through mechanism for stiffness change has been proven effective, with the B-VSG capable of transitioning between states rapidly, providing a practical solution for applications where adaptive stiffness is crucial.

Extensive experiments and analyses focused on the mechanical properties of the bistable metamaterial were performed. These included examinations of how torsional stiffness varies with different geometric ratios and material properties, in particular the Young's modulus. Stability and dynamic behavior of the metamaterial were also tested. Performance tests and grip assessments on the final B-VSG designs revealed that the device could change its stiffness by 40.2%, with a stiffness change of 0.173 Nm, demonstrating its effectiveness in practical scenarios.

The use of bistable metamaterials in the B-VSG has proven to be highly promising for advancing robotic hands. This is especially true in tasks that require delicate and precise movements, such as prosthetics and fine assembly work in industrial settings. The capability to change stiffness on demand improves the versatility and efficiency of robotic systems, mirroring the adaptability and responsiveness seen in biological systems.

Overall, this research demonstrates the practical advantages and feasibility of using bistable metamaterials in variable stiffness actuators. The results offer a new approach to designing efficient and adaptable robotic systems, enhancing the capabilities of robotic manipulators.

9.1. Recommendations for Future Research

After completing this research, there are many improvements and future steps left to explore. Possible future research projects include:

- **Optimization of Metamaterial Design** Future research should focus on optimizing the unit cell design that was investigated in this research to enhance the performance of the metamaterial further. This includes exploring different configurations and materials that could provide more significant stiffness variations and improved durability.
- **Integration of Stiffness Changing Actuation Unit** Integrating the piston that is used to change the stiffness of the metamaterial into the metamaterial itself would allow for a smaller, more customizable design. The design would no longer be constrained to the stroke length of the piston and the piston can be designed to handle the required pressure to induce snap-through.
- **Long-term Reliability Studies** Conducting long-term reliability and fatigue studies of the bistable metamaterials within the actuator is crucial. Understanding how these materials perform over extended periods and under various load conditions will ensure their practical applicability and longevity.

- **Exploring New Applications** Beyond the demonstrated applications, future research should explore other potential areas where the incorporation of bistable metamaterials in actuators could be beneficial, such as the mechanical fuse mentioned in Chapter 7.
- **Improving the Dynamic Model and Developing a Control Strategy** In Chapter 7, a simplified dynamic model for the behaviour of a single bistable cell is proposed. This model needs to be improved and expanded to the metamaterial used in the final VSG design, to accurately predict the dynamic response of the actuator. Developing this model is crucial for the development of a control strategy and application of the VSA in robotic systems.
- **Further Characterization of the Metamaterial** Investigating the bistability region and performing more accurate stiffness measurements on the metamaterial could provide insights on how to improve the performance of the B-VSG.

By addressing these areas, future research can build on the foundation laid by this thesis, leading to more advanced and widely applicable variable stiffness actuators.

References

[1] R. McN. Alexander. “Three Uses for Springs in Legged Locomotion”. en. In: *The International Journal of Robotics Research* 9.2 (Apr. 1990). Publisher: SAGE Publications Ltd STM, pp. 53–61. DOI: 10.1177/027836499000900205. URL: https://doi.org/10.1177/027836499000900205 (visited on 11/28/2023).

[2] Saber Mahboubi et al. “Variable Stiffness Robotic Hand for Stable Grasp and Flexible Handling”. In: *IEEE Access* 6 (2018). Conference Name: IEEE Access, pp. 68195–68209. DOI: 10.1109/ACCESS.2018.2879633. URL: https://ieeexplore.ieee.org/abstract/document/8523683 (visited on 06/05/2024).

[3] Dimuthu DK Arachchige et al. “A novel variable stiffness soft robotic gripper”. In: *2021 IEEE 17th International Conference on Automation Science and Engineering (CASE)*. IEEE. 2021, pp. 2222–2227.

[4] Xizhe Zang et al. “A Novel Design of a Multi-Fingered Bionic Hand With Variable Stiffness for Robotic Grasp”. In: *Journal of Mechanisms and Robotics* 15.045001 (Nov. 2022). DOI: 10.1115/1.4055252. URL: https://doi.org/10.1115/1.4055252 (visited on 06/04/2024).

[5] Christopher J Stabile et al. “The role of stiffness in versatile robotic grasping”. In: *IEEE Robotics and Automation Letters* 7.2 (2022), pp. 4733–4740.

[6] B. Vanderborght et al. “Variable impedance actuators: A review”. In: *Robotics and Autonomous Systems* 61.12 (Dec. 2013), pp. 1601–1614. DOI: 10.1016/j.robot.2013.06.009. URL: https://www.sciencedirect.com/science/article/pii/S0921889013001188 (visited on 11/21/2023).

[7] Giorgio Grioli et al. “Variable stiffness actuators: The user’s point of view”. en. In: *The International Journal of Robotics Research* 34.6 (May 2015). Publisher: SAGE Publications Ltd STM, pp. 727–743. DOI: 10.1177/0278364914566515. URL: https://doi.org/10.1177/0278364914566515 (visited on 11/21/2023).

[8] Elif Hocaoglu et al. “Design, implementation, and evaluation of a variable stiffness transradial hand prosthesis”. In: *Frontiers in Neurorobotics* 16 (2022), p. 789210.

[9] Sebastian Wolf et al. “A new variable stiffness design: Matching requirements of the next robot generation”. In: *2008 IEEE International Conference on Robotics and Automation*. IEEE. 2008, pp. 1741–1746.

[10] A. Bicchi et al. “Fast and ”Soft-Arm” Tactics”. en. In: *IEEE Robotics & Automation Magazine* 11.2 (June 2004), pp. 22–33. DOI: 10.1109/MRA.2004.1310939. URL: http://ieeexplore.ieee.org/document/1310939/ (visited on 11/27/2023).

[11] Irfan Hussain et al. “Design and Control of a Discrete Variable Stiffness Actuator With Instant Stiffness Switch for Safe Human-Robot Interaction”. In: *IEEE Access* 9 (2021). Conference Name: IEEE Access, pp. 118215–118231. DOI: 10.1109/ACCESS.2021.3105587. URL: https://ieeexplore.ieee.org/abstract/document/9514838 (visited on 05/20/2024).

[12] Katia Bertoldi et al. “Flexible mechanical metamaterials”. en. In: *Nature Reviews Materials* 2.11 (Oct. 2017), p. 17066. DOI: 10.1038/natrevmats.2017.66. URL: https://www.nature.com/articles/natrevmats201766 (visited on 12/11/2023).

[13] P.R. Kuppens et al. “Monolithic binary stiffness building blocks for mechanical digital machines”. en. In: *Extreme Mechanics Letters* 42 (Jan. 2021), p. 101120. DOI: 10.1016/j.eml.2020.101120. URL: https://linkinghub.elsevier.com/retrieve/pii/S235243162030290X (visited on 12/19/2023).

[14] P. Sinha et al. “Programmable multi-physical mechanics of mechanical metamaterials”. en. In: *Materials Science and Engineering: R: Reports* 155 (Oct. 2023), p. 100745. DOI: 10.1016/j.mser.2023.100745. URL: https://linkinghub.elsevier.com/retrieve/pii/S0927796X23000311 (visited on 01/03/2024).

[15] Frederic H. Giraud et al. “Flexure Variable Stiffness Actuators”. en. In: *Advanced Intelligent Systems* 4.7 (2022), p. 2100282. DOI: 10.1002/aisy.202100282. URL: https://onlinelibrary.wiley.com/doi/abs/10.1002/aisy.202100282 (visited on 11/23/2023).

[16] Ahmad Rafsanjani et al. “Programming soft robots with flexible mechanical metamaterials”. en. In: *Science Robotics* 4.29 (Apr. 2019), eaav7874. DOI: 10.1126/scirobotics.aav7874. URL: https://www.science.org/doi/10.1126/scirobotics.aav7874 (visited on 12/15/2023).

[17] Amir Jafari et al. “Determinants for Stiffness Adjustment Mechanisms”. en. In: *Journal of Intelligent & Robotic Systems* 82.3 (June 2016), pp. 435–454. DOI: 10.1007/s10846-015-0253-8. URL: https://doi.org/10.1007/s10846-015-0253-8 (visited on 12/21/2023).

[18] Min Pan et al. “Soft Actuators and Robotic Devices for Rehabilitation and Assistance”. en. In: *Advanced Intelligent Systems* 4.4 (2022), p. 2100140. DOI: 10.1002/aisy.202100140. URL: https://onlinelibrary.wiley.com/doi/abs/10.1002/aisy.202100140 (visited on 11/27/2023).

[19] Nazek El-Atab et al. “Soft Actuators for Soft Robotic Applications: A Review”. en. In: *Advanced Intelligent Systems* 2.10 (2020). _eprint: https://onlinelibrary.wiley.com/doi/pdf/10.1002/aisy.202000128, p. 2000128. DOI: 10.1002/aisy.202000128. URL: https://onlinelibrary.wiley.com/doi/abs/10.1002/aisy.202000128 (visited on 11/27/2023).

[20] Ronald Ham et al. “Compliant actuator designs”. en. In: *IEEE Robotics & Automation Magazine* 16.3 (Sept. 2009), pp. 81–94. DOI: 10.1109/MRA.2009.933629. URL: http://ieeexplore.ieee.org/document/5233419/ (visited on 11/24/2023).

[21] Yuwang Liu et al. “Design and analysis of spring parallel variable stiffness actuator based on antagonistic principle”. en. In: *Mechanism and Machine Theory* 140 (Oct. 2019), pp. 44–58. DOI: 10.1016/j.mechmachtheory.2019.05.016. URL: https://linkinghub.elsevier.com/retrieve/pii/S0094114X18317488 (visited on 11/28/2023).

[22] Thomas G. Sugar. “A novel selective compliant actuator”. In: *Mechatronics* 12.9 (Nov. 2002), pp. 1157–1171. DOI: 10.1016/S0957-4158(02)00021-1. URL: https://www.sciencedirect.com/science/article/pii/S0957415802000211 (visited on 11/28/2023).

[23] Sebastian Wolf et al. “Variable Stiffness Actuators: Review on Design and Components”. In: *IEEE/ASME Transactions on Mechatronics* 21.5 (Oct. 2016). Conference Name: IEEE/ASME Transactions on Mechatronics, pp. 2418–2430. DOI: 10.1109/TMECH.2015.2501019. URL: https://ieeexplore.ieee.org/abstract/document/7330025 (visited on 11/21/2023).

[24] Simon Guest. “The stiffness of prestressed frameworks: A unifying approach”. en. In: *International Journal of Solids and Structures* 43.3-4 (Feb. 2006), pp. 842–854. DOI: 10.1016/j.ijsolstr.2005.03.008. URL: https://linkinghub.elsevier.com/retrieve/pii/S0020768305001198 (visited on 01/12/2024).

[25] Bram Vanderborght et al. “Comparison of Mechanical Design and Energy Consumption of Adaptable, Passive-compliant Actuators”. en. In: *The International Journal of Robotics Research* 28.1 (Jan. 2009). Publisher: SAGE Publications Ltd STM, pp. 90–103. DOI: 10.1177/0278364908095333. URL: https://doi.org/10.1177/0278364908095333 (visited on 11/28/2023).

[26] I. Sardellitti et al. “A position and stiffness control strategy for variable stiffness actuators”. en. In: *2012 IEEE International Conference on Robotics and Automation*. St Paul, MN, USA: IEEE, May 2012, pp. 2785–2791. DOI: 10.1109/ICRA.2012.6224672. URL: http://ieeexplore.ieee.org/document/6224672/ (visited on 11/28/2023).

[27] Ronald Van Ham et al. “MACCEPA, the mechanically adjustable compliance and controllable equilibrium position actuator: Design and implementation in a biped robot”. In: *Robotics and Autonomous Systems* 55.10 (Oct. 2007), pp. 761–768. DOI: 10.1016/j.robot.2007.03.001.

URL: https://www.sciencedirect.com/science/article/pii/S0921889007000371 (visited on 11/27/2023).

[28] Bram Vanderborght et al. “MACCEPA 2.0: compliant actuator used for energy efficient hopping robot Chobino1D”. In: *Autonomous Robots* 31 (2011), pp. 55–65.

[29] Jung-Jun Park et al. “Safe joint mechanism based on passive compliance for collision safety”. In: *Recent Progress in Robotics: Viable Robotic Service to Human: An Edition of the Selected Papers from the 13th International Conference on Advanced Robotics*. Springer. 2008, pp. 49–61.

[30] Jung-Jun Park et al. “Safe joint mechanism using inclined link with springs for collision safety and positioning accuracy of a robot arm”. In: *2010 IEEE International Conference on Robotics and Automation*. IEEE. 2010, pp. 813–818.

[31] Nikos G Tsagarakis et al. “A new variable stiffness actuator (CompAct-VSA): Design and modelling”. In: *2011 IEEE/RSJ International Conference on Intelligent Robots and Systems*. IEEE. 2011, pp. 378–383.

[32] Amir Jafari et al. “A novel actuator with adjustable stiffness (AwAS)”. In: *2010 IEEE/RSJ International Conference on Intelligent Robots and Systems*. IEEE. 2010, pp. 4201–4206.

[33] Amir Jafari et al. “A new actuator with adjustable stiffness based on a variable ratio lever mechanism”. In: *IEEE/ASME Transactions on Mechatronics* 19.1 (2012), pp. 55–63.

[34] Stefan S Groothuis et al. “The vsaUT-II: A novel rotational variable stiffness actuator”. In: *2012 IEEE International Conference on Robotics and Automation*. IEEE. 2012, pp. 3355–3360.

[35] Matteo Fumagalli et al. “The mVSA-UT: A miniaturized differential mechanism for a continuous rotational variable stiffness actuator”. In: *2012 4th IEEE RAS & EMBS International Conference on Biomedical Robotics and Biomechatronics (BioRob)*. IEEE. 2012, pp. 1943–1948.

[36] Byeong-Sang Kim et al. “Design and control of a variable stiffness actuator based on adjustable moment arm”. In: *IEEE Transactions on Robotics* 28.5 (2012), pp. 1145–1151.

[37] Jiantao Sun et al. “A Novel Design of Serial Variable Stiffness Actuator Based on an Archimedean Spiral Relocation Mechanism”. en. In: *IEEE/ASME Transactions on Mechatronics* 23.5 (Oct. 2018), pp. 2121–2131. DOI: 10.1109/TMECH.2018.2854742. URL: https://ieeexplore.ieee.org/document/8409317/ (visited on 11/28/2023).

[38] Hung Vu Quy et al. “A novel mechanism for varying stiffness via changing transmission angle”. In: *2011 IEEE International Conference on Robotics and Automation*. IEEE. 2011, pp. 5076–5081.

[39] Sebastian Wolf et al. “The DLR FSJ: Energy based design of a variable stiffness joint”. In: *2011 IEEE international conference on robotics and automation*. IEEE. 2011, pp. 5082–5089.

[40] Manuel G Catalano et al. “Vsa-hd: From the enumeration analysis to the prototypical implementation”. In: *2010 IEEE/RSJ International Conference on Intelligent Robots and Systems*. IEEE. 2010, pp. 3676–3681.

[41] Toshio Morita et al. “Design and development of a new robot joint using a mechanical impedance adjuster”. In: *Proceedings of 1995 IEEE International Conference on Robotics and Automation*. Vol. 3. IEEE. 1995, pp. 2469–2475.

[42] Chad English et al. “Implementation of variable joint stiffness through antagonistic actuation using rolamite springs”. In: *Mechanism and Machine Theory* 34.1 (Jan. 1999), pp. 27–40. DOI: 10.1016/S0094-114X(97)00103-1. URL: https://www.sciencedirect.com/science/article/pii/S0094114X97001031 (visited on 12/06/2023).

[43] Jonathan W Hurst et al. “The actuator with mechanically adjustable series compliance”. In: *IEEE Transactions on Robotics* 26.4 (2010), pp. 597–606.

[44] Frank Daerden. “Conception and realization of pleated pneumatic artificial muscles and their use as compliant actuation elements”. In: *Vrije Universiteit Brussel* (1999), p. 176.

[45] Giovanni Tonietti et al. “Design and control of a variable stiffness actuator for safe and fast physical human/robot interaction”. In: *Proceedings of the 2005 IEEE international conference on robotics and automation*. IEEE. 2005, pp. 526–531.

[46] Riccardo Schiavi et al. “VSA-II: A novel prototype of variable stiffness actuator for safe and performing robots interacting with humans”. In: *2008 IEEE International Conference on Robotics and Automation*. IEEE. 2008, pp. 2171–2176.

[47] Manuel G Catalano et al. “VSA-CubeBot: A modular variable stiffness platform for multiple degrees of freedom robots”. In: *2011 IEEE international conference on robotics and automation*. IEEE. 2011, pp. 5090–5095.

[48] Florian Petit et al. “Bidirectional antagonistic variable stiffness actuation: Analysis, design & implementation”. In: *2010 IEEE International Conference on Robotics and Automation*. IEEE. 2010, pp. 4189–4196.

[49] Gianluca Palli et al. “Design of a Variable Stiffness Actuator Based on Flexures”. en. In: *Journal of Mechanisms and Robotics* 3.3 (Aug. 2011), p. 034501. DOI: 10.1115/1.4004228. URL: https://asmedigitalcollection.asme.org/mechanismsrobotics/article/doi/10.1115/1.4004228/468359/Design-of-a-Variable-Stiffness-Actuator-Based-on (visited on 01/02/2024).

[50] Xujin Yuan et al. “Recent progress in the design and fabrication of multifunctional structures based on metamaterials”. In: *Current Opinion in Solid State and Materials Science* 25.1 (Feb. 2021), p. 100883. DOI: 10.1016/j.cossms.2020.100883. URL: https://www.sciencedirect.com/science/article/pii/S1359028620300814 (visited on 12/12/2023).

[51] David J. Levine et al. “Materials with Electroprogrammable Stiffness”. en. In: *Advanced Materials* 33.35 (2021), p. 2007952. DOI: 10.1002/adma.202007952. URL: https://onlinelibrary.wiley.com/doi/abs/10.1002/adma.202007952 (visited on 01/08/2024).

[52] Alireza Mohammadi et al. “A bioinspired 3D-printable flexure joint with cellular mechanical metamaterial architecture for soft robotic hands”. en. In: *International Journal of Bioprinting* 9.3 (Mar. 2023), p. 696. DOI: 10.18063/ijb.696. URL: https://accscience.com/journal/IJB/9/3/10.18063/ijb.696 (visited on 12/20/2023).

[53] Romik Khajehtourian et al. “Soft Adaptive Mechanical Metamaterials”. In: *Frontiers in Robotics and AI* 8 (2021). URL: https://www.frontiersin.org/articles/10.3389/frobt.2021.673478 (visited on 01/08/2024).

[54] Daniela Rus et al. “Spotlight on origami robots”. In: *Science Robotics* 3.15 (Feb. 2018). Publisher: American Association for the Advancement of Science, eaat0938. DOI: 10.1126/scirobotics.aat0938. URL: https://www.science.org/doi/full/10.1126/scirobotics.aat0938 (visited on 11/24/2023).

[55] Zhenishbek Zhakypov et al. “Designing minimal and scalable insect-inspired multi-locomotion millirobots”. en. In: *Nature* 571.7765 (July 2019). Number: 7765 Publisher: Nature Publishing Group, pp. 381–386. DOI: 10.1038/s41586-019-1388-8. URL: https://www.nature.com/articles/s41586-019-1388-8 (visited on 12/08/2023).

[56] Pietro Bilancia et al. “Virtual and physical prototyping of a beam-based variable stiffness actuator for safe human-machine interaction”. In: *Robotics and Computer-Integrated Manufacturing* 65 (Oct. 2020), p. 101886. DOI: 10.1016/j.rcim.2019.101886. URL: https://www.sciencedirect.com/science/article/pii/S0736584519303850 (visited on 11/24/2023).

[57] Xiong Li et al. “Structure-Controlled Variable Stiffness Robotic Joint Based on Multiple Rotary Flexure Hinges”. In: *IEEE Transactions on Industrial Electronics* 68.12 (Dec. 2021). Conference Name: IEEE Transactions on Industrial Electronics, pp. 12452–12461. DOI: 10.1109/TIE.2020.3044795. URL: https://ieeexplore.ieee.org/abstract/document/9301345 (visited on 11/24/2023).

[58] Matthew F. Berwind et al. “A Hierarchical Programmable Mechanical Metamaterial Unit Cell Showing Metastable Shape Memory”. en. In: *Advanced Engineering Materials* 20.11 (Nov. 2018), p. 1800771. DOI: 10.1002/adem.201800771. URL: https://onlinelibrary.wiley.com/doi/10.1002/adem.201800771 (visited on 01/03/2024).

[59] M. Fleisch et al. “Functional mechanical metamaterial with independently tunable stiffness in the three spatial directions”. en. In: *Materials Today Advances* 11 (Sept. 2021), p. 100155. DOI: 10.1016/j.mtadv.2021.100155. URL: https://linkinghub.elsevier.com/retrieve/pii/S2590049821000254 (visited on 12/19/2023).

[60] Amir A. Zadpoor. “Mechanical meta-materials”. en. In: *Materials Horizons* 3.5 (2016), pp. 371–381. DOI: 10.1039/C6MH00065G. URL: http://xlink.rsc.org/?DOI=C6MH00065G (visited on 12/14/2023).

[61] Johan Christensen et al. “Vibrant times for mechanical metamaterials”. In: *Mrs Communications* 5.3 (2015), pp. 453–462.

[62] George Neville Greaves et al. “Poisson’s ratio and modern materials”. In: *Nature materials* 10.11 (2011), pp. 823–837.

[63] Tanmoy Mukhopadhyay et al. “Programmable stiffness and shape modulation in origami materials: Emergence of a distant actuation feature”. In: *Applied Materials Today* 19 (June 2020), p. 100537. DOI: 10.1016/j.apmt.2019.100537. URL: https://www.sciencedirect.com/science/article/pii/S2352940719306572 (visited on 11/22/2023).

[64] Xin Fang et al. “Programmable gear-based mechanical metamaterials”. en. In: *Nature Materials* 21.8 (Aug. 2022). Number: 8 Publisher: Nature Publishing Group, pp. 869–876. DOI: 10.1038/s41563-022-01269-3. URL: https://www.nature.com/articles/s41563-022-01269-3 (visited on 12/11/2023).

[65] Hongbin Fang et al. “Programmable Self-Locking Origami Mechanical Metamaterials”. en. In: *Advanced Materials* 30.15 (2018), p. 1706311. DOI: 10.1002/adma.201706311. URL: https://onlinelibrary.wiley.com/doi/abs/10.1002/adma.201706311 (visited on 12/11/2023).

[66] Navid Mehreganian et al. “Structural Mechanics of Negative Stiffness Honeycomb Metamaterials”. en. In: *Journal of Applied Mechanics* 88.5 (May 2021), p. 051006. DOI: 10.1115/1.4049954. URL: https://asmedigitalcollection.asme.org/appliedmechanics/article/doi/10.1115/1.4049954/1096925/Structural-Mechanics-of-Negative-Stiffness (visited on 01/08/2024).

[67] Marius A. Wagner et al. “Programmable, active lattice structures: Unifying stretch-dominated and bending-dominated topologies”. en. In: *Extreme Mechanics Letters* 29 (May 2019), p. 100461. DOI: 10.1016/j.eml.2019.100461. URL: https://linkinghub.elsevier.com/retrieve/pii/S2352431618302724 (visited on 01/08/2024).

[68] Shaowei Zhu et al. “A novel bi-material negative stiffness metamaterial in sleeve-type via combining rigidity with softness”. en. In: *Composite Structures* 262 (Apr. 2021), p. 113381. DOI: 10.1016/j.compstruct.2020.113381. URL: https://linkinghub.elsevier.com/retrieve/pii/S0263822320333079 (visited on 01/08/2024).

[69] Aditya Lele et al. “Snap-through and stiffness adaptation of a multi-stable Kirigami composite module”. In: *Composites Science and Technology* 182 (Sept. 2019), p. 107750. DOI: 10.1016/j.compscitech.2019.107750. URL: https://www.sciencedirect.com/science/article/pii/S0266353819313375 (visited on 12/19/2023).

[70] Yinding Chi et al. “Bistable and Multistable Actuators for Soft Robots: Structures, Materials, and Functionalities”. en. In: *Advanced Materials* 34.19 (2022). _eprint: https://onlinelibrary.wiley.com/doi/pdf/10.1002/adma.202110384, p. 2110384. DOI: 10.1002/adma.202110384. URL: https://onlinelibrary.wiley.com/doi/abs/10.1002/adma.202110384 (visited on 11/22/2023).

[71] Joshua Kaufmann et al. “Harnessing the Multistability of Kresling Origami for Reconfigurable Articulation in Soft Robotic Arms”. In: *Soft Robotics* 9.2 (Apr. 2022). Publisher: Mary Ann Liebert, Inc., publishers, pp. 212–223. DOI: 10.1089/soro.2020.0075. URL: https://www.liebertpub.com/doi/full/10.1089/soro.2020.0075 (visited on 12/19/2023).

[72] Xiaojun Tan et al. “Design, fabrication, and characterization of multistable mechanical metamaterials for trapping energy”. en. In: *Extreme Mechanics Letters* 28 (Apr. 2019), pp. 8–21. DOI: 10.1016/j.eml.2019.02.002. URL: https://linkinghub.elsevier.com/retrieve/pii/S2352431618301901 (visited on 12/14/2023).

[73] Baocai Chen et al. “Novel multifunctional negative stiffness mechanical metamaterial structure: Tailored functions of multi-stable and compressive mono-stable”. en. In: *Composites Part B: Engineering* 204 (Jan. 2021), p. 108501. DOI: 10.1016/j.compositesb.2020.108501. URL: https://linkinghub.elsevier.com/retrieve/pii/S1359836820335484 (visited on 12/12/2023).

[74] Tian Chen et al. “A reprogrammable mechanical metamaterial with stable memory”. en. In: *Nature* 589.7842 (Jan. 2021). Number: 7842 Publisher: Nature Publishing Group, pp. 386–390. DOI: 10.1038/s41586-020-03123-5. URL: https://www.nature.com/articles/s41586-020-03123-5 (visited on 12/11/2023).

[75] Jia-Xin Wang et al. “A novel chiral metamaterial with multistability and programmable stiffness”. en. In: *Smart Materials and Structures* 30.6 (Apr. 2021). Publisher: IOP Publishing, p. 065006. DOI: 10.1088/1361-665X/abf994. URL: https://dx.doi.org/10.1088/1361-665X/abf994 (visited on 12/19/2023).

[76] Janav P. Udani et al. “Programmable mechanical metastructures from locally bistable domes”. In: *Extreme Mechanics Letters* 42 (Jan. 2021), p. 101081. DOI: 10.1016/j.eml.2020.101081. URL: https://www.sciencedirect.com/science/article/pii/S2352431620302674 (visited on 12/19/2023).

[77] Jiahao Shi et al. “Programmable Multistable Perforated Shellular”. en. In: *Advanced Materials* 33.42 (2021). _eprint: https://onlinelibrary.wiley.com/doi/pdf/10.1002/adma.202102423, p. 2102423. DOI: 10.1002/adma.202102423. URL: https://onlinelibrary.wiley.com/doi/abs/10.1002/adma.202102423 (visited on 01/09/2024).

[78] Aryan Sinha. “Kirigami-inspired metamaterials for programming constitutive laws: Mixed-mode multidirectional auxeticity and contact-induced stiffness modulation”. en. In: *OPEN ACCESS* (Dec. 2022).

[79] Boyuan Tian et al. “Hybrid artificial muscle: enhanced actuation and load-bearing performance via an origami metamaterial endoskeleton”. en. In: *Materials Horizons* 10.7 (2023). Publisher: Royal Society of Chemistry, pp. 2398–2411. DOI: 10.1039/D3MH00551H. URL: https://pubs.rsc.org/en/content/articlelanding/2023/mh/d3mh00551h (visited on 01/04/2024).

[80] Sattam Sengupta et al. “Harnessing the anisotropic multistability of stacked-origami mechanical metamaterials for effective modulus programming”. en. In: *Journal of Intelligent Material Systems and Structures* 29.14 (Aug. 2018). Publisher: SAGE Publications Ltd STM, pp. 2933–2945. DOI: 10.1177/1045389X18781040. URL: https://doi.org/10.1177/1045389X18781040 (visited on 12/19/2023).

[81] Hang Yang et al. “1D and 2D snapping mechanical metamaterials with cylindrical topology”. en. In: *International Journal of Solids and Structures* 204-205 (Nov. 2020), pp. 220–232. DOI: 10.1016/j.ijsolstr.2020.08.023. URL: https://linkinghub.elsevier.com/retrieve/pii/S0020768320303280 (visited on 02/02/2024).

[82] Yi Wu et al. “Programming Soft Shape-Morphing Systems by Harnessing Strain Mismatch and Snap-Through Bistability: A Review”. en. In: *Materials* 15.7 (Jan. 2022). Number: 7 Publisher: Multidisciplinary Digital Publishing Institute, p. 2397. DOI: 10.3390/ma15072397. URL: https://www.mdpi.com/1996-1944/15/7/2397 (visited on 01/03/2024).

[83] Jia-Xin Wang et al. “A novel programmable composite metamaterial with tunable Poisson’s ratio and bandgap based on multi-stable switching”. en. In: *Composites Science and Technology* 219 (Mar. 2022), p. 109245. DOI: 10.1016/j.compscitech.2021.109245. URL: https://linkinghub.elsevier.com/retrieve/pii/S0266353821006011 (visited on 01/04/2024).

[84] Hang Yang et al. “Multi-stable mechanical metamaterials by elastic buckling instability”. en. In: *Journal of Materials Science* 54.4 (Feb. 2019), pp. 3509–3526. DOI: 10.1007/s10853-018-3065-y. URL: http://link.springer.com/10.1007/s10853-018-3065-y (visited on 02/02/2024).

[85] Neville Hogan et al. “The physical basis of analogies in physical system models”. In: *The mechatronics handbook*. CRC Press/Balkema, 2002.

[86] Hazem I Ali et al. “A review of pneumatic actuators (modeling and control)”. In: *Australian Journal of Basic and Applied Sciences* 3.2 (2009), pp. 440–454.

[87] Matheus S. Xavier et al. “Soft Pneumatic Actuators: A Review of Design, Fabrication, Modeling, Sensing, Control and Applications”. In: *IEEE Access* 10 (2022), pp. 59442–59485. DOI: 10.1109/ACCESS.2022.3179589. URL: https://ieeexplore.ieee.org/document/9785890/ (visited on 05/16/2024).

[88] M. Rismalia et al. “Infill pattern and density effects on the tensile properties of 3D printed PLA material”. en. In: *Journal of Physics: Conference Series* 1402.4 (Dec. 2019). Publisher: IOP Publishing, p. 044041. DOI: 10.1088/1742-6596/1402/4/044041. URL: https://dx.doi.org/10.1088/1742-6596/1402/4/044041 (visited on 05/14/2024).

[89] Kumaresan Rajan et al. “Fused deposition modeling: process, materials, parameters, properties, and applications”. en. In: *The International Journal of Advanced Manufacturing Technology* 120.3 (May 2022), pp. 1531–1570. DOI: 10.1007/s00170-022-08860-7. URL: https://doi.org/10.1007/s00170-022-08860-7 (visited on 05/14/2024).

[90] Brian N Turner et al. “A review of melt extrusion additive manufacturing processes: I. Process design and modeling”. In: *Rapid Prototyping Journal* 20.3 (2014), pp. 192–204. DOI: 10.1108/RPJ-01-2013-0012.

[91] R. J. Urbanic et al. “Fused Deposition Modeling Design Rules for Building Large, Complex Components”. In: *Computer-Aided Design and Applications* 13.3 (May 2016). Publisher: Taylor & Francis _eprint: https://doi.org/10.1080/16864360.2015.1114393, pp. 348–368. DOI: 10.1080/16864360.2015.1114393. URL: https://doi.org/10.1080/16864360.2015.1114393 (visited on 05/14/2024).

[92] Micaela Ribeiro et al. “Interface geometries in 3D multi-material prints by fused filament fabrication”. In: *Rapid Prototyping Journal* 25.1 (Jan. 2018). Publisher: Emerald Publishing Limited, pp. 38–46. DOI: 10.1108/RPJ-05-2017-0107. URL: https://doi.org/10.1108/RPJ-05-2017-0107 (visited on 05/14/2024).

[93] Bastiaan Florijn et al. “Programmable Mechanical Metamaterials”. In: *Physical Review Letters* 113.17 (Oct. 2014). Publisher: American Physical Society, p. 175503. DOI: 10.1103/PhysRevLett.113.175503. URL: https://link.aps.org/doi/10.1103/PhysRevLett.113.175503 (visited on 12/12/2023).

[94] F.J. Harewood et al. “Comparison of the implicit and explicit finite element methods using crystal plasticity”. en. In: *Computational Materials Science* 39.2 (Apr. 2007), pp. 481–494. DOI: 10.1016/j.commatsci.2006.08.002. URL: https://linkinghub.elsevier.com/retrieve/pii/S0927025606002278 (visited on 05/20/2024).

[95] A. Srirekha et al. “Infinite to finite: An overview of finite element analysis”. en-US. In: *Indian Journal of Dental Research* 21.3 (Sept. 2010), p. 425. DOI: 10.4103/0970-9290.70813. URL: https://journals.lww.com/ijdr/fulltext/2010/21030/infinite_to_finite__an_overview_of_finite_element.24.aspx (visited on 05/20/2024).

[96] Michael Chung et al. “On the optimization of low-cost FDM 3D printers for accurate replication of patient-specific abdominal aortic aneurysm geometry”. en. In: *3D Printing in Medicine* 4.1 (Jan. 2018), p. 2. DOI: 10.1186/s41205-017-0023-2. URL: https://doi.org/10.1186/s41205-017-0023-2 (visited on 04/25/2024).

[97] Nicholas B. Bolus et al. “A 3D-Printed, Adjustable-Stiffness Knee Brace with Embedded Magnetic Angle Sensor”. In: *2018 40th Annual International Conference of the IEEE Engineering in Medicine and Biology Society (EMBC)*. ISSN: 1558-4615. July 2018, pp. 1624–1627. DOI: 10.1109/EMBC.2018.8512600. URL: https://ieeexplore.ieee.org/abstract/document/8512600 (visited on 05/14/2024).

[98] Conor G Harris et al. “Additive manufacturing with soft TPU–adhesion strength in multimaterial flexible joints”. In: *Frontiers in Mechanical Engineering* 5 (2019), p. 37.

[99] Thiago Boaventura et al. “Dynamic torque control of a hydraulic quadruped robot”. In: *2012 IEEE international conference on robotics and automation*. IEEE. 2012, pp. 1889–1894.

[100] Matteo Laffranchi et al. “A variable physical damping actuator (VPDA) for compliant robotic joints”. In: *2010 IEEE International Conference on Robotics and Automation*. IEEE. 2010, pp. 1668–1674.

[101] Yangsheng Xu et al. “Stabilization and path following of a single wheel robot”. In: *IEEE/ASME Transactions on Mechatronics* 9.2 (2004), pp. 407–419.

[102] Haoyong Yu et al. “Control design of a novel compliant actuator for rehabilitation robots”. In: *Mechatronics* 23.8 (Dec. 2013), pp. 1072–1083. DOI: 10.1016/j.mechatronics.2013.08.004. URL: https://www.sciencedirect.com/science/article/pii/S0957415813001542 (visited on 11/28/2023).

[103] J.W. Hurst et al. “An actuator with physically variable stiffness for highly dynamic legged locomotion”. en. In: *IEEE International Conference on Robotics and Automation, 2004. Proceedings. ICRA ’04. 2004*. New Orleans, LA, USA: IEEE, 2004, 4662–4667 Vol.5. DOI: 10.1109/ROBOT.2004.1302453. URL: http://ieeexplore.ieee.org/document/1302453/ (visited on 11/27/2023).

[104] N.G. Tsagarakis et al. “A compact soft actuator unit for small scale human friendly robots”. In: *2009 IEEE International Conference on Robotics and Automation*. ISSN: 1050-4729. May 2009, pp. 4356–4362. DOI: 10.1109/ROBOT.2009.5152496. URL: https://ieeexplore.ieee.org/abstract/document/5152496 (visited on 11/28/2023).

[105] M. Zinn et al. “Playing it safe [human-friendly robots]”. In: *IEEE Robotics & Automation Magazine* 11.2 (June 2004). Conference Name: IEEE Robotics & Automation Magazine, pp. 12–21. DOI: 10.1109/MRA.2004.1310938. URL: https://ieeexplore.ieee.org/abstract/document/1310938 (visited on 11/28/2023).

[106] Sašo Jezernik et al. “Robotic Orthosis Lokomat: A Rehabilitation and Research Tool”. en. In: *Neuromodulation: Technology at the Neural Interface* 6.2 (2003). _eprint: https://onlinelibrary.wiley.com/doi/pdf/10.1046/j.1525-1403.2003.03017.x, pp. 108–115. DOI: 10.1046/j.1525-1403.2003.03017.x. URL: https://onlinelibrary.wiley.com/doi/abs/10.1046/j.1525-1403.2003.03017.x (visited on 11/27/2023).

[107] Samuel K. Au et al. “Biomechanical Design of a Powered Ankle-Foot Prosthesis”. In: *2007 IEEE 10th International Conference on Rehabilitation Robotics*. ISSN: 1945-7901. June 2007, pp. 298–303. DOI: 10.1109/ICORR.2007.4428441. URL: https://ieeexplore.ieee.org/abstract/document/4428441?casa_token=8W0vFHM9AJcAAAAA:du4VI5F0UktuADz4dO-BT8DK_W4Z3wdQ5co-C71qpXKbp9MpASri1TXw51YKW-TXm2G7V36_ (visited on 11/27/2023).

[108] Joseph K. Hitt et al. “The SPARKy (Spring Ankle With Regenerative Kinetics) Project: Design and Analysis of a Robotic Transtibial Prosthesis With Regenerative Kinetics”. en. In: American Society of Mechanical Engineers Digital Collection, May 2009, pp. 1587–1596. DOI: 10.1115/DETC2007-34512. URL: https://dx.doi.org/10.1115/DETC2007-34512 (visited on 11/27/2023).

[109] Bram Vanderborght et al. “Development of a compliance controller to reduce energy consumption for bipedal robots”. en. In: *Autonomous Robots* 24.4 (May 2008), pp. 419–434. DOI: 10.1007/s10514-008-9088-5. URL: https://doi.org/10.1007/s10514-008-9088-5 (visited on 11/27/2023).

[110] E.T. Filipov et al. “Mechanical characteristics of the bistable origami hypar”. en. In: *Extreme Mechanics Letters* 25 (Nov. 2018), pp. 16–26. DOI: 10.1016/j.eml.2018.10.001. URL: https://linkinghub.elsevier.com/retrieve/pii/S2352431618300907 (visited on 12/14/2023).

[111] David Dureisseix. “An Overview of Mechanisms and Patterns with Origami”. en. In: *International Journal of Space Structures* 27.1 (Mar. 2012). Publisher: SAGE Publications Ltd STM, pp. 1–14. DOI: 10.1260/0266-3511.27.1.1. URL: https://doi.org/10.1260/0266-3511.27.1.1 (visited on 01/04/2024).

[112] Doh-Gyu Hwang et al. “Tunable Mechanical Metamaterials through Hybrid Kirigami Structures”. en. In: *Scientific Reports* 8.1 (Feb. 2018). Number: 1 Publisher: Nature Publishing Group, p. 3378. DOI: 10.1038/s41598-018-21479-7. URL: https://www.nature.com/articles/s41598-018-21479-7 (visited on 01/08/2024).

[113] Fuwen Hu et al. “An Origami Flexiball-Inspired Metamaterial Actuator and Its In-Pipe Robot Prototype”. en. In: *Actuators* 10.4 (Apr. 2021). Number: 4 Publisher: Multidisciplinary Digital Publishing Institute, p. 67. DOI: 10.3390/act10040067. URL: https://www.mdpi.com/2076-0825/10/4/67 (visited on 01/08/2024).

[114] Zhaowen Lin et al. “Folding at the Microscale: Enabling Multifunctional 3D Origami-Architected Metamaterials”. en. In: *Small* 16.35 (2020), p. 2002229. DOI: 10.1002/smll.202002229. URL: https://onlinelibrary.wiley.com/doi/abs/10.1002/smll.202002229 (visited on 01/08/2024).

[115] Sicong Shan et al. “Multistable Architected Materials for Trapping Elastic Strain Energy”. In: *Advanced Materials* 27.29 (2015), pp. 4296–4301. DOI: 10.1002/adma.201501708. URL: https://onlinelibrary.wiley.com/doi/abs/10.1002/adma.201501708 (visited on 12/12/2023).

Part IV

Appendices

A

Additional Background

A.1. Stiffness in Linear Elastic Material

Equation A.2 shows how axial stiffness, Young's modulus, and the cross-sectional area, which is perpendicular to the load direction, are related in a linear elastic material. Using Equations A.1 and A.2, the axial stiffness can be derived from the stress-strain curve of linear elastic material, if the effective length and cross-sectional area of the material is known.

$$\sigma = E\epsilon, \tag{A.1}$$

where σ is the stress acting on the material, E is the Young's modulus of the material and ϵ is strain of the material.

$$k_l = \frac{E * A}{x_e}, \tag{A.2}$$

where k_l is the axial stiffness, E is the Young's modulus of the material, A is the cross-sectional area, and x_e is the effective length of the elastic material.

For linear axial springs, the relation between force and displacement is Equation A.3. Which shows the relation between the force ($F(x)$) acting on the spring, the variation of length of the spring (x) and a spring constant (k_l). Since the relation between the force and the variation in length is linear, the axial stiffness of linear elastic springs is equal to the spring constant. The stiffness of a linear elastic spring can be observed in Equation A.4.

$$F(x) = k_l * x \tag{A.3}$$

$$K = \frac{F(x)}{x} = k_l \tag{A.4}$$

In linear elastic material, the slope of the stress-strain curve is equal to the Young's modulus of the material. While in linear springs, the gradient of the force-displacement curve is equal to the stiffness of the material. However, not every material or mechanism is linear elastic. Nonlinear elastic mechanisms, whose force-displacement curves are quadratic, cubic or even exponential, exist. Examples of these are given in Figure A.1. These relations can no longer be expressed using Hooke's Law, but could require more advanced material models, such as the neo-Hookian or Mooney-Rivlin model.

A.2. Variable Impedance Actuators

VSAs are part of a broader category of actuators called variable impedance actuators (VIAs). Lets start by explaining the difference concept of a VIA and its opposite, the non-VIA or rigid actuator. A rigid actuator is essentially a device capable of moving to a specific position or following a predetermined path. Once it reaches its intended position, the actuator should maintain that position against external forces (as long as

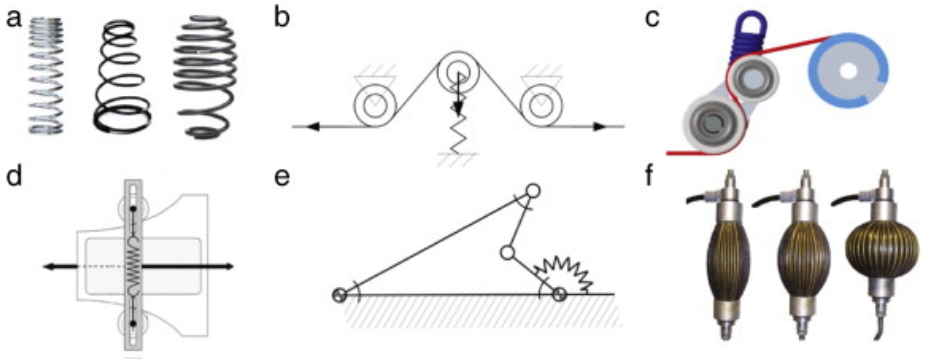

Figure A.1: Examples of mechanisms that produce nonlinear elastic characteristics [6].

they remain within the force limits of the device). In other terms, it acts as a positional source with very high, ideally infinite, mechanical impedance [6].

Impedance refers to the system's resistance to motion in response to an applied force. This term covers a broader scope than stiffness, which is a mechanical property describing a material's (or system's) resistance to deformation under an applied force. While stiffness specifically addresses resistance to deformation, impedance is a more inclusive term. Compliance represents the inverse of stiffness, and admittance complements impedance.

Many types of VIA exist, Ham et al. [20] categorized VIAs depending on how their stiffness and damping are achieved. A primary division can be established among *active impedance by control*, *inherent compliance actuators*, *inherent damping actuators*, *inertial actuators*, and combinations thereof. An example of variable active impedance by control is the quadruped HyQ by Boaventura et al. [99]. The HyQ utilizes the high-bandwidth torque control possible in hydraulics to achieve active compliance by a wide impedance range. An example of an inherent damping actuator is a piezoelectric-based friction damper by Laffranchi et al. [100]. Their variable physical damping actuator uses parallely connected piezo stacks to generate a braking force. An example of an inertial actuator where a mass is used to storage kinetic energy, not a spring or damper, is a spinning flywheel. The flywheel can act as a gyroscope or used to store energy [101]. This report will focus on inherent compliance actuators and examples of this type of VIA will therefore be given throughout this section.

VIAs based on inherent compliance incorporate a built-in passive element, such as a spring capable of storing energy, as noted by Ham et al.[20]. This classification can be further divided into mechanisms where the compliant element maintains a constant stiffness, known as *fixed compliance*, while variable impedance is managed through software, and systems with *adaptable compliance*, wherein stiffness adjusts through mechanical reconfiguration. VSAs belong to the class of adaptable compliance actuators. The advantage of adaptable compliance systems lies in the impressive bandwidth of passive compliance allowing for the absorption of impact shocks and efficient energy storage. Typically, these systems exhibit low intrinsic damping for effective energy storage and retrieval [6].

A.2.1. Fixed Compliance Actuators

The Series Elastic Actuator (SEA) is a widely recognized fixed compliance actuator, featuring a spring arranged in series with a robust actuator. The chosen spring dictates the fixed actuator stiffness, making it impossible to alter the physical stiffness during operation [6][20]. SEAs are made up of actuators connected to elastic elements and loads in series. These elastic elements have three primary functions [15]:

- Efficiently storing and releasing energy.
- Transforming the force control problem into a position control problem using the relation between elastic deformation and output force.
- Minimizing peak forces on the motor and user during impact, enhancing safety.

The widespread use of SEAs in robotics is attributed to their notable force/torque control capabilities and low output impedance [102]. However, despite their broad applications, SEAs are known also for

undesirable characteristics such as fixed stiffness, bulky structures, and substantial weight [37]. Additionally, their inability to adapt stiffness to varying loads and conditions can lead to undesired oscillations [103].

Some examples of SEAs are: 1) The ComPact© soft actuator designed for the iCub robot [104], which incorporates six linear springs for the compliant element positioned between the three-spoke structure of the motor-side reduction drive and the three spokes of the output link. 2) Distributed Elastically Coupled Macro Mini Actuation (DECMMA) [105], where an SEA is placed in parallel with a smaller motor to recover control bandwidth in high frequencies.

A.2.2. Differences between Fixed Compliance Actuators & Adaptable Compliance Actuators

SEAs and VSAs are very similar. Both type of actuators use a intrinsic compliant element to provide shock resistance, energy storage, and stable force control. In addition, SEAs and VSAs are (generally) both composed of the following elements [15]:

- Output Link, the point that interacts with the environment.
- (Multiple) Compliant Elements, these are often springs.
- Transmissions, which define the kinematics, speed, and force characteristics of the actuator.

The main difference between the two actuators is that VSAs have some actuator that controls the compliance of the system. Because of this SEAs have a more limited performance, but are usually less complex. In contrast to SEAs, VSAs introduce additional actuators, elastic elements, connectors, friction reducers, and diverse mechanisms to attain variable stiffness [6][17], thereby increasing mechanical complexity. This literature review will focus on VSAs because of the wider range of applications and higher performance.

A.2.3. Application of Adaptable Compliance Actuators

VSAs find application in a variety of robot prototypes, each tailored for specific purposes. For instance, the development of robot hands and arms prioritizes safety, robustness, and dynamic performance improvements, facilitating tasks like throwing or hammering [17]. In these systems, joint stiffness can be mechanically adjusted within the VSA or through control algorithms, or a combination of both [23]. Current applications that necessitate adaptable compliance can be divided into two main categories: those that improve *human-robot interaction* and those that improve *natural dynamics*. The classification of these groups is depends on the core objective of compliance within the application, as discussed by Ham et al. [20]. It is essential to recognize that the capability to alter stiffness is often considered a desirable feature rather than an absolute necessity.

Application of variable stiffness in human-robot interaction usually revolves around safety, both for human and robot, and comfort for the human. In industrial robots, compliant joints enhance safety during collaborative tasks between robots and humans. An actuator with adaptable compliance can increase stiffness for better positioning and decrease stiffness for faster movements [10]. Also, robotic toys benefit from compliance in actuation since this prevents damage caused by children imposing unintended motions on stiffly driven robotic toys and provides a more natural feel [20]. In gait rehabilitations, adding compliance to actuators helps absorb large position errors, preventing harm to the wearer in cases of severe spasms [106]. An actuator that can tune stiffness improves robustness to external perturbations and model errors. These model errors or perturbations could be caused by a change in the environment of the robot, the dynamics of the robot itself or a change in the dynamics of the human that is interaction with it. Robustness to external perturbation is required in tasks that require low-position error, such as hammering, screw-driving or drawing.

In addition to applications of variable stiffness in human-robot interaction, variable stiffness opens a door to more natural dynamics. In robotic prosthetics, for instance, adaptable compliance allows optimization for a wide range of circumstances and desired motions, enhancing comfort, energy efficiency, and avoiding gait pattern pathologies. For example, in a transtibial prosthesis, the compliance is predetermined during the design phase and is set to an average value, creating a fixed natural frequency for the device. Consequently, only under specific conditions of ground stiffness and walking speed, the device provides a comfortable experience for the user [107][108]. Also, in walking and running robots, actuators with adaptable compliance maximize energy storage and release during motion phases, and varying joint stiffness adjusts the natural frequency for slower or faster walking [27][109].

A.3. Design Conflicts in Variable Stiffness Actuator Design

In the design phase of VSAs, there exists a clear conflict between several factors. The existing contradictions in actuator attributes is summarized by Wolf et al. [23] as the conflict between:

- **Size, Weight & Cost**: VSAs are primarily designed for robotic arms and legs, aiming for compactness to meet crucial size and weight constraints. The weight of VSAs directly impacts system performance by influencing payload capacity, link inertia, and active/passive bandwidth. Yet, incorporating top-notch VSAs in commercial robots is expected to come with higher costs.
- **Output Power**: While a VSAs spring can provide a momentary power boost when preloaded, continuous and reliable output power is determined by the motor(s) capabilities. Continuous output power is the result of the nominal speed multiplied by the nominal torque of the positioning motor(s). Electric motors can offer a brief burst of maximum torque for dynamic applications, enabling achievable velocity to exceed nominal velocity at less than nominal torque. Maximum speed is possible at zero external load.
- **Potential energy**: Assuming full accessibility of the spring's energy through passive actuator deflection, the maximum elastic energy of the VSA is the same as that of the spring. The elastic energy is constrained by the potential energy capacity of the spring. The elastic energy stored in the VSA under axial deformation and torsion have already been given in Equation **??** and 4.2. The stiffness setup σ affects this capacity and spring pretension reduces the energy capacity. For practical reasons, some VSAs set a limit on maximum deflection (ϕ_{max}) rather than strictly adhering to potential energy capacity.
- **Stiffness Range**: A wide stiffness range is beneficial for tasks with cyclic movements and is especially in stiffness variation at constant load use-cases. The time to change the stiffness is influenced by the stiffness variation principle.
- **Efficiency**: Efficient energy transformation from kinematic to potential energy is very important for robots with VSAs. Minimizing friction, especially in the actuator mechanism, is essential to prevent unintended energy loss. Stiffness-adjusting motors can save energy, considering factors like using a small motor with a high transmission ratio for faster stiffness adjustments or a nonbackdrivable gear for occasional stiffness changes.
- **Accuracy**: Accuracy, repeatability, and predictability concerns with VSAs are highly dependent on the quality of models, parts, sensors, and design. High-resolution sensors are essential for precision, considering factors like hysteresis, temperature drifts, time delays, limited bandwidth, and careful selection of position sensors. Indirect measurement methods are often favored to avoid challenges with sensor placements.

A.4. Performance Analysis of VSA Classes & Compliant Behaviour

The design determinants proposed by Jafari et al. [17] can be used as tools to analytically determine the best suited motor configuration and method of stiffness variation. The determinants offer a guideline to select between the previously discussed classes of VSA and the type of compliant element based on performance analyses. The relevant determinants can be selected based on the relevant key attributes, discusses in Section 2.1.3. One could think of many crucial determinants. A design determinant could be the speed at which stiffness can be adjusted, or the range over which the stiffness can be adjusted, these determinants highly depend on the application of the VSA. In this subsection five determinant will be highlighted. Jafari et al. analysed every class of VSA and the compliant elements currently present in these classes with respect to these five determinants. The results from the analytical evaluation of the five classes and compliant element elastic behaviours, based on these determinants, can be observed in Figures A.2a-A.2e. The abbreviations of the classes from Section 2.1.4 are denoted in Table A.1. These determinants are:

- **Required energy to adjust the stiffness**: The method of changing the stiffness is dependent on the type of VSA, however in every class of VSA the actuators have to spent energy to change the stiffness of the VSA. This determinant is analysed by calculating the required energy to adjust the stiffness between two arbitrary values, while the link is deviated from its equilibrium by a constant distance.

- **Required force to maintain the stiffness**: To analyse this, the forces that the actuator has to hold to keep the stiffness at an arbitrary high constant value are calculated.
- **Energy efficiency of stiffness adjustment**: In an ideal situation, the energy consumed during stiffness adjustment is equal to the potential energy added to the spring by the same stiffness adjustment. The difference between these two can be used to benchmark a VSM on efficiency.
- **Accessibility to the maximum energy storage**: In the ideal situation, all energy that is stored in the springs because of deflection, can be utilized as output potential energy by the system. The accessibility is denoted as the ratio between maximum energy storage and output potential energy.
- **Coupling between the deflection and the stiffness**: The coupling or decoupling between deflection and stiffness depends highly on the intended application of the VSA. The coupling factor can be derived using the degree of correlation between deflection and stiffness.

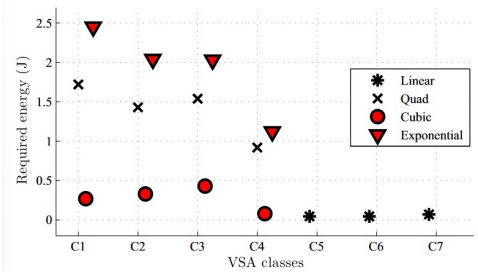

(a) Energy required to change the stiffness over an arbitrary range while the output link is deviated from its equilibrium position by an arbitrary distance, using different types of springs from C1 to C7

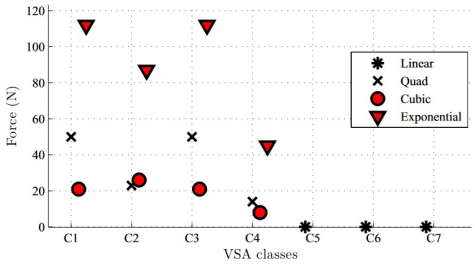

(b) Force requirement to keep the maximum stiffness (arbitrary value) using different types of springs in C1 to C7

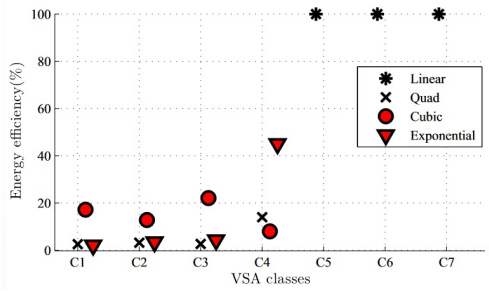

(c) Energy efficiency of stiffness adjustment over an arbitrary range using different types of springs in C1 to C7

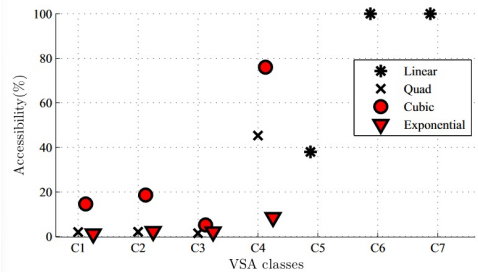

(d) Accessibility to the maximum energy storage in C1 to C7 with different types of springs

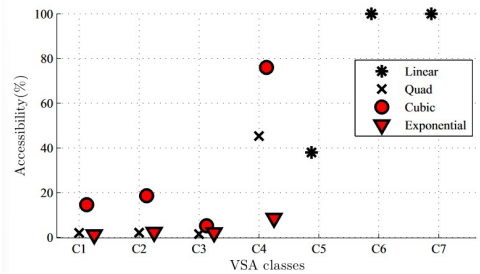

(e) Evaluation of coupling between deflection and stiffness in C1 to C7 with different types of springs

Figure A.2: Evaluation performance of different classes of VSAs and different compliant element elastic behaviour with respect to the five determinants, by Jafari et al. [17]

As mentioned, other determinants exists depending on the application of the VSA. During the design process, these determinants offer analytical guidance, if the correct determinants are identified and analysed.

Table A.1: Abbreviation of VSA classes

Class of VSA	Abbreviation
Unidirectional antagonistic	C1
Cross-coupled antagonistic	C2
Bidirectional antagonistic	C3
Changing pretension of nonlinear spring	C4
Changing load-spring transmission ratio via lever arm ratio	C5
Changing load-spring transmission ratio via transmission angle	C6
Changing effective physical properties	C7

A.5. Metamaterials

Positioned between natural materials with inherent mechanical properties and large-scale structures with highly specific designs, metamaterials hold an intermediate position in this spectrum [60]. Most recently, advancements in the online reprogrammability of metamaterials have been made. These materials can, because of their internal geometric arrangement and material used in the unit cells, change their properties, such as shear and bending stiffness, friction coefficient, Poisson's ratio, wave propagation characteristics and volume expansion factor [74]. These are categorized as active metamaterials, since their geometric arrangements can be controlled by external fields such as temperature and magnetism.

A.6. What are Mechanical Metamaterials?

Natural materials typically have specific mechanical properties. For example, Poisson's ratio, which measures how much a material contracts perpendicularly to an applied force during uniaxial loading, is generally positive in most engineered and natural materials, with a few exceptions [62]. Additionally, the mechanical and physical characteristics of many natural materials are connected. Cellular materials, for instance, show a power-law relationship between elastic modulus, density, and porosity [60]. The inherent limitations in natural materials limit design options and practical applications. Hence, there is a growing interest in creating materials with specific mechanical and physical properties, and this is the main focus of mechanical metamaterials [60]. In today's era, mechanical metamaterials are becoming essential materials with significant potential for applications in various high-end engineering and physical systems [64].

A.6.1. Categories of Mechanical Metamaterials

Zadpoor [60] has identified different categories of mechanical metamaterials, which are extremal materials, negative metamaterials (i.e. materials with negative moduli) and ultra-property metamaterial. These categories will be briefly discussed in the following subsections. These categories are not mutually exclusive. For instance, FMMs can be both extremal and exhibit negative moduli.

Extremal materials

Extremal materials are materials that are extremely stiff in specific directions, while being very complaint in other directions. The eigenvalues in the elasticity tensor of the material determine the behaviour of a material under load in any of the six directions. A very small eigenvalue results in high compliance in the direction corresponding to the particular eigenvalue, while a very large eigenvalue indicates stiffness. Extremal materials are categorized based on the number of small eigenvalues present in their elasticity tensor. The subcategories of extremal material are *unimode*, *bimode*, *trimode*, *quadramode* and *pentamode*, based on the number of small eigenvalues present that are in the elasticity tensor.

Ultra-property metamaterial

Ultra-property metamaterials are materials that combine high stiffness, high strength, high toughness or low mass-density. These properties are inherently difficult to combine, but such material would have many structural applications. Some biological matter show ultra-property behaviour, because of this many researchers have been trying to develop ultra-property metamaterials by taking inspiration from nature.

Negative metamaterials
Negative metamaterials refer to metamaterials characterized by negative moduli, such as a negative bulk modulus or negative elastic modulus. Materials exhibiting positive stiffness deform in the direction of the applied force, generating a restoring force that tries to return the material to its original shape, resisting deformation in the process. Alternatively, materials with negative stiffness deform in the opposite direction to the applied force, creating an assisting force that facilitates the deformation.

Materials with positive stiffness deform in the direction of applied force and form a restoring force that tries to restore the original shape of the deformed material, thereby resisting deformation. Materials with negative stiffness, on the other hand, deform in a direction opposite to the direction of the applied force and form an assisting force, thereby assisting the deformation.

Negative compressibility or negative stiffness lacks thermodynamic stability, meaning the elasticity tensor must be positively definite, resulting in materials that are inherently unstable. A simple system that can demonstrate negative stiffness is a planar beam buckled under compression. Recent in-depth studies have explored reversible and irreversible nonlinear mechanical properties, especially those associated with elastic buckling instability. For example, the research by Yang and Ma. [81] that has focused on self-recovering and multistable mechanical metamaterials, showcasing applications in shape-reconfigurable intelligent materials, reusable shock/impact resistance, energy trapping and absorption, as well as vibration isolation, sound, and control of elastic wave propagation.

A.6.2. Geometrical structures that allow for Stiffness Adaptation

As mentioned previously, metamaterials are build up using small structures called unit cells, which combined individual responses create the macro-response of the structure. Geometric structures of FMMs can be classified based on the shape of their unit cells. The unit cell can be classified as *constrained 1D beams*, *2D curved planes*, *3D shells*, *compliant mechanisms* or *balloon structures*. These can be connected in 1D chains, 2D networks or 3D volumetric shapes [70]. In literature, FMM used in stiffness modulation are generally made out of 2D curved planes [110], 3D shells [71] or complaint mechanisms [15]. Therefore, this review will be limited to these three categories.

Two types of structural mechanisms that fall in the 2D plane or 3D shell category are origami and kirigami structures. Origami is the famous ancient Japanese art of folding paper, while kirigami is another ancient Japanese art that uses both folds and cuts in paper [78]. A benefit in using origami and kirigami patterns to create 2D and 3D engineering structures lies in the increased stiffness at the folding creases. This means that when bending stiffness has increasing in the folding direction, the overall rigidity of the structure is increased as well [111]. Another benefit, which is exclusive to kirigami structures, is the possibility to combine major and minor cuts to achieve highly tunable mechanical responses [112]. In many origami-based metastructural pattern, researchers have extensively studied how stiffness changes with varying geometric dimensions. Also, they have shown that forcefully distorting specific origami units, can lead to a notable increase in stiffness. However, these distortions change the fundamental behavior of origami or kirigami structures, making them unable to recover and non-repeatable when subjected to cyclic loading [78], making distorted origami units practically unsuited for applications such as VSAs.

Origami and kirigami patterns are increasingly being used in the design of mechanical metamaterials. These materials offer a programmable stiffness, enabling them to adjust and react to external loads, boundary conditions, and their operating environment [63], for example the novel kirigami-inspired hybrid metamaterial with programmable deformation-dependent stiffness and mixed-mode multidirectional auxeticity by Sinha and Mukhopadhyay [78]. Structural deformation in origami-based metamaterial has even transcended traditional deformations such as bending, stretching, twisting, spiraling and coiling to more advanced deformation patterns such as actuating a magneto-responsive flexiball-inspired origami metamaterial [113]. In recent years, many researchers have found inspiration in origami and kirigami to expand the realm of FMMs, even enabling an origami-based structure that achieves variable stiffness at micro-scale [114].

In recent years, chiral metamaterials for stiffness modulation are being developed also, which are not confined to one of the three previously mentioned categories. For instance, Wang et al. [75] proposed a chiral metamaterial structure that is stackable to realise multistability and is able to achieve multiple stiffness modes. Chirality means the inability to coincide with its mirror image. Chiral structures are designed by attaching flexible beams to a central rigid node in a tangential direction.

B

Supplementary Figures

Energy trapping due to Buckling Instabilities
Strain energy trapping caused by buckling instabilities occurs when materials or structures suddenly deform upon exceeding a critical load. This deformation, known as buckling, localizes energy in certain areas of the structure. Such energy trapping can only happen in bistable systems because in these systems, the strain energy remains stored even after the load is removed. In contrast, in simple stable or monostable systems, any stored strain energy is released when the load is removed. Bistable systems retain this energy due to the presence of a local minimum in strain energy in their second stable state. An example of energy trapping in 1D beams is shown in Figure B.1.

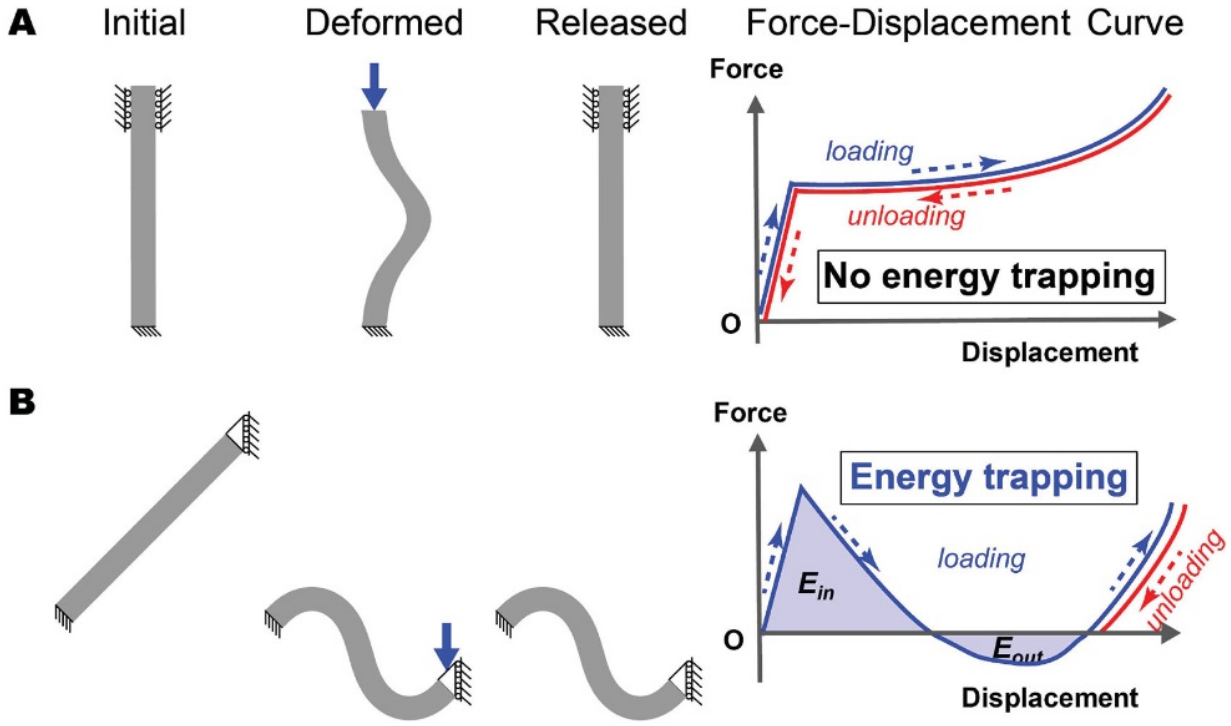

Figure B.1: Deformation of 1D beams A) Simple stability deformation of a 1D beam B) Energy trapping in a constrained 1D beam due to bistability [115]

Stiffness Difference in Planar Structure
This research explores the difference in torsional stiffness in a cylindrical bistable cell, employing a 2D visualization to demonstrate how this stiffness variation arises. The visualization represents the planar metamaterial described by Yang and Ma [84]. In Figure B.2, the difference in deformation between the closed and open state of the unit cell is visualized. The vertical support beams of the bistable cell bend, illustrating the importance the flexural modulus of these beams has on the stiffness of the entire structure.

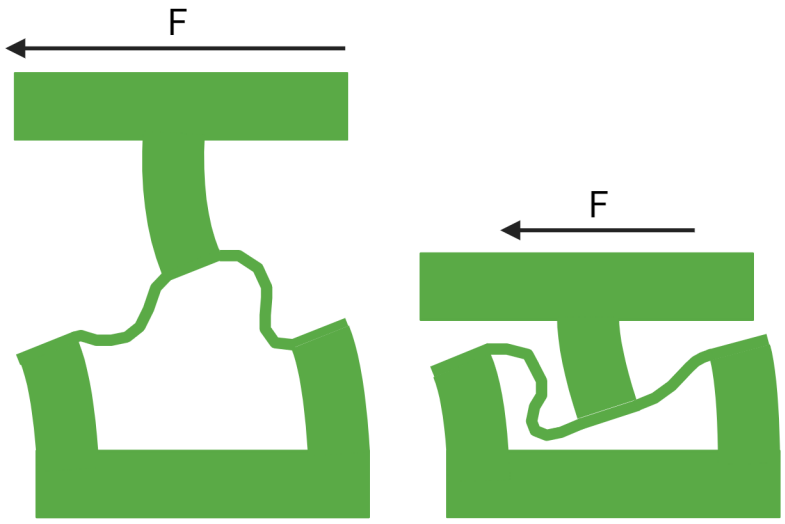

Figure B.2: Visualized stiffness difference in the 2D structure proposed by Yang and Ma [84].

3D Visualization of Stiffness depending on Geometric Ratios
The torsional stiffness of the bistable cell was assessed using different geometric ratios b/l and $t2/t1$, as shown in Figure 6.3. For each ratio, the torsional stiffness was simulated through finite element analysis (FEA). Figure B.3 displays a 3D surface plot of the stiffness for each geometric ratio within the specified region from Figure 6.3. Figure B.3 includes red dots marking the specific data points, and the surface is created using linear interpolation. Due to the linear interpolation, the representation at the edges of the region was incorrect. To address this, the edges were smoothed during post-processing. The plot illustrates the stiffness landscape for both the open and closed states of the bistable cell.

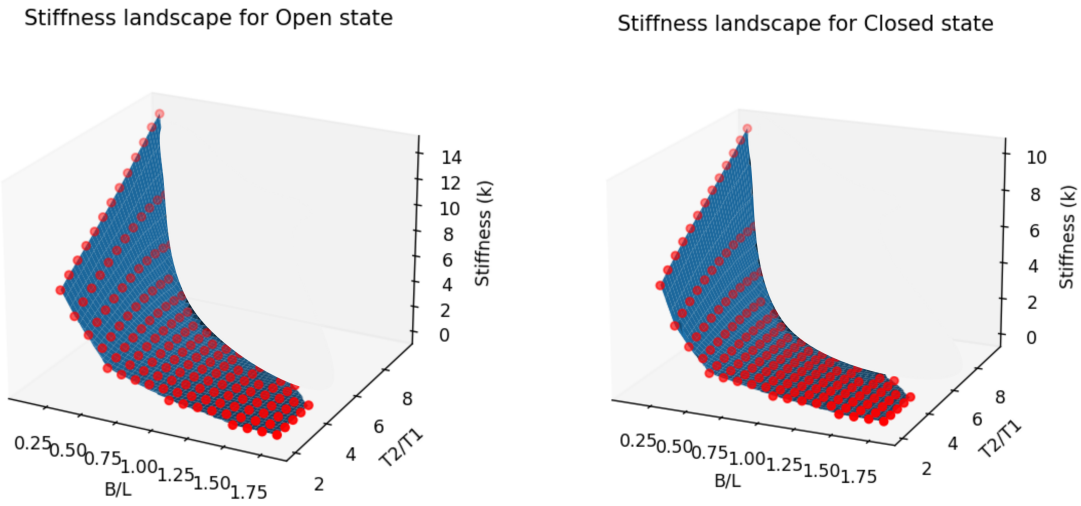

Figure B.3: The stiffness landscapes that result from the FEA regarding the geometric analysis. The red dots are the investigated data points. The blue surface constructed using linear interpolation between the data points.

Experimental Setup to Investigate Dynamic Behaviour of the Bistable Cell
Figure B.4 depicts the experimental setup employed to record the motion trajectory of the bistable cell after it was rotated. The setup features a high-speed camera and studio lighting to ensure optimal illumination. The captured footage was then analyzed using motion tracking software to extract the motion data.

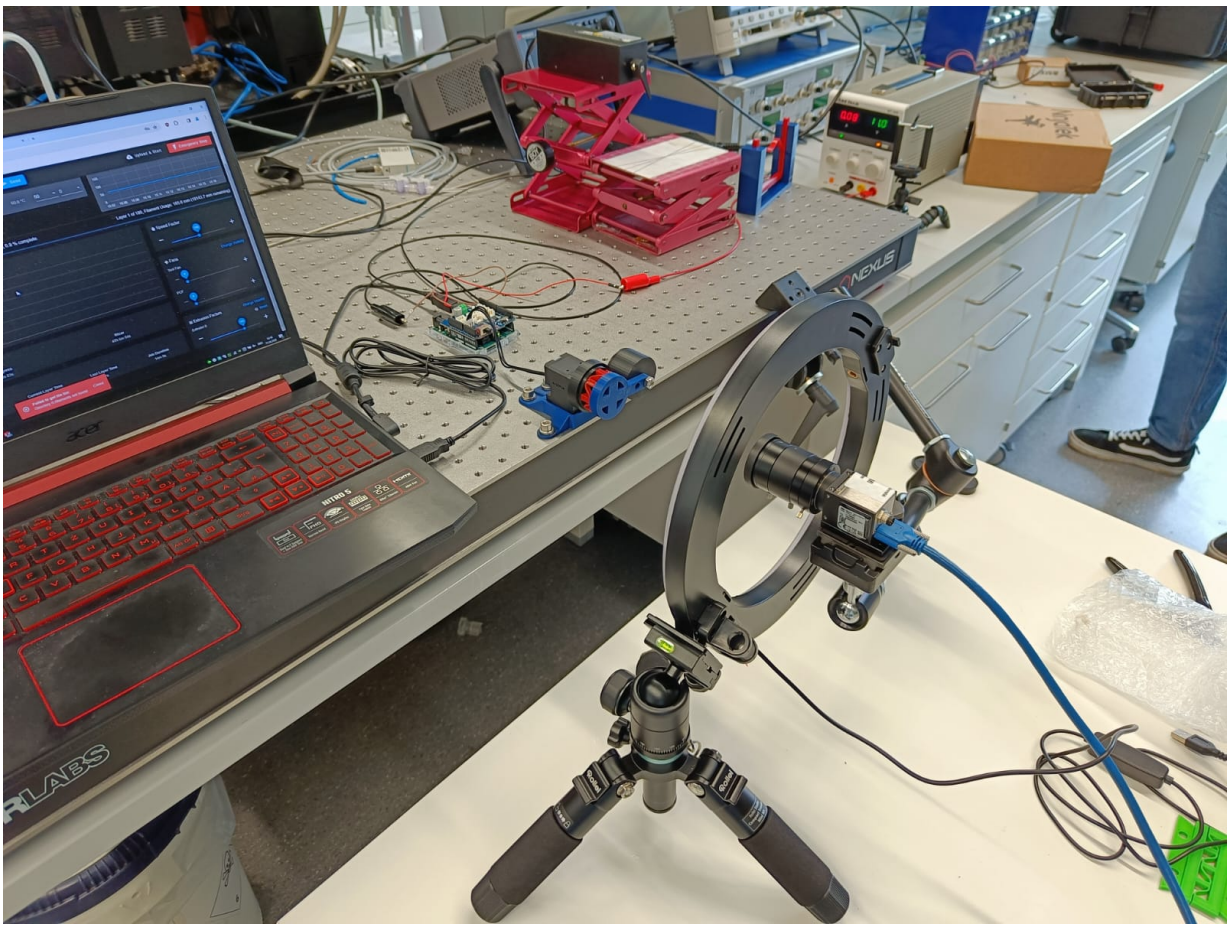

Figure B.4: Setup of the dynamic test. Using a high speed camera to record the dynamic behaviour of the bistable cell.

Biaxial Testing Machine
In this study's stability analysis and the experimental validation of the FEAs, a Zwick&Roell biaxial tensile-torsion test machine was used. This machine is depicted in Figure B.5. The samples were attached between the testing machine's load cell and motor. Additionally, a specially designed clamp was used to secure the samples in the gripper of the testing machine.

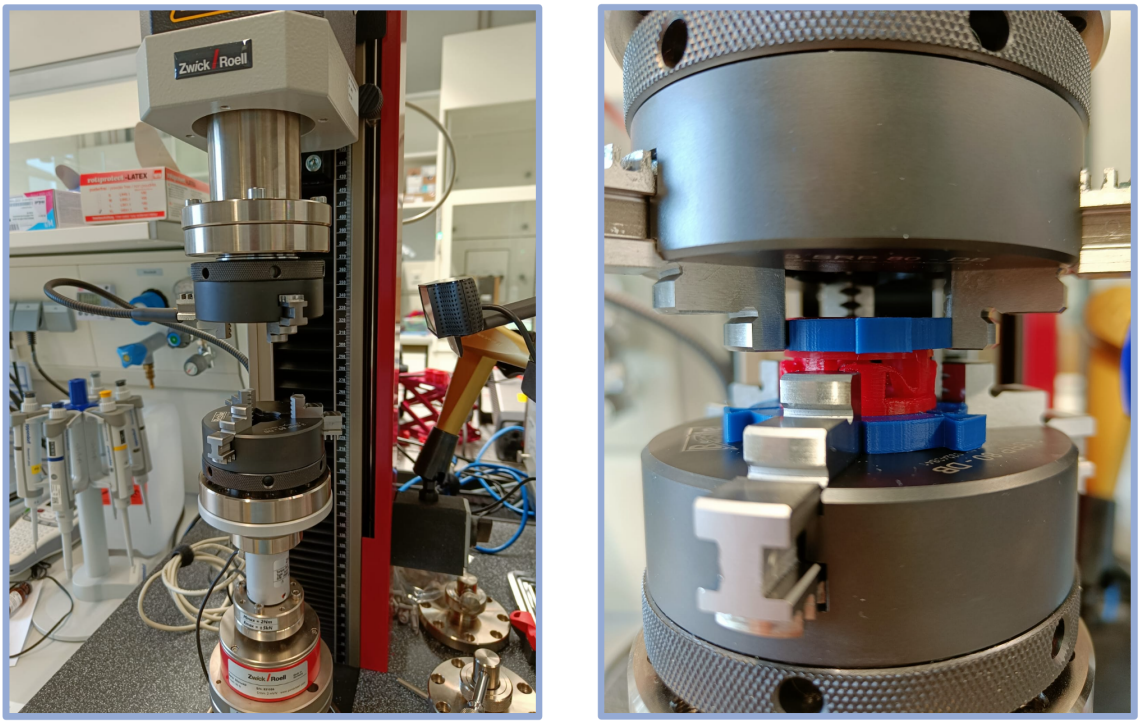

a) The biaxial testing machine

b) Sample structure mounted on the machine

Figure B.5: The biaxial testing machine by ZwickRoell used in this research.

Torque-Angle Data obtained from the Biaxial Testing Machine

After testing the samples in the biaxial testing machine, the raw data obtained is displayed in Figure B.6, illustrating three distinct load cycles. By plotting the torque against the angle and distinguishing the peaks and valleys in the data, the stiffness values can be derived.

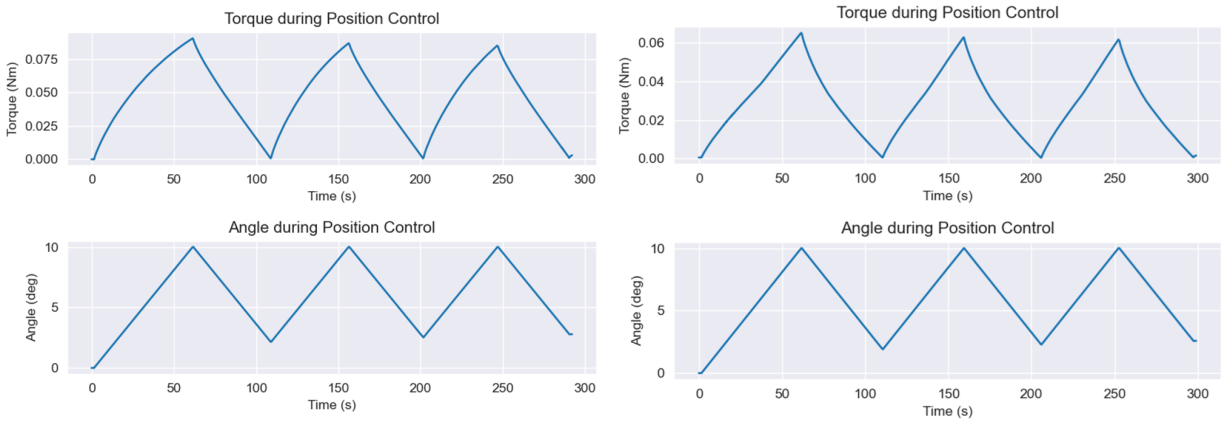

Figure B.6: Example of experimentally obtained data, where the torque and angle are plotted against time for position-controlled measurements.

Soft Pneumatic Actuator Prototype and Mold Design

In the final design of this thesis, rigid pistons were utilized. However, another approach involves using custom soft pneumatic actuators made from silicone, as depicted in Figure B.7a. To create these actuators,

silicone is poured into a mold, shown in Figure B.7b. For applications requiring a linear pneumatic actuator, the balloon should be designed with a bellowed configuration.

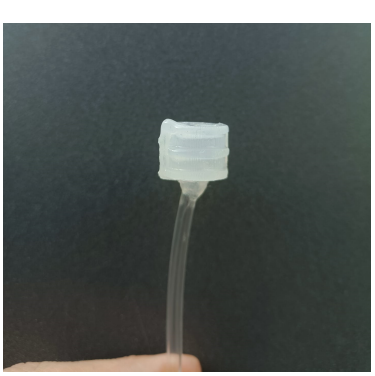

(a) Soft pneumatic actuator

(b) 3D printed molds to fabricate soft pneumatic actuators

Figure B.7: Example of soft pneumatic actuator and complementary mold design.

Mold Design for Bistable Cell

To increase the customizability of the unit cell, a new mold design was introduced, allowing for broader material use and improved mechanical interlocks. The process involves creating parts of the unit cell with PLA through FDM printing, which are then inserted into the mold. The mold is filled with a liquid polymer that cures to form the final cylindrical unit cell, as shown in Figure B.8.

However, optimizing this injection molding technique proved to be too time-intensive for the scope of the research. Given that the PLA and TPU combination was effective, further development of this mold was discontinued due to time constraints, although the method remains promising for future work.

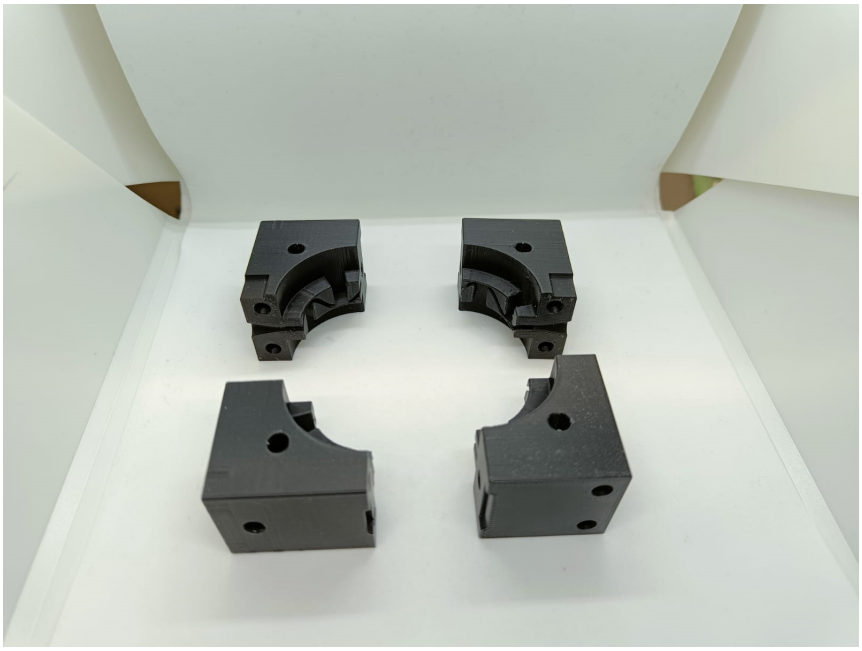

Figure B.8: Mold design used to make multi-material bistable cells

Torque-Angle Data: Changing the Young's Modulus

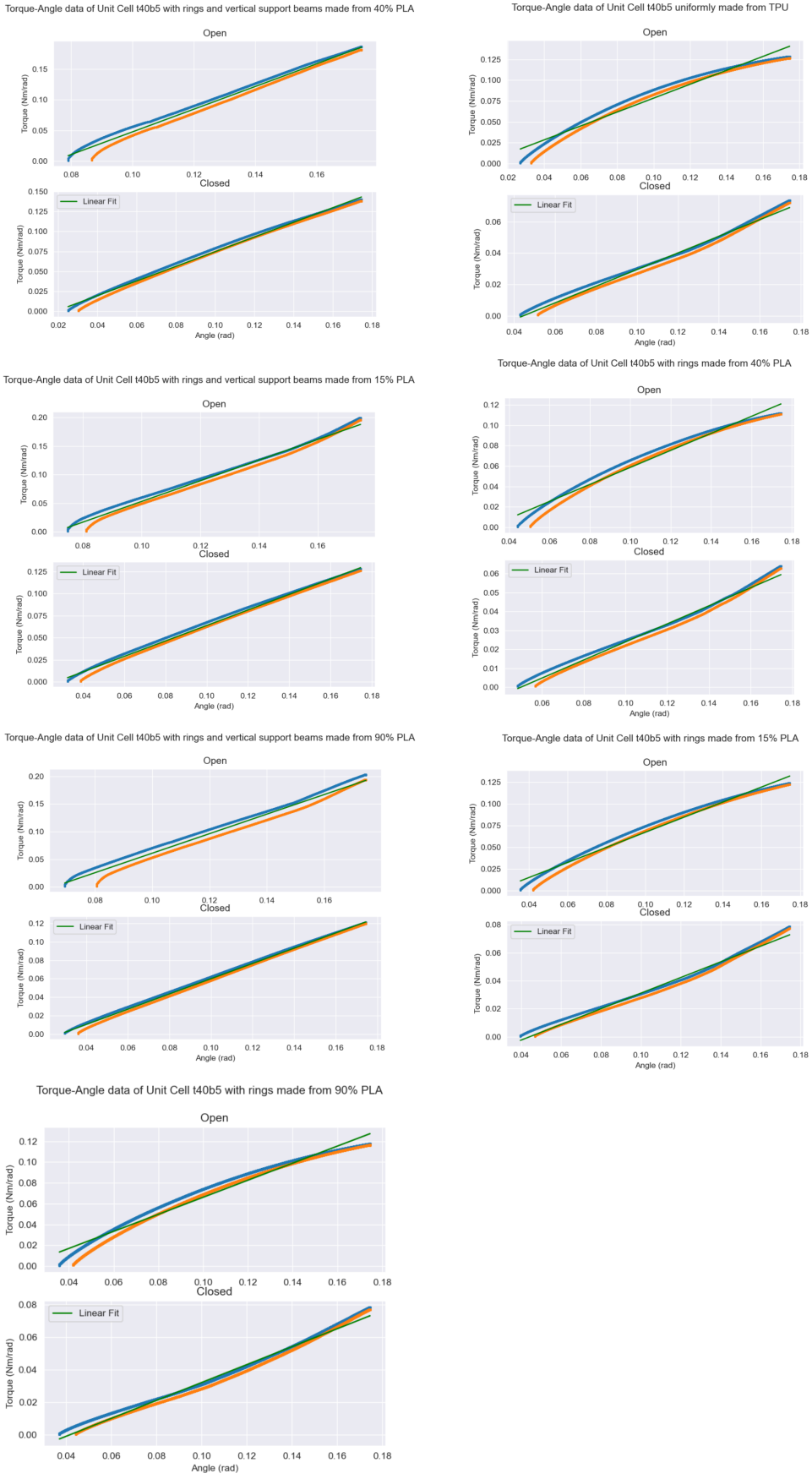

Figure B.9: Obtained data from validation experiments to assess the influence of changing the Young's modulus of certain section of the structure

Torque-Angle Data: Changing Geometric Ratios

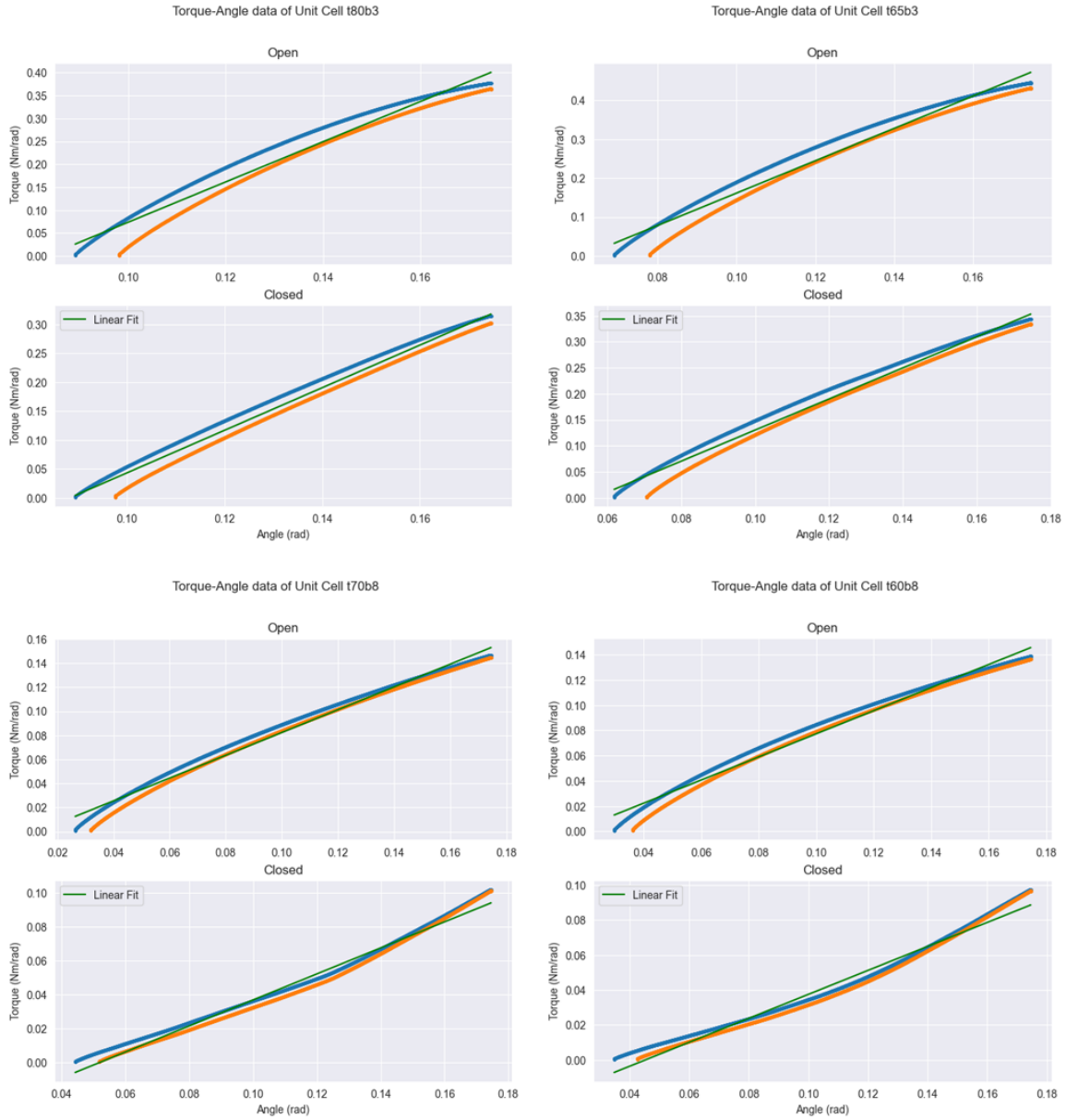

Figure B.10: Obtained data from validation experiments to assess the influence of changing certain geometric ratios of the unit cell.

Experimental Setup of Actuated Prototype with Pneumatic Actuator

The stiffness in the actuated concept is adjusted using a standard miniature piston. Two syringes are attached to the piston, each connected to one of the piston's in-/outlets, as shown in Figure B.11. This setup enables the structure to quickly transition between states by applying pressure to the piston. This method simplifies stiffness control to the operation of a single linear pneumatic actuator.

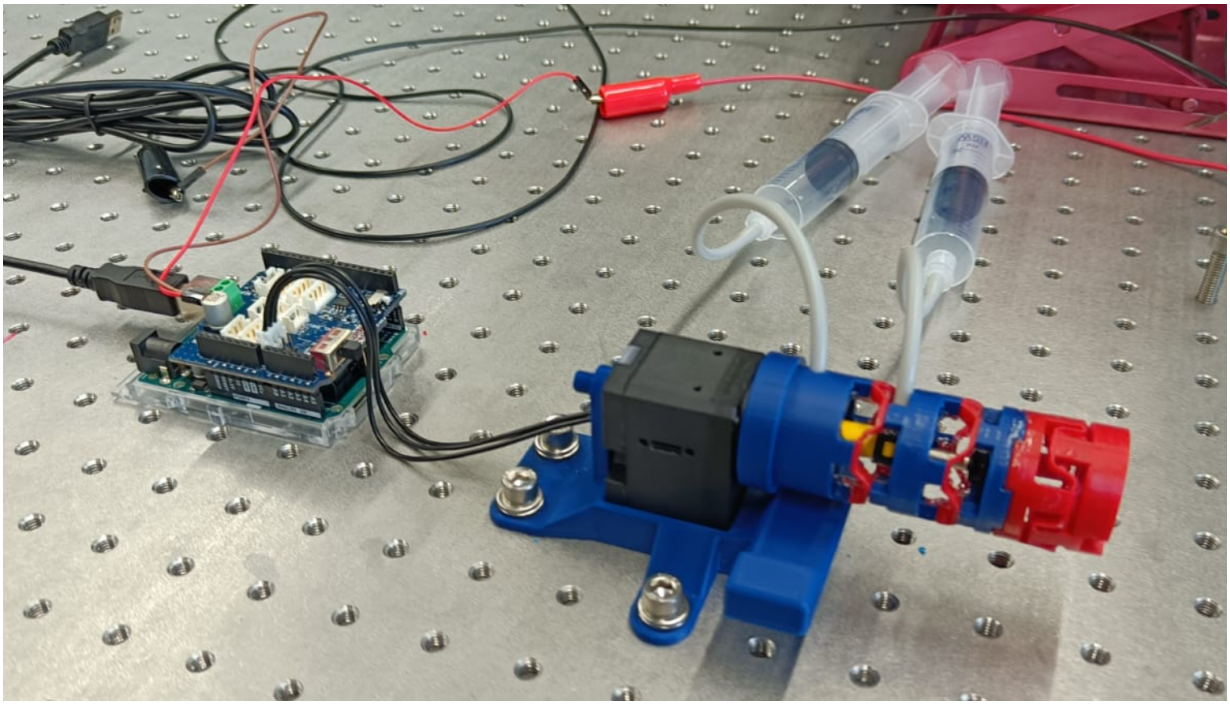

Figure B.11: Two syringes are connected to the linear pneumatic actuator to manually change the state of the metamaterial.

Grip Force Measurements on the Final Design of the B-VSG

The grip force exerted by a single end effector of the final prototype is measured using a load cell. Only a single end effector is used in the B-VSG, which is mounted on the Franka Panda robot arm. The setup of the measurement in visible in Figure B.12.

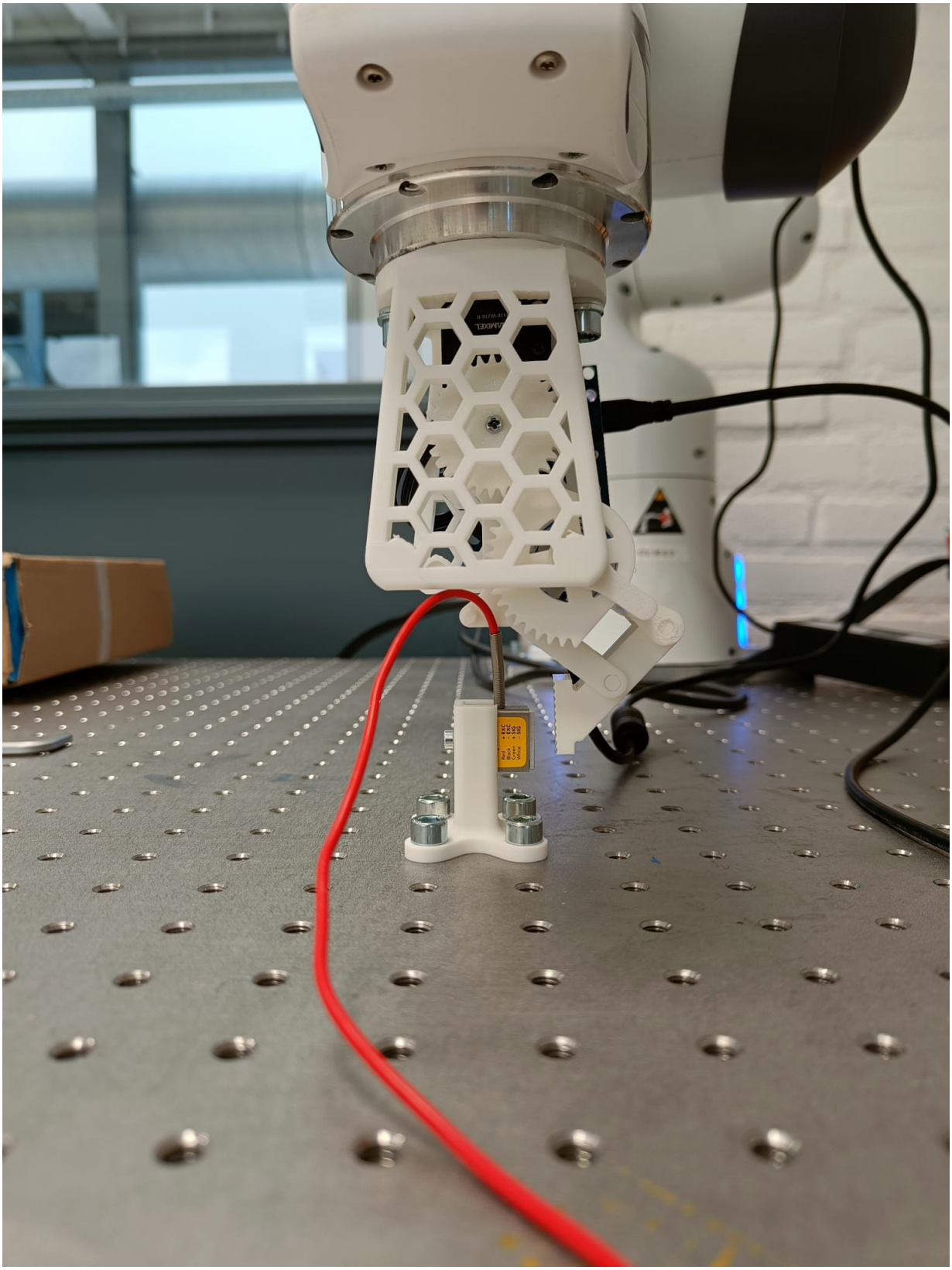

Figure B.12: Grip force measurements on the final design using a load cell (in the middle)

C

Python Code

The Python script below was employed to systematically create numerous SAT files, which were then utilized for finite element analyses in Abaqus.

```python
import win32com.client
import time

def get_active_solidworks_model():
    try:
        # Connect to the running instance of SolidWorks
        swApp = win32com.client.GetActiveObject("SldWorks.Application")
        swApp.Visible = True

        # Get the active document
        swModel = swApp.ActiveDoc
        if swModel is None:
            raise Exception("No active SolidWorks document found.")

        print("Connected to the active SolidWorks document.")
        return swModel, swApp
    except Exception as e:
        print(f"Failed to connect to SolidWorks: {e}")
        raise

def read_and_modify_text_file(file_path, line_number, new_content):
    with open(file_path, 'r') as file:
        lines = file.readlines()

    if 0 <= line_number - 1 < len(lines):
        lines[line_number - 1] = new_content + "\n"
        print("Line changed")
    else:
        print("Line number is out of range.")

    with open(file_path, 'w') as file:
        file.writelines(lines)

def rebuild_solidworks_model(swModel):
    swModel.ForceRebuild3(False)

def save_as_new_file(swModel, base_path, file_name_suffix_t1, file_name_suffix_b):
    new_file_path = f"{base_path}_t_{file_name_suffix_t1}_b_{file_name_suffix_b}.SAT"  # Adjust the extension as needed
    swModel.SaveAs(new_file_path)
    print(f"File saved as: {new_file_path}")


# Paths
text_file_path = "file/path"
base_file_path = "file/path"

# Start value and step size for file naming
start_value_t = 20
step_size_t = 5
```

```
50
51 start_value_b = 1
52 step_size_b = 1
53
54 file_name_suffix_t = start_value_t
55
56 # Operations
57 swModel, swApp = get_active_solidworks_model()
58 print("Active document found")
59
60 t2s = ['"t2"= "t1" * 2','"t2"= "t1" * 2.5','"t2"= "t1" * 3','"t2"= "t1" * 3.5','"t2"= "t1" * 4'
    ,'"t2"= "t1" * 4.5','"t2"= "t1" * 5','"t2"= "t1" * 5.5','"t2"= "t1" * 6','"t2"= "t1" * 6.5'
    ,'"t2"= "t1" * 7','"t2"= "t1" * 7.5','"t2"= "t1" * 8','"t2"= "t1" * 8.5','"t2"= "t1" * 9','
    "t2"= "t1" * 9.5']
61 bs = ['"b"= 0.1 * "l"','"b"= 0.2 * "l"','"b"= 0.3 * "l"','"b"= 0.4 * "l"','"b"= 0.5 * "l"','"b
    "= 0.6 * "l"','"b"= 0.7 * "l"','"b"= 0.8 * "l"','"b"= 0.9 * "l"','"b"= 1 * "l"','"b"= 1.1 *
     "l"','"b"= 1.2 * "l"','"b"= 1.3 * "l"','"b"= 1.4 * "l"','"b"= 1.5 * "l"','"b"= 1.6 * "l"',
    '"b"= 1.7 * "l"','"b"= 1.8 * "l"']
62
63 for t2 in t2s:
64     file_name_suffix_b = start_value_b
65     read_and_modify_text_file(text_file_path, 3, t2)
66     for b in bs:
67         read_and_modify_text_file(text_file_path, 5, b)
68         rebuild_solidworks_model(swModel)
69         time.sleep(5)
70         save_as_new_file(swModel, base_file_path, f"{file_name_suffix_t}", f"{
    file_name_suffix_b}")
71         file_name_suffix_b += step_size_b
72     file_name_suffix_t += step_size_t
73
74 print("Active SolidWorks document used, text file modified, part rebuilt and saved under new
    names")
```

Listing C.1: Python script to generate different SAT files